# MECHANISTIC-EMPIRICAL MODELING AND DESIGN MODEL DEVELOPMENT OF GEOSYNTHETIC REINFORCED FLEXIBLE PAVEMENTS

FHWA/MT-01-002/99160-1A

*Final Report*

*prepared for*
THE STATE OF MONTANA
DEPARTMENT OF TRANSPORTATION

*in cooperation with*
THE U.S. DEPARTMENT OF TRANSPORTATION
FEDERAL HIGHWAY ADMINISTRATION
and the
Idaho, Kansas, Minnesota, New York, Texas, Wisconsin
and Wyoming Departments of Transportation and the
Western Transportation Institute at Montana State University

*November 2001*

*prepared by*
Dr. Steven W. Perkins
Montana State Univeristy

RESEARCH PROGRAM

# MECHANISTIC-EMPIRICAL MODELING AND DESIGN MODEL DEVELOPMENT OF GEOSYNTHETIC REINFORCED FLEXIBLE PAVEMENTS: FINAL REPORT

**FHWA/MT-01-002/99160-1A**

*Final Report*

*Prepared for the*
STATE OF MONTANA
DEPARTMENT OF TRANSPORTATION
RESEARCH, DEVELOPMENT AND TECHNOLOGY TRANSFER PROGRAM
in cooperation with the
U.S. DEPARTMENT OF TRANSPORTATION
FEDERAL HIGHWAY ADMINISTRATION
and the
Idaho, Kansas, Minnesota, New York, Texas, Wisconsin and Wyoming
Departments of Transportation
and the
Western Transportation Institute at Montana State University

October 1, 2001

*Prepared by*

Dr. Steven W. Perkins
Associate Professor
Department of Civil Engineering
Western Transportation Institute
Montana State University – Bozeman
Bozeman, Montana 59717
Office Telephone: 406-994-6119
Fax: 406-994-6105
E-Mail: stevep@ce.montana.edu

**TECHNICAL REPORT STANDARD PAGE**

| 1. Report No. | 2. Government Accession No. | 3. Recipient's Catalog No. |
|---|---|---|
| **FHWA/MT-01-002/99160–1A** | | |

| 4. Title and Subtitle | 5. Report Date |
|---|---|
| **Mechanistic-Empirical Modeling and Design Model Development of Geosynthetic Reinforced Flexible Pavements: Final Report** | **October 1, 2001** |
| | 6. Performing Organization Code **MSU G&C #428573** |
| 7. Author<br>**Steven W. Perkins, Ph.D., P.E.** | 8. Performing Organization Report No. |
| 9. Performing Organization Name and Address<br>**Department of Civil Engineering**<br>**205 Cobleigh Hall**<br>**Montana State University**<br>**Bozeman, Montana 59717** | 10. Work Unit No.<br>11. Contract or Grant No.<br>**99160** |
| 12. Sponsoring Agency Name and Address<br>**Montana Department of Transportation**<br>**Research Section**<br>**2701 Prospect Avenue**<br>**P.O. Box 201001**<br>**Helena, Montana 59620-1001** | 13. Type of Report and Period Covered<br>**Final: October 1, 1998 – October 1, 2001**<br>14. Sponsoring Agency Code<br>**5401** |

15. Supplementary Notes
**Preparation in cooperation with the U.S. Department of Transportation, Federal Highway Administration**

16. Abstract

Research over the past 20 years has demonstrated the benefit provided by geosynthetics when placed within or at the bottom of base aggregate layers in flexible pavement systems for the purpose of reinforcement. The primary benefits demonstrated include an extension of service life of the pavement and/or a reduction in the structural section for equivalent service life. These benefits have been defined primarily in terms of a Traffic Benefit Ratio (*TBR*) defining the increase in service life of the pavement and a Base Course reduction Ratio (*BCR*) defining the reduction in base aggregate thickness permissible by the use of reinforcement.

Previous experimental work involving the construction and loading of reinforced pavement test sections has demonstrated that values of benefit are strongly dependent on pavement design parameters such as thickness of the structural section and strength and/or stiffness of the subgrade, and properties and type of geosynthetic used. A recently completed report by the Geosynthetic Materials Association, GMA, (Berg et al., 2000) concluded that given the absence of a suitable method for analytically quantifying reinforcement benefit, benefit values for use in design should at present be based on purely empirical methods involving direct observation of benefit from test sections having pavement design conditions and a geosynthetic reinforcement similar to the design being considered. A NCHRP Synthesis, in print at the time this report was prepared (Christopher et al., 2001), provides a survey of geosynthetic base reinforcement usage amongst all U.S. State transportation agencies and found that the primary reasons for lack of usage were the absence of a suitable design method for defining reinforcement benefit and the corresponding inability to define cost-benefit for reinforced pavement systems.

This project was undertaken to provide an analytically based method for the determination of reinforcement benefit. The method developed is expressed solely in terms of design equations used to calculate reinforcement benefit in terms of pavement structural thickness, subgrade strength and several properties related to the geosynthetic. These design equations are based on the results of over 465 pavement cross-sections analyzed using a finite element response model and empirical damage models specifically developed for this project. The 465 cases analyzed involved the systematic variation of parameters that are believed to be the most critical in terms of their impact on reinforcement benefit.

The finite element model developed involves elastic-plastic material models for the asphalt concrete, base aggregate and subgrade layers, and an anisotropic linear elastic model for the geosynthetic. Membrane elements are used for the geosynthetic where these elements are capable of carrying load in tension but have no resistance to bending or compression. The material models and parameters used for the asphalt concrete, base aggregate and subgrade are shown to relate to common pavement design properties for these materials.

Empirical distress models were developed to relate stress and strain response measures from the finite element model to pavement performance and ultimately reinforcement benefit. The distress models were calibrated from test section results given in Perkins (1999a). The distress models developed and the corresponding observed distress feature in the test sections reported in Perkins (1999a) was permanent surface deformation (rutting) caused by permanent vertical strain in the base and subgrade layers. As such, the design model proposed in this report specifically addresses the pavement distress feature of rutting. A method for evaluating the effective increase in the resilient modulus of the base aggregate layer with reinforcement for the purpose of evaluating asphalt concrete fatigue cracking criteria is suggested.

Three classes of finite element (FE) response models were developed. The first was for an unreinforced pavement cross-section. Results from unreinforced cross-sections were later compared to those with reinforcement to define reinforcement benefit. The second class of FE model was one in which reinforcement was modeled by preventing all lateral motion of the bottom of the base aggregate. This class of model allowed for definition of reinforcement benefit for a condition of maximum reinforcement potential (perfect reinforcement). While the reinforcement is not explicitly modeled in this model class, the effect of the modeling technique is to simulate a reinforcement product with an infinite tensile

stiffness and an infinitely stiff geosynthetic/aggregate shear interface. Results from the second class of FE model were compared to those of the unreinforced pavement to develop equations describing reinforcement benefit for the case of perfect reinforcement. These equations account for variations in asphalt concrete and base aggregate thickness, and subgrade strength.

The influence of geosynthetic properties was evaluated by creating a third class of FE model. In this model, the geosynthetic was explicitly accounted for by including a geosynthetic sheet, modeled with membrane elements, between the base aggregate and subgrade layer. Results from cases using this FE model were used to develop expressions for reduction factors applied to benefit seen for the cases of perfect reinforcement to account for the geosynthetic material properties varied in the study.

The anisotropic, linear-elastic material model used for the geosynthetic allowed for the variation of four basic geosynthetic material properties. These properties included the elastic modulus in the strong and weak principal directions of the material, the in-plane Poisson's ratio and the in-plane shear modulus. The design method is based on the use of a secant tensile modulus measured at 2 % axial strain from a wide-width tension test, ASTM D 4595 (ASTM, 2001a), for later definition of the elastic modulus. Reinforcement benefit is seen to be most heavily influenced by these two parameters (i.e. elastic modulus in the strong and weak principal material directions).

Geosynthetic in-plane Poisson's ratio and shear modulus are most likely related to the type and structure of the geosynthetic. Test methods and reported values for these parameters are not currently available. As such, the design method does not allow for the specific input of these two parameter values. Rather the method requires that one of two benefit reduction factors be specified for each material parameter. The two choices for benefit reduction factors correspond to good or poor values for these material parameters. Calibration of the design model from test section results using two geogrid and one geotextile product has resulted in recommended values for these products, which serve as a starting point when selecting values for other products.

The influence of base aggregate-geosynthetic shear interaction is accounted for empirically by calibration of the design method against results from published test sections, where this influence is also expressed in terms of a benefit reduction factor. Since the design method was calibrated from test section results using two types of geosynthetics, reduction factors for interface shear were developed for each type of material.

Design equations were developed for reinforcement benefit defined in terms of a *TBR*, *BCR* or a combination of the two. Furthermore, benefit defined in terms of *TBR* and/or *BCR* was broken into components associated with reinforcement effects on the subgrade, reinforcement effects on the base aggregate, and combined effects on the total pavement system. Since distress models were developed for effects in the subgrade and effects in the base aggregate layer, calibration of the design model required that separate benefit values be determined. The generally conservative nature of the design method suggests that benefit values for the total system be used.

The design model was calibrated and verified by comparison to test section results reported in Perkins (1999a), where these results were analyzed to derive experimental definitions of benefit for reinforcement effects in the base aggregate and subgrade layers. Further validation of the model was accomplished by comparison to other test section results available in the literature as summarized in Berg et al. (2000).

The design model is shown to provide generally conservative estimates of reinforcement benefit when compared to available test section results. The model is shown to be sensitive to design parameters of asphalt concrete and base aggregate thickness, subgrade strength, geosynthetic tensile modulus and tensile modulus ratio and other geosynthetic elastic material model properties. The model tends to show variations of benefit with these design parameters that are consistent with general application guidelines developed in Berg et al. (2000). Several examples are described to illustrate the use of the model and to illustrate the construction and life-cycle cost benefit that can result from the use of reinforcement.

This report provides a detained description of the finite element response model, the material models used in the FE model, calibration of the material models and how these models relate to commonly used pavement layer material models, and the steps followed to develop the design model. Limitations for use of the model are described in Sections 7.8 and Appendix B. Section 8 of the report provides a summary of the equations developed for the design model and provides suggestions for how the design model can be extended to situations not specifically addressed in the project. The design equations have been programmed into a spreadsheet program that is also described in Section 8 and can be downloaded from the following URL: http://www.mdt.state.mt.us/departments/researchmgmt/grfp/grfp.html. Appendix B of the report provides a summary of the design model as it relates to its use in practice. The material provided in Appendix B constitutes a design guideline based on the design model developed in this project. Examples are provided in Appendix B to illustrate the use of the design model and the cost-benefit for the examples given.


| 17. Key Words | | 18. Distribution Statement | |
|---|---|---|---|
| **Pavements, Highways, Geogrid, Geotextile, Geosynthetic, Reinforcement, Base Course, Finite Element Model, Numerical Modeling, Design, Montana** | | **Unrestricted. This document is available through the National Technical Information Service, Springfield, VA 21161.** | |
| 19. Security Classif. (of this report) **Unclassified** | 20. Security Classif. (of this page) **Unclassified** | 21. No. of Pages **170** | 22. Price |

# PREFACE

## DISCLAIMER

The opinions, findings and conclusions expressed in this publication are those of the author and not necessarily those of the Federal Highway Administration, the Idaho, Kansas, Minnesota, New York, Montana, Texas, Wisconsin and Wyoming Departments of Transportation or the Western Transportation Institute.

## ALTERNATE FORMAT STATEMENT

MDT attempts to provide reasonable accommodations for any known disability that may interfere with a person participating in any service, program or activity of the department. Alternative accessible formats of this document will be provided upon request. For further information, call (406) 444-7693 or TTY (406) 444-7696.

## NOTICE

The authors, the State of Montana and the Federal Highway Administration do not endorse products or manufacturers. Trade and manufacturers names appear herein solely because they are considered essential to the object of the report.

# ACKNOWLEDGEMENTS

The author gratefully recognizes the generous financial and technical support of the Montana, Idaho, Kansas, Minnesota, New York, Texas, Wisconsin and Wyoming Departments of Transportation and the Western Transportation Institute at Montana State University. The technical review provided by Mr. William Vischer of the Region 1 Engineering USDA Forest and formally of the Montana Department of Transportation provided significant substance to the report. The technical contribution of Mr. Yan Wang and Dr. Mike Edens is gratefully recognized. The Amoco Fabrics and Fibers Company and Tensar Earth Technologies, Incorporated graciously donated geosynthetic materials for preceding projects leading up to this work. They and the Tenax Corporation provided geosynthetic product information used in this report. Dr. Muralee Muraleetharan of the University of Oklahoma and Dr. Kim Mish of Lawrence Livermore National Laboratory generously provided source code and support for development of a user defined material model.

# TABLE OF CONTENTS

# LIST OF TABLES

# LIST OF FIGURES

# CONVERSION FACTORS

The following conversion factors are required for interpretation of results contained in this report.

1 m = 3.28 ft
1 mm = 0.0394 in
1 kN = 225 lb
1 kN/m = 68.6 lb/ft
1 kPa = 0.145 psi
1 $MN/m^3$ = $7.94 \times 10^{-6}$ $lb/ft^3$

# EXECUTIVE SUMMARY

Research over the past 20 years has demonstrated the benefit provided by geosynthetics when placed within or at the bottom of base aggregate layers in flexible pavement systems for the purpose of reinforcement. The primary benefits demonstrated include an extension of service life of the pavement and/or a reduction in the structural section for equivalent service life. These benefits have been defined primarily in terms of a Traffic Benefit Ratio (*TBR*) defining the increase in service life of the pavement and a Base Course reduction Ratio (*BCR*) defining the reduction in base aggregate thickness permissible by the use of reinforcement.

Previous experimental work involving the construction and loading of reinforced pavement test sections has demonstrated that values of benefit are strongly dependent on pavement design parameters such as thickness of the structural section and strength and/or stiffness of the subgrade, and properties and type of geosynthetic used. A recently completed report by the Geosynthetic Materials Association, GMA, (Berg et al., 2000) concluded that given the absence of a suitable method for analytically quantifying reinforcement benefit, benefit values for use in design should at present be based on purely empirical methods involving direct observation of benefit from test sections having pavement design conditions and a geosynthetic reinforcement similar to the design being considered. A NCHRP Synthesis, in print at the time this report was prepared (Christopher et al., 2001), provides a survey of geosynthetic base reinforcement usage amongst all U.S. State transportation agencies and found that the primary reasons for lack of usage were the absence of a suitable design method for defining reinforcement benefit and the corresponding inability to define cost-benefit for reinforced pavement systems.

This project was undertaken to provide an analytically based method for the determination of reinforcement benefit. The method developed is expressed solely in terms of design equations used to calculate reinforcement benefit in terms of pavement structural thickness, subgrade strength and several properties related to the geosynthetic. These design equations are based on the results of over 465 pavement cross-sections analyzed using a finite element response model and empirical damage models specifically developed for this project. The 465 cases analyzed involved the systematic variation of parameters that are believed to be the most critical in terms of their impact on reinforcement benefit.

The finite element model developed involves elastic-plastic material models for the asphalt concrete, base aggregate and subgrade layers, and an anisotropic linear elastic model for the geosynthetic. Membrane elements are used for the geosynthetic where these elements are capable of carrying load in tension but have no resistance to bending or compression. The material models and parameters used for the asphalt concrete, base aggregate and subgrade are shown to relate to common pavement design properties for these materials.

Empirical distress models were developed to relate stress and strain response measures from the finite element model to pavement performance and ultimately reinforcement benefit. The distress models were calibrated from test section results given in Perkins (1999a). The distress models developed and the corresponding observed distress feature in the test sections reported in Perkins (1999a) was permanent surface deformation (rutting) caused by permanent vertical strain in the base and subgrade layers. As such, the design model proposed in this report specifically addresses the pavement distress feature of rutting. A method for evaluating the effective increase in the resilient modulus of the base aggregate layer with reinforcement for the purpose of evaluating asphalt concrete fatigue cracking criteria is suggested.

Three classes of finite element (FE) response models were developed. The first was for an unreinforced pavement cross-section. Results from unreinforced cross-sections were later compared to those with reinforcement to define reinforcement benefit. The second class of FE model was one in which reinforcement was modeled by preventing all lateral motion of the bottom of the base aggregate. This class of model allowed for definition of reinforcement benefit for a condition of maximum reinforcement potential (perfect reinforcement). While the reinforcement is not explicitly modeled in this model class, the effect of the modeling technique is to simulate a reinforcement product with an infinite tensile stiffness and an infinitely stiff geosynthetic/aggregate shear interface. Results from the second class of FE model were compared to those of the unreinforced pavement to develop equations describing reinforcement benefit for the case of perfect reinforcement. These equations account for variations in asphalt concrete and base aggregate thickness, and subgrade strength.

The influence of geosynthetic properties was evaluated by creating a third class of FE model. In this model, the geosynthetic was explicitly accounted for by including a geosynthetic sheet, modeled with membrane elements, between the base aggregate and subgrade layer. Results from cases using this FE model were used to develop expressions for reduction factors applied to benefit seen for the cases of perfect reinforcement to account for the geosynthetic material properties varied in the study.

The anisotropic, linear-elastic material model used for the geosynthetic allowed for the variation of four basic geosynthetic material properties. These properties included the elastic modulus in the strong and weak principal directions of the material, the in-plane Poisson's ratio and the in-plane shear modulus. The design method is based on the use of a secant tensile modulus measured at 2 % axial strain from a wide-width tension test, ASTM D 4595 (ASTM, 2001a), for later definition of the elastic modulus. Reinforcement benefit is seen to be most heavily influenced by these two parameters (i.e. elastic modulus in the strong and weak principal material directions).

Geosynthetic in-plane Poisson's ratio and shear modulus are most likely related to the type and structure of the geosynthetic. Test methods and reported values for these parameters are not currently available. As such, the design method does not allow for the specific input of these two parameter values. Rather the method requires that one of two benefit reduction factors be specified for each material parameter. The two choices for benefit reduction factors correspond to good or poor values for these material parameters. Calibration of the design model from test section results using two geogrid and one geotextile product has resulted in recommended values for these products, which serve as a starting point when selecting values for other products.

The influence of base aggregate-geosynthetic shear interaction is accounted for empirically by calibration of the design method against results from published test sections, where this influence is also expressed in terms of a benefit reduction factor. Since the design method was calibrated from test section results using two types of geosynthetics, reduction factors for interface shear were developed for each type of material.

Design equations were developed for reinforcement benefit defined in terms of a *TBR*, *BCR* or a combination of the two. Furthermore, benefit defined in terms of *TBR* and/or *BCR* was broken into components associated with reinforcement effects on the subgrade, reinforcement effects on the base aggregate and combined effects on the total pavement system. Since distress models were developed for effects in the subgrade and effects in the base aggregate layer, calibration of the design model required that separate benefit values be determined. The

generally conservative nature of the design method suggests that benefit values for the total system be used.

The design model was calibrated and verified by comparison to test section results reported in Perkins (1999a), where these results were analyzed to derive experimental definitions of benefit for reinforcement effects in the base aggregate and subgrade layers. Further validation of the model was accomplished by comparison to other test section results available in the literature as summarized in Berg et al. (2000).

The design model is shown to provide generally conservative estimates of reinforcement benefit when compared to available test section results. The model is shown to be sensitive to design parameters of asphalt concrete and base aggregate thickness, subgrade strength, geosynthetic tensile modulus and tensile modulus ratio and other geosynthetic elastic material model properties. The model tends to show variations of benefit with these design parameters that are consistent with general application guidelines developed in Berg et al. (2000). Several examples are described to illustrate the use of the model and to illustrate the construction and life-cycle cost benefit that can result from the use of reinforcement.

This report provides a detained description of the finite element response model, the material models used in the FE model, calibration of the material models and how these models relate to commonly used pavement layer material models, and the steps followed to develop the design model. Limitations for use of the model are described in Sections 7.8 and Appendix B. Section 8 of the report provides a summary of the equations developed for the design model and provides suggestions for how the design model can be extended to situations not specifically addressed in the project. The design equations have been programmed into a spreadsheet program that is also described in Section 8 and can be downloaded from the following URL: http://www.mdt.state.mt.us/departments/researchmgmt/grfp/grfp.html. Appendix B of the report provides a summary of the design model as it relates to its use in practice. The material provided in Appendix B constitutes a design guideline based on the design model developed in this project. Examples are provided in Appendix B to illustrate the use of the design model and the cost-benefit for the examples given.

## 1.0 INTRODUCTION

This project has followed a completed project sponsored by the Montana Department of Transportation (MDT), which is described in Perkins (1999a). The preceding project was experimentally based and provided stress, strain and deformation response measures of geosynthetic reinforced flexible pavements. This completed project, and other research conducted over the past 20 years, has demonstrated the benefit that geosynthetics can provide when placed within or at the bottom of base aggregate layers in flexible pavement systems for the purpose of reinforcement. The primary benefits that have been demonstrated include an extension of service life of the pavement and/or a reduction in the structural section. These benefits have been defined primarily in terms of a Traffic Benefit Ratio (*TBR*), defining the increase in service life of the pavement, and a Base Course reduction Ratio (*BCR*), defining the reduction in base aggregate thickness permissible by the use of reinforcement.

Previous experimental work involving the construction and loading of reinforced pavement test sections has demonstrated that values of benefit are strongly dependent on pavement design parameters such as thickness of the structural section and strength and/or stiffness of the subgrade, and properties and type of geosynthetic used. A recently completed report by the Geosynthetic Materials Association, GMA (Berg et al., 2000) concluded that given the absence of a suitable method for analytically quantifying reinforcement benefit, benefit values for use in design should at present be based on purely empirical methods involving direct observation of benefit from test sections having pavement design conditions and a geosynthetic reinforcement similar to the design being considered. A NCHRP Synthesis currently in print (Christopher et al., 2001) provided a survey of geosynthetic base reinforcement usage amongst all U.S. State transportation agencies and found that the primary reasons for lack of usage were the absence of a suitable design method for defining reinforcement benefit and the corresponding inability to define cost-benefit for reinforced pavement systems.

This project was undertaken to provide an analytically based method for the determination of reinforcement benefit. The design model developed is described in terms of generic pavement design parameters and geosynthetic properties that are believed to be reflective of how these materials behave in this application. The design model is developed by first developing a numerical, finite element response model having structural components for the geosynthetic reinforcement. Empirical distress models are used to relate response measures from the FE

response model to long term pavement performance and serves as a means of describing reinforcement benefit between comparative reinforced and unreinforced pavements. The response and distress models, together referred to as the mechanistic-empirical model, are then used to predict reinforcement benefit for a broad range of pavement design conditions and geosynthetic properties. Results from this parametric study are then expressed in terms of regression equations relating benefit to these input parameters. The resulting design model is calibrated against results from tests sections described in Perkins (1999a) and further validated by comparison of design model predictions to other available results summarized in Berg et al. (2000).

A companion report has been prepared for this project (Perkins 2001a), which summarizes work performed to evaluate a more rigorous numerical model designed to predict the cyclic loading response of unreinforced and reinforced pavements.

## 2.0 LITERATURE REVIEW

The purpose of this literature review is to present material relating to the work described in this report. This includes observed performance of geosynthetic reinforced flexible pavements, existing design techniques for geosynthetic reinforced pavements, a recently proposed standard of practice for the design of flexible pavements with geosynthetic reinforcement, mechanistic-empirical modeling of flexible pavements, modeling of geosynthetic reinforced flexible pavements, and tension and interface testing practices for geosynthetics.

### 2.1 Geosynthetic Reinforced Flexible Pavement Performance

The concept of using geosynthetics to provide reinforcement in flexible pavement systems was introduced and developed in the late 1980's. Since this time, numerous experimentally based studies have been conducted to examine the performance of flexible pavement systems reinforced with geosynthetics. Many of these studies have been summarized by Perkins and Ismeik (1997a,b) and more recently by Berg et al. (2000). The latter is a report prepared by the Geosynthetics Materials Association (GMA) for the American Association of State Highway Transportation Officials (AASHTO) Subcommittee on Materials Technical Section 4E, which has the overall responsibility for the subject of geosynthetics within AASHTO. This subcommittee formed a Task Force on the subject of geosynthetic reinforcement of flexible

pavement systems and established interaction with industry represented by the GMA. Through a review of existing research, the report provided qualitative application guidelines and a recommended standard of practice. The former is summarized within this section and provides guidance for the selection of certain design approaches proposed later in this report as well as providing a means of comparison for the recommendations developed in this project. The standard of practice is summarized in Section 2.3 and is discussed in further detail in Section 9 in light of information developed in this project.

The use of geosynthetics for reinforcement when placed at the bottom or within the base course aggregate layer of a flexible pavement generally provides benefit by improving the service life and/or providing equivalent performance with a reduced structural section. The principal categories of pavement distress are rutting due to permanent deformation in the base and subgrade layers, asphalt concrete fatigue cracking, asphalt concrete low temperature cracking, rutting due to asphalt concrete high temperature flow, surface raveling, loss of skid resistance, contamination and/or saturation of base aggregate layers and frost heave. Base reinforcement is applicable for the support of vehicular traffic over the life of the pavement and is designed to address the pavement distress mode of permanent surface deformation or rutting and possibly asphalt fatigue cracking.

The principle mechanism responsible for reinforcement in paved roadways is one generally referred to as *base course lateral restraint* and is schematically illustrated in Figure 2.1.1. Vehicular loads applied to the roadway surface create a lateral spreading motion of the base course aggregate. Tensile lateral strains are created in the base below the applied load as the material moves down and out away from the load. The geosynthetic restrains the base thus reducing or restraining this lateral movement. The term *lateral restraint* involves several components of reinforcement including: (i) restraint of lateral movement of base aggregate; (ii) increase in modulus of base aggregate due to confinement; (iii) improved vertical stress distribution on the subgrade due to increased base modulus; and (iv) reduced shearing in the top of the subgrade. These mechanisms, most of which were experimentally verified in the study by Perkins (1999a), lead to a reduction in vertical strain in the base and subgrade layers.

The benefits of reinforcement on the design of flexible pavements are generally expressed in terms of an extension of life of the pavement or an allowable reduction in base course thickness. An extension of life of the pavement is typically expressed in terms of a Traffic

Benefit Ratio (*TBR*). *TBR* is defined as the ratio of the number of traffic loads between an otherwise identical reinforced and unreinforced pavement that can be applied to reach a particular pavement permanent surface deformation. *TBR* indicates the additional amount of traffic loads that can be applied to a pavement when a geosynthetic is added, with all other pavement materials and geometry being equal.

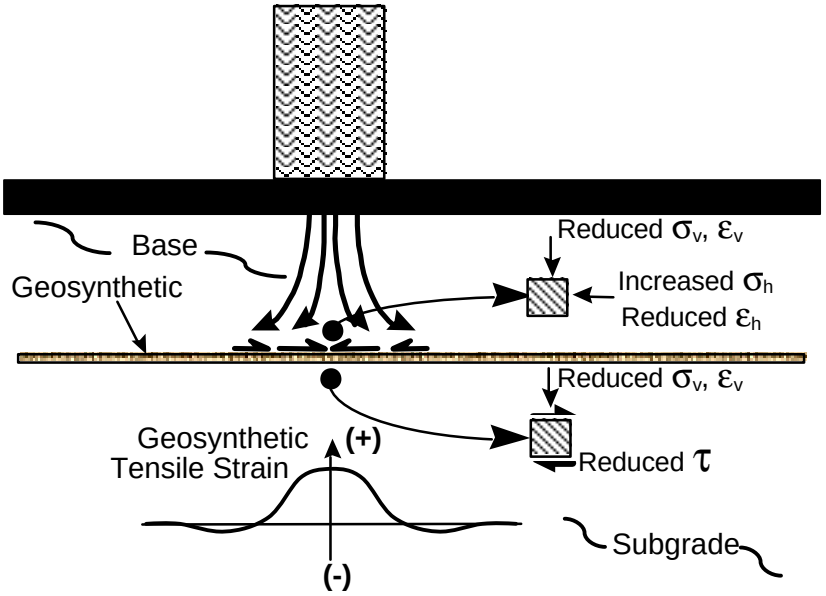


**Figure 2.1.1** Schematic illustration of base reinforcement mechanisms.

The benefit of reducing the base aggregate thickness is typically defined by a Base Course reduction Ratio (*BCR*). *BCR* defines the percentage reduction in the base course thickness of a reinforced pavement such that equivalent life is obtained between the reinforced and the unreinforced pavement with the greater aggregate thickness. Since *TBR* as defined above does not involve a reduced base course layer, the resulting *TBR* corresponds to a *BCR* of 0 and is denoted as $TBR_{BCR=0}$. Similarly, the *BCR* defined above is for equal life or for a *TBR* of 1 and is denoted by $BCR_{TBR=1}$. Combinations of *BCR* and *TBR* are possible if the base course thickness is not reduced by the full amount yielding equivalent life. A number of combinations of *TBR* between 1 and $TBR_{BCR=0}$ and *BCR* between 0 and $BCR_{TBR=1}$ are possible as schematically illustrated in Figure 2.1.2.

Based on the studies reviewed in Berg et al. (2000), values of $TBR_{BCR=0}$ up to 10 can generally be anticipated for roadways resting on a subgrade with a California bearing ratio (*CBR*)

≤ 8. Values of $BCR_{TBR=1}$ up to 50 % can be anticipated for subgrade *CBR* values lying between 3 and 8. For subgrade *CBR* less than 3, the margin of safety for reduction of base course thickness becomes smaller and designs using a *BCR* must be treated with caution. Existing information to date indicates that reinforcement benefit begins to diminish quickly for subgrade *CBR* values greater than 8. Tables 2.1.1 and 2.1.2 from Berg et al. (2000) provide a more detailed listing of the variables that are believed to influence reinforcement benefit for flexible pavements.

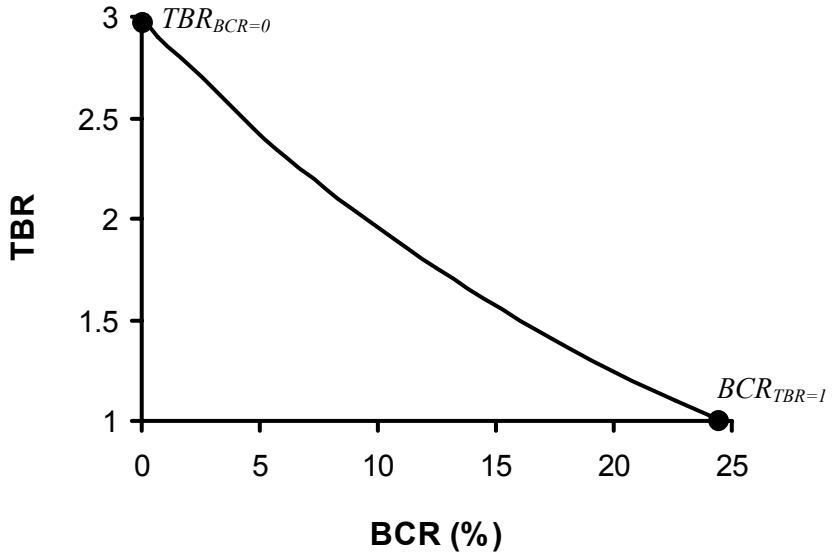


**Figure 2.1.2** Schematic illustration of combinations of *TBR* and *BCR*.

From Tables 2.1.1 and 2.1.2, several critical design variables that influence the effect of the reinforcement are noted. The strength and/or stiffness of the subgrade appears to be a critical design parameter as discussed above. Currently available studies generally show little reinforcement benefit for subgrade *CBR* in excess of 8. Recommendations in Berg et al. (2000) were expressed in terms of *CBR* because this is the pavement design variable for the subgrade most commonly reported in the studies reviewed. The thickness of the structural section appears to have a significant impact on reinforcement benefit. Very few studies are available that used a thickness for the asphalt concrete (AC) greater than 75 mm. Several studies have shown that as the thickness of the base course aggregate becomes greater than approximately 250 mm, reinforcement benefit begins to decrease. It should be noted, however, that several studies have demonstrated significant values of *TBR* for base aggregate thicknesses as great as 400 mm. In contrast to a reduction of reinforcement benefit for thick structural sections, several studies have

demonstrated that sections that are designed for a low number of traffic passes (i.e. under designed sections) are not appreciably influenced by base reinforcement.

**Table 2.1.1** Variables influencing reinforcement effect (after Berg et al., 2000).

| Pavement Component | Variable | Range from Test Studies/ Remarks | Condition where Reinforcement Appears to Provide Most Benefit |
|---|---|---|---|
| Geosynthetic | Structure | Rigid (extruded) and flexible (knitted and woven) geogrids, woven and nonwoven geotextiles, geogrid-geotextile composites | See Table 2.1.2 |
| | Modulus (@ 2% and/or 5% strain) | 100 kN/m to 750 kN/m | Higher modulus improves potential for performance |
| | Location | Geogrid | Moderate load ($\leq$ 80 kN axle load): Bottom of thin bases ($\leq$ 250 mm), middle for thick (>300 mm) bases<br>Heavy load (> 80kN axle load): Bottom for thin bases ($\leq$ 300 mm), middle for thick bases (>350mm) |
| | | Geotextile | Bottom of base, on the subgrade |
| | | Geogrid-geotextile composite | Bottom of open-graded base OGB |
| | Surface | Slick versus rough | Rough |
| | Geogrid Aperture | 15 mm to 64 mm | > $D_{50}$ of adjacent base/subbase |
| | Aperture Stiffness | Rigid to flexible | Rigid |
| Subgrade Condition | Soil Type | SP, SM, CL, CH, ML, MH, Pt | No relation noted |
| | Strength | *CBR* from 0.5 to 27 | *CBR* $\leq$ 8<br>($M_R \leq$ 80 MPa) |
| Subbase | Thickness | 0 to 300 mm | No subbase |
| | Particle Angularity | Rounded to angular | Angular |
| Base | Thickness | 40 mm to 640 mm | $\leq$ 250 mm for moderate loads |
| | Gradation | Well graded to poorly graded | Well graded |
| | Angularity | Angular to subrounded | Angular |
| Pavement | Type | Asphalt, concrete, unpaved | Asphalt and unpaved |
| | Thickness | 25 mm to 180 mm | 75 mm |
| | Resilient Modulus | Not typically measured | Unknown |
| Design | Pavement loading | 200 kPa to 1800 kPa | Does not perform on significantly under-designed pavements |
| Construction | Pre-rutting | None in lab to pre-rutted in field | Unknown |

**Table 2.1.2** Qualitative application guidelines for geosynthetic type (after Berg et al., 2000).

| Roadway Design Conditions | | Geosynthetic Type | | | | | |
|---|---|---|---|---|---|---|---|
| Subgrade | Base/Subbase Thickness [1] (mm) | Geotextile | | Geogrid [2] | | GG-GT Composite | |
| | | Nonwoven | Woven | Extruded | Knitted or Woven | Open-graded Base [3] | Well Graded Base |
| *CBR* < 3 ($M_R$ <30 MPa) | 150 – 300 | ❹ | ● | ● | ❑ | ● | ⑤ |
| | > 300 | ❹ | ❹ | ◗ | ◗ | ◗ | ⑤ |
| 3≤ *CBR*≤ 8 (30≤ $M_R$ ≤ 80) | 150 – 300 | ⑥ | ◗ | ● | ❑ | ● | ⑤ |
| | > 300 | ⑥ | ⑥ | ◗[7] | ❑ | ❑ | ⑤ |
| *CBR* > 8 ($M_R$ >80 MPa) | 150 – 300 | ❍ | ❍ | ◗ | ❑ | ❑ | ⑤ |
| | > 300 | ❍ | ❍ | ❍ | ❍ | ❍ | ⑤ |

Key: ● — usually applicable ◗ — applicable for some (various) conditions
❍ — usually not applicable ❑ — insufficient information at this time ⑤ — see note

Notes:
1. Total base or subbase thickness with geosynthetic reinforcement. Reinforcement may be placed at bottom of base or subbase, or within base for thicker (usually > 300 mm) thicknesses. Thicknesses less than 150 mm not recommended for construction over soft subgrade. Placement of less than 150 mm over a geosynthetic not recommended.
2. For open-graded base or thin bases over wet, fine-grained subgrades, a separation geotextile should be considered with geogrid reinforcement.
3. Potential assumes base placed directly on subgrade. A subbase also may provide filtration.

❹ Reinforcement usually applicable, but typically addressed as a subgrade stabilization application.
⑤ Geotextile component of composite likely is not required for filtration with a well graded base course; therefore, composite reinforcement usually not applicable.
⑥ Separation and filtration application; reinforcement usually not applicable.
7. Usually applicable when placed up in the base course aggregate. Usually not applicable when placed at the bottom of the base course aggregate.

The type of geosynthetic used and its corresponding mechanical properties have a significant influence on reinforcement benefit. In general, the tensile modulus of the geosynthetic is recognized as a critical design parameter with reinforcement benefit increasing with increasing modulus. Since dynamic strains induced in the geosynthetic are relatively small for this application, a secant modulus value for a low value of strain is believed to be the most descriptive design parameter. Secant modulus values are generally not reported, however, for values of axial strain less than 2 %. Furthermore, common roadway traffic speeds result in a

loading strain rate that can be as much as 100 times greater than that employed in wide-width tension tests, such as ASTM D 4595 (ASTM, 2001a).

Existing literature has not explicitly addressed the effect of the ratio of modulus in the machine and cross machine directions of the geosynthetic, but it is expected that both values are important. Since pavement loading is generally modeled as an axisymmetric loading condition and actual roadway traffic involves loading in both directions of the material, use of the highest modulus value would ignore the greater strains experienced in the orthogonal and less stiff direction of the geosynthetic and the negative impact this would have on pavement performance.

The type and structure of the geosynthetic appears to influence reinforcement benefit. For geogrids, limited data indicates that the stiffness of the aperture impacts reinforcement benefit with increased aperture rigidity corresponding to greater benefit. The integral junctions with rigid geogrids generally correspond to a greater potential for load transfer between the two principal directions of the material and may offer a stiffer response under confined biaxial loading. Limited existing literature tends to show that rigid, extruded geogrids offer greater benefit in comparison to flexible geogrids and geotextiles, and is indicated in Table 2.1.2 by the greater range of conditions for application of these types of geogrids. Clear distinctions between flexible geogrids and geotextiles are not possible based on information currently available.

Geosynthetic/base aggregate interface properties may also be partly responsible for differences in reinforcement benefit seen between geogrids and geotextiles. Geotextiles generally rely upon surface friction for interaction while geogrids provide interaction though direct bearing of aggregate against cross members of the mesh. Most previous studies have not reported information from direct shear or pull out tests making it difficult to quantify differences in interaction between different products. Complicating this, most direct shear and pull out tests are designed to provide gross frictional properties once ultimate shearing loads have been induced. Since this reinforcement application corresponds to a condition where shear displacements between the geosynthetic and the aggregate are relatively small, existing interface tests may not be capable of providing meaningful information for small shear displacements. Intuitively, however, it should be expected that small displacement interface shear properties have an effect on reinforcement benefit.

## 2.2 Design Solutions for Geosynthetic Reinforced Pavements

Design methods proposed for geosynthetic reinforcement of flexible pavements have been based on either empirical or analytical considerations, or analytical methods modified by experimental data. Several studies have been summarized by Perkins and Ismeik (1997b) with others summarized by Berg et al. (2000). Empirical methods have been typically developed for a specific geosynthetic product or products and for a particular set of design conditions. These methods are thereby limited by the conditions upon which they were developed. Of the few analytical solutions that have been proposed, none have been found to address the many variables that have been experimentally shown to impact resulting benefit.

**Table 2.2.1** Summary of empirical design methods for geosynthetic reinforced pavements (after Berg et al., 2000).

| Source | Geo-synthetic Type | Range of Subgrade *CBR* Strength (%) | Design Method and Basis | Geosynthetic Reinforcement Modification | Distress Mode | Design Format | Empirical Support | Range of Improvement |
|---|---|---|---|---|---|---|---|---|
| Mirafi (1982) | Specific Geotextile | 1-6 | Modified AASHTO 72 | Layer coefficient ratio equal to reinforced to unreinforced layer coefficients | Not stated | Equations and charts | | *BCR* = 7 - 18 % |
| Penner et al. (1985) | Specific Geogrid | 4.3-5.7 | Modified AASHTO 81 | Structural number modifier based on unreinforced base layer thickness | Rut depth (20 mm) | Equations and charts | Cyclic plate load tests (Haas et al. 1988) | *BCR* = 30 – 50 % |
| Webster (1993) | Specific Geogrid | 3-8 | FAA, 1978 | Direct extrapolation from test track results | Rut depth (25 mm) | Charts | Test tracks (Webster, 1993) | *BCR* = 5 – 45 % |
| Tensar (1996) | Specific Geogrids | 1.9 | Modified AASHTO 93 | Life extension and base course reduction from empirically determined *TBR* | Rut depth (20-30 mm) | Equations, charts and computer program | Test tracks (Collin et al., 1996) | *TBR* = 1.5 - 10 |
| Colbond (1998) | Specific Geo-composite | 1.5 - 4.5 | Design life extension per FEM analysis | Reduction of asphalt cracking | Asphalt concrete cracking | Charts | | *TBR* = 1.1 – 1.3 |
| Colbond (1998) | Specific Geo-composite | Not stated | German road design | Increase in bearing capacity of the unsurfaced road | Bearing capacity | Equations and charts | Plate load tests (Meyer and Elias, 1999) | *BCR* = 32 – 56 % |
| Zhao and Foxworthy (1999) | Specific Geogrid | ≤ 18 | Modified AASHTO 93 | Layer coefficient ratio, LCR, equal to reinforced to unreinforced layer coefficients | Rut depth | Equations and spread sheet | Cyclic plate load tests and test tracks | Not specifically stated |

Six methods falling within the category of empirical methods have been identified and are listed in Table 2.2.1. The earliest method was developed in 1982 and was developed for a specific geotextile product. The method relied upon the use of the 1972 AASHTO pavement design method and produced values of *BCR* between 7 and 18 %.

Penner et al. (1985) presented an empirical design approach stemming from the experimental work of Haas et al. (1988). The approach used the AASHTO 1981 Interim Guide as a basis for comparing results and developing base course equivalency charts. The structural number (*SN*) of each control section was calculated assuming layer coefficients of 0.4 for the asphalt layer and 0.14 for the granular base layer. The subgrade soil support value (*S*) was determined from the *CBR* strength and ranged from 4.3-5.7. The values for *SN* and *S* were then used in the AASHTO method to determine the total equivalent 80 kN single-axle load applications, which ranged from 60,000 to 10,000,000 applications. A load correction factor was calculated for each section by dividing the number of 80 kN single-axle load applications by the actual number of load applications necessary to cause failure, where failure was defined as a rut depth of 20 mm. This load correction factor was intended to account for differences in loading conditions between the experiments and actual field moving wheel loads. For the control sections, these ratios ranged from 3.5 to 10. The factor implies that had the laboratory section been subjected to actual field loads, a rut depth of 20 mm would have developed after a number of load applications equal to the number seen in the experiments multiplied by the load correction factor.

This load correction factor was then taken to apply to the reinforced sections within a particular test loop. The load correction factor for each reinforced section was then used to calculate the 80 kN single-wheel load applications by multiplying the actual number of load applications experienced in the laboratory tests by the corresponding correction factor. From the AASHTO method, a *SN* for that section was determined. A structural number for the reinforced granular base was then calculated by subtracting the asphalt layer component from the total *SN*. A reinforced layer coefficient was then calculated by dividing the *SN* for the reinforced base by its corresponding thickness. The ratio of the reinforced to unreinforced layer coefficients was calculated by using the layer coefficient for the unreinforced granular base given above. For equivalent base layer *SN*'s, the ratio of reinforced to unreinforced layer coefficients is equal to the ratio of unreinforced to reinforced base layer thickness. The ratio of reinforced to unreinforced layer coefficients was plotted against the reinforced base thickness and was shown to decrease as the reinforced base thickness approached 250 mm when the geogrid was placed at the bottom of the base. Additional improvement in the layer coefficient ratio was noted for a base thickness of 250 mm when the geogrid was placed in the middle of the base. Webster

(1993) produced a design chart similar to that of Haas et al. (1988) by direct comparison and extrapolation of test results for sections of equivalent base course thickness.

The method proposed by Tensar (1996) is based on the test section work performed by Collin et al. (1996). The method relies on the identification of *TBR* for the application. Charts are given defining *TBR* as a function of base course thickness for three levels of rut depth (20, 25 and 30 mm). The values of *TBR* listed in these charts were generated from the test section work of Collin et al. (1996) and pertain to a subgrade with an average *CBR* of 1.9. With the definition of *TBR*, a life-cycle analysis could be performed by extending the life of the roadway or the AASTHO '93 guide could be used to calculate a *BCR* value. Test sections were not conducted to verify *BCR* values determined through this method.

Colbond (1998) developed a method that fits within the framework of the German practice for roadway design. This practice relies upon achieving a particular bearing capacity of the base-subgrade system prior to proceeding with the placement of surfacing material. Plate load tests are typically conducted to evaluate the modulus of the system. Tests reported by Meyer and Elias (1999) serve as empirical support for the method.

Zhao and Foxworthy (1999) also used the AASHTO design method to determine a layer coefficient ratio for the granular base, which equaled the ratio of the reinforced to unreinforced layer coefficients. Values of this ratio were determined from experiments using one geogrid and subgrades with different *CBR* strengths and ranged from 2 to 1.5, with values greater than 1.5 being obtained for *CBR* strengths less than 3. This ratio was used as a multiplication factor on the depth of the reinforced base inside the equation for structural number, implying that for an equivalent structural number, the unreinforced base could be reduced by 33 to 50 %.

Three methods falling within the category of methods based on analytical considerations have been identified. Davies and Bridle (1990) developed an analytical technique to determine the development of permanent deformation (rut depth) with load cycle of reinforced pavements. The displacement response of the pavement under a single monotonic load application was predicted using an energy method. An expression for the potential energy of the pavement system was developed as a function of the central displacement of the applied load. The general shape of the surface displacement profile was assumed to match that seen in previously published studies. The geosynthetic layer provided an additional energy component to the system as it deformed and was shown to increase the component of strain energy provided by the

base layer of the pavement. Both the base layer and the geosynthetic were assumed to provide a component of strain energy as they functioned as a structural member in bending, even though both materials have little flexural rigidity.

The development of permanent deformation with increasing load cycle was predicted by varying the stiffness parameters of the subgrade. Permanent deformation was assumed to be negligible in the base layer. The stiffness parameters of the subgrade during loading were assumed to be less than those during unloading. Each set of stiffness parameters were assumed to vary with increasing load cycle, with the difference between the two sets becoming less at an ever decreasing rate. The net effect of this type of material model was a prediction of rut depth that increased with load cycle at a decreasing rate. The values and variation of these parameters were determined primarily from the results of repeated load experiments on reinforced pavement test sections. In this way, the material parameters were empirically derived from the tests for which the parameters are being used to predict. Use of this technique will require that these parameters be related to material properties, such as resilient modulus, that can be more readily determined from element tests.

Sellmeijer (1990) formulated a model for the behavior of a soil-geotextile-aggregate system that accounted for both the membrane action and lateral restraint function of the geotextile. While an AC layer was not specifically included in the model, the model was said to be suitable for paved roads owing to its ability to analyze situations where only small rut depths were permissible. The model used an elastic-plastic model for the aggregate. The subgrade was taken as a rigid-perfectly plastic material. Interaction between the soil and geotextile was accounted for using a simple law of friction. The function of lateral restraint was shown to increase the mean stress and stiffness in the aggregate layer. The model was not compared to experimental results.

Colbond (1998) has presented a method based in part on the work of Liu et al. (1998). The method involves the examination of crack initiation and propagation in the asphalt concrete for reinforced base layers through a finite element study. The number of load cycles necessary to create asphalt fatigue was examined, with life increasing by 10 to 30 % with the addition of reinforcement (i.e. *TBR* = 1.1 to 1.3). This work was not compared to results from experimental test sections.

## 2.3 Summary of an Existing Recommended Standard of Practice

The document developed by the GMA for the AASHTO Subcommittee on Materials Technical Section 4E (Berg et al., 2000) contained a recommended standard of practice (SOP) based on the research and case histories reviewed for the report. This SOP has now been adopted by the AASHTO Subcommittee and is contained in the AASHTO Designation PP 46-01 (AASHTO 2001). The purpose of this section is to summarize the recommended standard of practice given by Berg et al. (2000) for the purpose of identifying how research described in this report can be used within the SOP.

The recommended SOP given in Berg et al. (2000) relies upon the assessment of reinforcement benefit as defined by a Traffic Benefit Ratio (*TBR*), a Base Course reduction Ratio (*BCR*) or a combination of the two. Reinforcement benefit defined in terms of *TBR* and *BCR* is then used to modify an existing unreinforced pavement design.

The steps involved in the recommended SOP consist of:

Step 1. Initial assessment of applicability of the technology.

Step 2. Design of the unreinforced pavement.

Step 3. Definition of the qualitative benefits of reinforcement for the project.

Step 4. Definition of the quantitative benefits of reinforcement (*TBR* and/or *BCR*).

Step 5. Design of the reinforced pavement using the benefits defined in Step 4.

Step 6. Analysis of life-cycle costs.

Step 7. Development of a project specification.

Step 8. Development of construction drawings and bid documents.

Step 9. Construction of the roadway.

Step 1 involves assessing the project related variables described in Tables 2.1.1 and 2.1.2 and making a judgment on whether the project conditions are favorable or unfavorable for reinforcement to be effective and what types of reinforcement products (as defined in Table 2.1.2) are appropriate for the project. Step 2 involves the design of a conventional unreinforced typical pavement design cross-section or a series of cross sections, if appropriate, for the project. Any acceptable design procedure can be used for this step. Step 3 involves an assessment of the qualitative benefits that will be derived by the addition of the reinforcement. The two main benefits that should be assessed are whether the geosynthetic will be used for an extension of the life of the pavement (i.e. the application of additional vehicle passes), a reduction of the base

aggregate thickness or a combination of the two. Berg et al. (2000) has listed additional secondary benefits that should also be considered.

Step 4 requires the definition of the value, or values, of benefit (*TBR* and/or *BCR*) that will be used in the design of the reinforced pavement. In the absence of a suitable solution for the definition of these values, Berg et al. (2000) suggested that these values be determined through empirical means by a careful comparison of project design conditions, as defined in previous steps, to conditions present in studies reported in the literature. In the absence of suitable comparison studies, an experimental demonstration method involving the construction of reinforced and unreinforced pavement test sections has been suggested and described in Berg et al. (2000) and may be used for the definition of benefit for the project conditions. The research described in this report is designed to provide for a quantitative solution for values of benefit defined in terms of *TBR* and/or *BCR*.

Step 5 involves the direct application of *TBR* or *BCR* to modify the unreinforced pavement design defined in Step 2. *TBR* can be directly used to define an increased number of vehicle passes that can be applied to the pavement while *BCR* can be used to define a reduced base aggregate thickness such that equal life results. If combinations of *TBR* and *BCR* are provided, each can be used according to the usage described above for a combined effect.

With the unreinforced and reinforced pavement designs defined, a life-cycle cost analysis should be performed to assess the economic benefit of reinforcement. This step will dictate whether it is economically beneficial to use the geosynthetic reinforcement. Remaining steps involve the development of project specifications, construction drawings, bid documents and plans for construction monitoring. Berg et al. (2000) has presented a draft specification that may be adopted for this application.

The research described in this report provides a quantitative and general means of identifying values of benefit defined in terms of *TBR* and/or *BCR* needed for Step 4 of the recommended SOP. The design model developed for the definition of *TBR* and/or *BCR* values is general in the sense that it can be used to assess benefit values for a wide range of pavement design conditions and reinforcement products.

## 2.4 Mechanistic-Empirical Modeling of Flexible Pavements

Mechanistic-empirical modeling of flexible pavements relies upon the use of a numerical model to describe the response of the pavement system to an externally applied load representative of the traffic to which the roadway will be subjected. The response extracted from the model is typically a measure of stress, strain or deflection for one or several critical points within the pavement system. Several types of numerical or response models are available for pavement analysis and design. Multi-layered elastic (MLE) programs, such as DAMA (Asphalt Institute, 1991), ELSYM5 (Kopperman et al., 1986) and KENLAYER (Huang, 1993) rely upon the solution of differential equations for layered elastic systems. Finite element (FE) models, such as ILLI-PAVE (1990) and MICH-PAVE (Harichandran et al., 1989) typically consist of two-dimensional axi-symmetric models.

Response models typically use elastic material models for the asphalt concrete (AC), base aggregate and subgrade layers. These material models may be linear or non-linear and may be isotropic or anisotropic. Models using nonlinear elastic material models generally express the elastic modulus, or resilient modulus, as a function of stress state, whereas linear elastic models treat the elastic modulus of the materials as a constant for all stress states. A common non-linear elastic model for relating the resilient modulus of aggregates to stress state is given by Equation 2.4.1 (Seed et al., 1967), where $M_R$ is resilient modulus, $q$ is the bulk stress defined as the sum of the three principal stresses and $k_1$ and $k_2$ are material constants. Chen et al. (1995) has provided a summary of response models commonly used for pavement modeling. (Refer to Appendix A for a listing of all notation used in this report).

$$M_R = k_1 q^{k_2} \tag{2.4.1}$$

The response measures extracted from response models are typically related to long-term pavement performance through empirically derived damage models. The two most common types of damage models are those that relate the tensile strain in the bottom of the asphalt to asphalt fatigue life and ones that use the vertical compressive strain in the top of the subgrade to control permanent deformation of the pavement structure. The later was introduced by Dorman and Metcalf (1965) and was later expressed in the form of Equation 2.4.2, where $N$ is the number

of load cycles necessary to reach a certain permanent deformation of the pavement surface, $e_v$ is the vertical strain in the top of the subgrade and $A$ and $B$ are constants.

$$N = Ae_v^{-B} \tag{2.4.2}$$

## 2.5 Modeling of Geosynthetic Reinforced Pavements

A number of studies have been conducted to examine the utility of finite element programs to predict the response of roadways reinforced with geosynthetics. Several of these studies have been performed in conjunction with experimental studies such that comparisons between model predictions and experimental results could be made. For the studies discussed below, Table 2.3.1 has been created to summarize the major features associated with each study's model.

Barksdale et al. (1989) adapted an existing finite element model to predict the response seen in the experimental portion of their study. The prediction of tensile strain in the base material was essential in determining the level of tensile strain developed in the geosynthetic, which in turn determined, in part, the benefit provided by the reinforcement. The cross-anisotropic linear elastic model used for the base was the only model capable of simultaneously predicting the lateral tensile strains in the bottom of the base and the small vertical strains in the bottom and upper part of that layer, as observed in the laboratory experiments.

The finite element model was calibrated and verified by using data from an unreinforced pavement section from a previous study and from the test data generated from one of the experimental test series of their study. The unreinforced pavement section used for calibration was strong in comparison to the sections described for their study. The finite element model was capable of predicting measured variables to within +/- 20 % for the strong unreinforced section. For the weaker sections used in the study described as part of their work, the finite element predictions were not as good. The strain in the geosynthetic was over predicted by about 33 % when the geosynthetic was located in the bottom of the base. It was under predicted by about 14 % when located in the middle of the layer. The vertical stress and vertical strain on the top of the subgrade was under predicted by about 50 %. The lateral strains were also under predicted by about 50 %.

**Table 2.5.1** Summary of Finite Element Studies of Geosynthetic Reinforced Pavements.

| | Author | | | | | | |
|---|---|---|---|---|---|---|---|
| | Barksdale et al. (1989) | Burd & Houlsby (1986) | Burd & Brocklehurst (1990) | Burd & Brocklehurst (1992) | Dondi (1994) | Miura et al. (1990) | Wathugala et al. (1996) |
| Analysis Type | Axi-symmetric | Plane strain | Plane strain | Plane strain | Three-dimensional | Axi-symmetric | Axi-symmetric |
| AC Constitutive Model | Isotropic, non-linear elastic | None | None | None | Isotropic, linear elastic | Isotropic, linear elastic | Isotropic elastoplastic, D-P |
| AC Thickness (mm) | Variable | None | None | None | 120 | 50 | 89 |
| Base Constitutive Model | Anisotropic, linear elastic | Isotropic, elastoplastic, Matusoka | Isotropic, elastoplastic, Matusoka | Isotropic, elastoplastic, Matusoka | Isotropic, elastoplastic, D-P | Isotropic, linear elastic | Isotropic, elastoplastic, D-P |
| Base Thickness (mm) | Variable | 75 | 300 | 300 | 300 | 150 | 140 |
| Geosynthetic Constitutive Model | Isotropic, linear elastic | Isotropic, linear elastic | Isotropic, linear elastic | Isotropic, linear elastic | Isotropic, linear elastic | Isotropic, linear elastic | Isotropic, elastoplastic, von Mises |
| Geosynthetic Element Type | Membrane | Membrane | Membrane | Membrane | Membrane | Truss | Solid continuum |
| Geosynthetic Thickness (mm) | None | None | None | None | None | None | 2 |
| Interface Elements & Model | Linear elastic-perfectly plastic | None | None | Elastoplastic, Mohr-Coulomb | Elastoplastic, Mohr-Coulomb | Linear elastic joint element | None |
| Subbase Constitutive Model | None | None | None | None | None | Isotropic, linear elastic | Isotropic, elastoplastic,HiSS $\delta_o$ |
| Subbase Thickness (mm) | None | None | None | None | None | 200 | 165 |
| Subgrade Constitutive Model | Isotropic, non-linear elastic | Isotropic, elastoplastic, von Mises | Isotropic, elastoplastic, von Mises | Isotropic, elastoplastic, von Mises | Isotropic, elastoplastic, Cam-Clay | Isotropic, linear elastic | Isotropic, elastoplastic, HiSS $\delta_o$ |
| Load Application | Monotonic | Monotonic, footing width = 75 mm | Monotonic, footing width = 500 mm | Monotonic, footing width = 500 mm | Monotonic, two rectangular areas, 240 mm x 180 mm | Monotonic, 200 mm diameter plate | Single cycle, peak pressure = 725 kPa on a 180 mm diameter plate |
| Remarks on Observed Improvement | Base layer could be reduced in thickness by 4-18 %. Greater improvement seen for sections with weak subgrade | Improvement seen after a penetration of 4 mm. Model over predicted improvement beyond a 4 mm displacement | Improvement seen after a penetration of 12 mm. Improvement increased with increasing geosynthetic stiffness. | Improvement seen after a penetration of 25 mm. | 15-20 % reduction in vertical displacement, fatigue life of section increased by a factor of 2-2.5 | 5 % reduction in vertical displacement. Improvement level did not match experimental results. | 20 % Reduction in Permanent Displacement |

D-P: Drucker-Prager

A parametric study was conducted with the finite element model to calculate the lateral tensile strain at the bottom of the AC layer and the vertical strain at the top of the subgrade for a single load application. This was used for evaluations of fatigue resistance and to indicate the degree of rutting that would occur, which in turn was used to evaluate the improvement in pavement performance when reinforcement was added. Reinforcement improvement was quantified as the reduction in aggregate base thickness for a reinforced roadway giving the same tensile strain (fatigue) and vertical strain (reflecting permanent deformation) as that for the unreinforced section. Improvement was seen to increase with increasing geosynthetic stiffness, and to decrease with increasing subgrade stiffness and asphalt thickness. Optimal improvement was seen when the geosynthetic was placed between the bottom of the base and 1/3 up into the base layer.

Barksdale et al. (1989) used the 1972 AASHTO design method to determine design thickness for the sections with subgrade *CBR* strengths ranging from 3 to 10 and for two different traffic loading conditions. Using the more stiff geosynthetic, reductions in base course thickness ranged between 4 to 16 % when improvement was based on equal lateral strain in the bottom of the AC layer and 6 to 18 % when improvement was based on equal vertical strain at the top of the subgrade. In general, more improvement was observed for sections with a weak subgrade and a thinner AC layer. The magnitude of benefit defined in this study is less than those for a preponderance of experimental studies as summarized by Berg et al. (2000). Barksdale et al. (1989) felt that the mechanisms modeled were more suited for geotextiles and that additional research was needed to define the mechanisms of improvement associated with geogrids and to develop suitable models.

Burd and Houlsby (1986) developed a large strain finite element model for the purpose of examining the experimental results of reinforced unpaved roads, but could be extended to include material elements representing an asphalt layer. The large strain formulation was included to account for the extensive rutting that can take place in unpaved roads. Interface elements were not included in the formulation, which implies perfect fixidity between the soil layers and the geosynthetic. The model was used to predict the response of a footing resting on a base layer with a geosynthetic layer placed between the base and the underlying subgrade. The model predictions were compared to experimental results and shown to match reasonably well. The experimental results showed a slight improvement in the load-displacement curve for the

reinforced footing for footing penetrations less than 4 mm, while the model did not show improvements of this kind until the footing penetration exceeded 4 mm. Beyond a penetration of 4 mm, the improvement exhibited by the reinforced footing became significant for both the model and the experimental results, with the model over predicting the experimental results at larger displacements and with this over prediction becoming more significant as the footing displacement increased.

Burd and Brocklehurst (1990) applied this same model to a larger footing. Similar to the results of Burd and Houlsby (1986) the model did not show improvements in the load-displacement curve until a settlement of 12 mm was reached. The model was used in a parametric study to demonstrate the importance of the geosynthetic stiffness on improvement levels.

Burd and Brocklehurst (1992) extended this model to include interface elements. The model was used to predict the response of a footing placed on a base material over top of a subgrade with reinforcement between the base and subgrade. The finite element analyses predicted negligible improvement in the load versus displacement response until a displacement of over 25 mm was reached. In general, the model with interface elements tended to show less improvement than the earlier version without these elements. In light of the results of Burd and Houlsby (1986), where model results were compared to experimental results, it appears that interface elements were needed only when large footing displacements were present.

Dondi (1994) used the commercial code ABAQUS to model a geosynthetic reinforced pavement. Load was applied to the pavement surface by two rectangular areas measuring 240 mm by 180 mm and representing a single pair of dual wheels. A distance of 120 mm separated the wheels. Each rectangular area experienced a peak loading pressure of 1500 kPa. Due to the loading geometry, a three-dimensional finite element analysis was performed. A cohesion of 60 kPa was assigned to the base course soil to avoid numerical instabilities. Different friction coefficients were used between the geosynthetic and the base and subgrade soils. Sections were analyzed with and without the geosynthetic layer and for two geosynthetics of differing elastic modulus.

The evaluation of stress and strain measures for elements in the base and in the subgrade indicated that the base layer experienced moderate increases in load carrying capacity for the reinforced cases while the strain in the subgrade was seen to decrease substantially for the

reinforced cases. The model indicated that the geosynthetic layer reduced the shear stresses and strains experienced by the subgrade. Vertical displacement of the loaded area was reduced by 15 to 20 % by the inclusion of the geosynthetic. The displacement of the unreinforced section was not indicated. An empirical power expression involving tensile strain in the AC layer was used to evaluate the fatigue life of the sections, showing that the life of the reinforced sections could be increased by a factor of 2 to 2.5 as compared to the unreinforced section.

Miura et al. (1990) performed a finite element analysis of a reinforced paved road in support of a laboratory and field experimental program. The section layer thicknesses were chosen to match the laboratory test sections. The results from the analysis of reinforced and unreinforced sections showed general agreement with results from the laboratory test sections where surface displacement and strain in the geosynthetic were plotted against distance from the centerline of the load. The improvement in the surface displacement for the reinforced section as compared to the unreinforced section was greatly underestimated by the finite element model as compared to the experimental results. The finite element model showed a reduction in displacement of 5 % while the experiment showed a 35 % reduction. The monotonic loading results from the finite element analysis were compared to the experimental results at 10,000 cycles of applied load. In this light, the finite element model was not intended to be an exact representation of the experiments but were intended more to shed light on the mechanisms involved in reinforcement.

Wathugala et al. (1996) used the commercial program ABAQUS to formulate a finite element model of a geogrid reinforced pavement. The base aggregate and subgrade soils were modeled using the hierarchical constitutive model developed by Desai et al. (1986) and Wathugala and Desai (1993). This model can account for non-linear behavior during non-virgin loading, which is particularly appropriate for cyclic loading applications. This feature was not used, however, with non-virgin loading modeled by a linear elastic response. No special interface models were used between the geogrid and the surrounding soil. The geosynthetic was given a thickness of 2.5 mm. The pavement section was analyzed with and without the geogrid layer. The addition of the geogrid was shown to reduce the permanent rut depth by approximately 20 % for a single cycle of load. This level of improvement was most likely due the flexural rigidity of the geosynthetic, which is an artificial feature arising from the material and element model used for the geosynthetic.

## 2.6 Tension and Interface Testing of Geosynthetics

Tensile properties of geosynthetics are most commonly determined through the use of wide-width tension tests, ASTM D 4595 (ASTM, 2001a). This test standard is currently developed for geotextiles while a draft standard exists for geogrids. Properties reported from these tests typically consist of ultimate strength and strength at 2 %, 5 % and perhaps at higher values of axial strain. Strength at various levels of axial strain can be used to determine a secant tensile modulus for that level of axial strain according to Equation 2.6.1, where $G_{SM}$ is the geosynthetic secant tensile modulus, $T_{ea}$ is the tensile strength at a certain level of axial strain and $e_a$ is the value of axial strain for which the modulus is determined and is in decimal form. It is not common for values of strength at axial strain levels less than 2 % to be reported. Since strength values for geosynthetics are often times different in the two principal directions of the material, it is common to perform tests in each of the two material directions (machine and cross-machine directions) and report values for each.

$$G_{sm} = \frac{T_{e_a}}{e_a} \tag{2.6.1}$$

Interface testing of geosynthetics and soil (or base aggregate) is commonly performed by conducting direct shear tests, ASTM D 5321 (ASTM, 2001a), and pull out tests, GRI GT6 or GG5 (GRI, 2001). Coefficients of interaction are typically computed for ultimate values of shearing resistance generally corresponding to large levels of displacement. Test protocols have not been developed for the accurate determination of small displacement shear resistance, as may be a more appropriate measure of interaction for base reinforcement applications.

# 3.0 PRIOR TEST SECTION WORK

Previous work supported by the Montana Department of Transportation focused on the construction and evaluation of geosynthetic reinforced pavement test sections constructed in a facility located at Montana State University (MSU). Test sections were constructed for the purpose of providing data to evaluate the mechanisms by which geosynthetics serve to reinforce flexible pavements and to provide data to which the models, developed as part of this work, could be compared. Perkins (1999a,b) provides detailed information describing the pavement test facility, the construction process, instrumentation used and results obtained. Other papers related

to this test section work are given in Perkins et al. (1998a,b, 1999). The purpose of Section 3 is to briefly describe the pavement test facility, the materials used, and to summarize the results from this previous study that are used for comparison to the finite element model and design model developed in this project.

## 3.1 Test Sections Constructed

The test sections used for the development of the design model described in this report are given in Table 3.1.1. Of these test sections, 5 are control sections with no reinforcement and 7 are test sections with either a geogrid or geotextile reinforcement. The geosynthetic products used are described in Section 3.1.2. Two types of subgrade were used for the test sections listed in Table 3.1.1. A clay subgrade represents a weak subgrade with a *CBR* of 1.5. The silty sand subgrade is a more competent material with a *CBR* of approximately 15. Additional details for these and the other pavement layer materials are given below.

**Table 3.1.1** Comparison test section variables.

| Section [a] | Nominal Base Thickness (mm) | Subgrade Type | Geosynthetic | Position |
|---|---|---|---|---|
| CS2 | 300 | Clay | Unreinforced | Unreinforced |
| CS5 | 300 | Clay | Geogrid B | Base/subgrade interface |
| CS6 | 300 | Clay | Geotextile | Base/subgrade interface |
| CS7 | 300 | Clay | Geogrid A | 100 mm above base/subgrade interface |
| CS8 | 300 | Clay | Unreinforced | Unreinforced |
| CS9 | 375 | Clay | Unreinforced | Unreinforced |
| CS10 | 375 | Clay | Geogrid A | Base/subgrade interface |
| CS11 | 300 | Clay | Geogrid A | Base/subgrade interface |
| SSS1 | 200 | Silty-sand | Unreinforced | Unreinforced |
| SSS2 | 200 | Silty-sand | Geogrid A | 40 mm above base/subgrade interface |
| SSS3 | 200 | Silty-sand | Geotextile | 40 mm above base/subgrade interface |
| SSS4 | 200 | Silty-sand | Unreinforced | Unreinforced |

[a] Nominal AC thickness = 75 mm for all sections.

### *3.1.1 Test Box and Loading Apparatus*

A test box was constructed having inside dimensions of 2 m in width and length and 1.5 m in height and was constructed of reinforced concrete. Figure 3.1.1 shows a schematic of the

pavement test facility. A load frame was constructed to rest and ride on I-beams set into the concrete walls. A load actuator, consisting of a pneumatic cylinder with a 305 mm diameter bore and a stroke of 75 mm, is used to apply a cyclic load to the pavement. A 50 mm diameter steel rod 300 mm in length extends from the piston of the actuator. The rod is rounded at its tip and fits into a cup welded on top of the load plate that rests on the pavement surface.

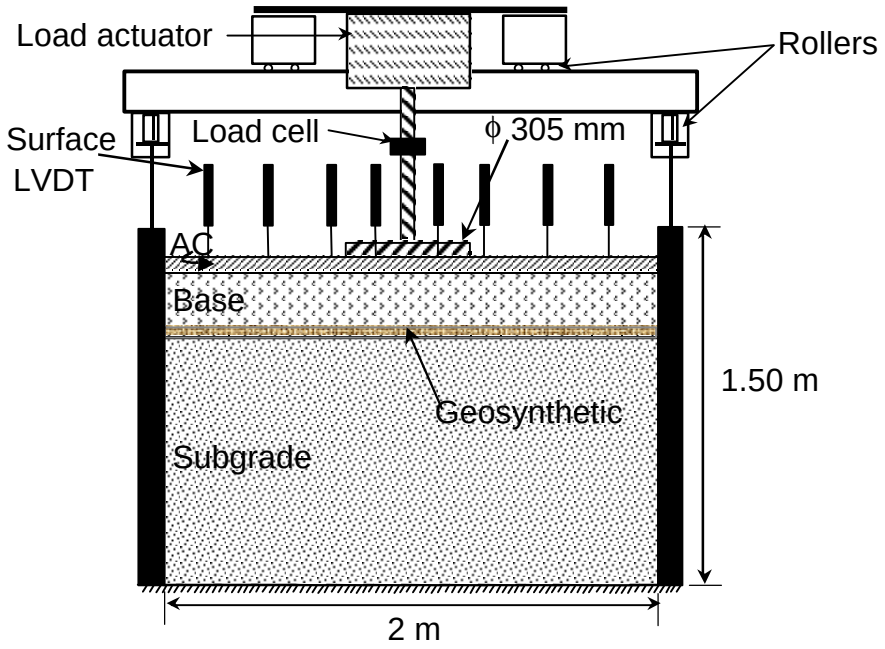


**Figure 3.1.1** Schematic diagram of the pavement test facility.

The load plate consists of a 305 mm diameter steel plate with a thickness of 25 mm. A 4 mm thick, waffled butyl-rubber pad was placed beneath the load plate in order to provide a uniform pressure and avoid stress concentrations along the plate's perimeter.

A binary solenoid regulator attached to a computer controlled the load-time history applied to the plate. The software controlling the load pulse was set up to provide the load or plate pressure pulse shown in Figure 3.1.2. This pulse has a linear load increase from zero to 40 kN over a 0.3 second rise time, followed by a 0.2 second period where the load is held constant, followed by a load decrease to zero over a 0.3 second period and finally followed by a 0.7 second period of zero load before the load cycle is repeated, resulting in a load pulse frequency of 0.67 Hz.

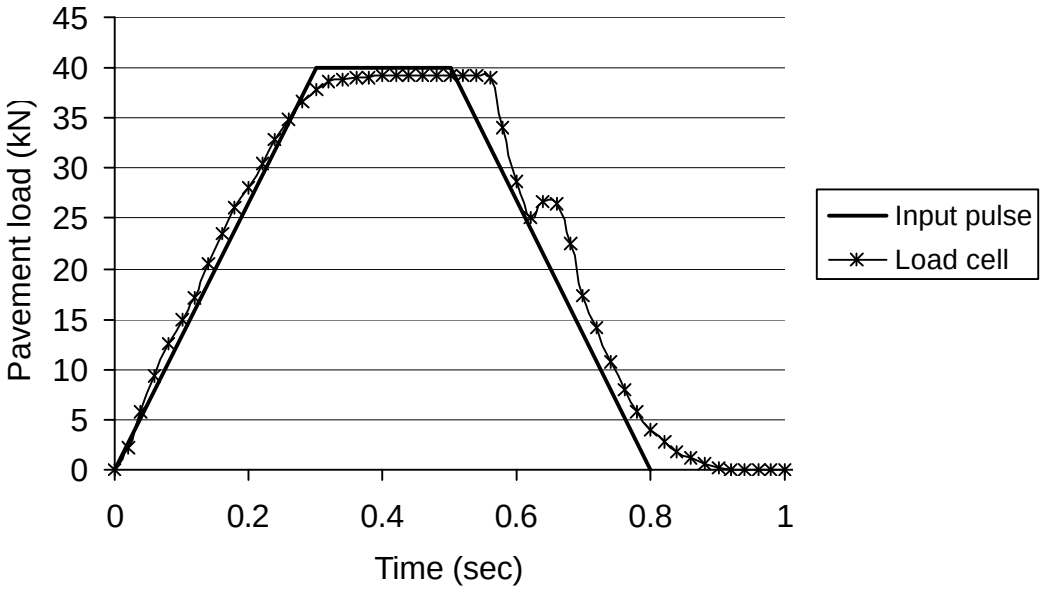


**Figure 3.1.2** Input load pulse and corresponding load cell measurement.

The prescribed maximum applied load of 40 kN resulted in a pavement pressure of 550 kPa. This load represents one-half of an 80 kN axle load from an equivalent single axle load (ESAL) and hence represents one ESAL. The load frequency was selected to allow the data acquisition system time to store data before the next load pulse was applied. The average peak plate pressure and standard deviation over the course of pavement loading is given in Section 3.1.4 for each test section reported. The pavement load typically did not return to zero following the application of each load cycle. The average minimum load over the course of pavement loading is also given in Section 3.1.4 for each test section. Also shown in Figure 3.1.2 is the corresponding output from the load cell for a typical load application. The hump seen on the descending branch of the curve is due to back venting of air pressure into the solenoid and was characteristic of all load pulses.

### *3.1.2 Pavement Layer Materials*

Hot-mix asphalt concrete was used for the test sections listed in Table 3.1.1. The aggregate gradation meets the Montana Department of Transportation specifications for a Grade A mix design. Asphalt cement used was PG-58/28 and asphalt content was approximately six percent. A grain size distribution for both the hot-mix aggregate is shown in Figure 3.1.3. As-constructed

properties of the AC for each test section are given in Section 3.1.4. Results from indirect tension resilient modulus tests are presented in Section 4.1.

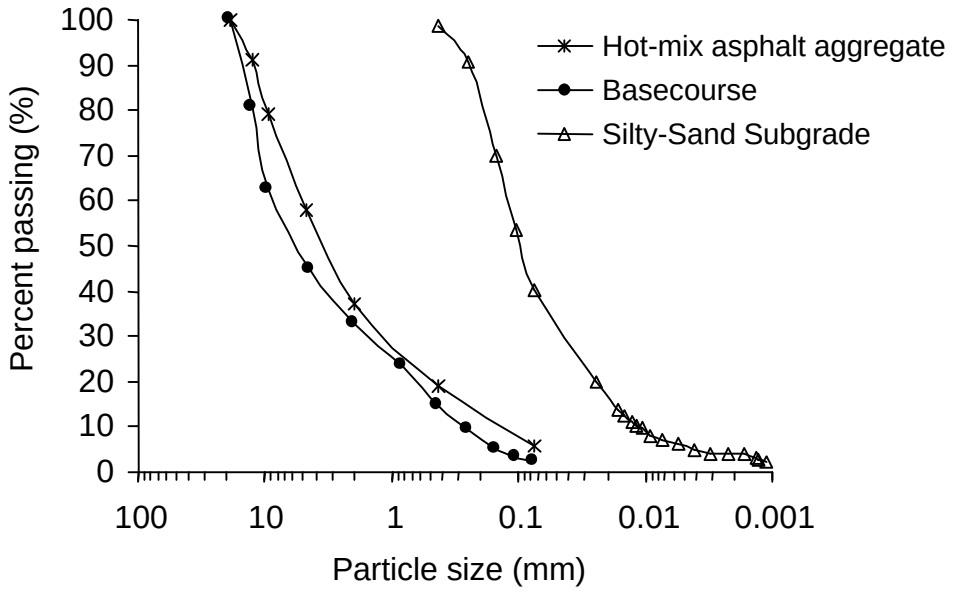


**Figure 3.1.3** Grain size distribution of AC and base aggregate and silty sand subgrade.

The geosynthetics used for the test sections shown in Table 3.1.1 are listed with their properties as reported by the manufacturers in Table 3.1.2.

A crushed-stone base course was used for all experimental test sections. The base course grain size distribution is shown in Figure 3.1.3, where it is seen that 100 % passes the 19 mm sieve. The material is classified as an A-1-a or a GW. Specific gravity of the material is 2.63. Modified Proctor tests resulted in a maximum dry unit weight of 21.5 kN/m$^3$ at an optimum moisture content of 7.2 %. This material was typically compacted at a moisture content of 6.3 % and to a dry unit weight of 21 kN/m$^3$. As-constructed properties of the base course for each test section are given in Section 3.1.4. A series of triaxial tests were performed on this material and are presented in Section 4.2 when the constitutive model for this material is described and calibrated. The triaxial tests yielded a drained friction angle of approximately 48 degrees.

To provide information on the influence of subgrade strength on reinforcement benefits, two subgrade materials were used in this study. A highly plastic clay subgrade was used to represent a soft subgrade while a silty-sand was used to represent a hard subgrade. The soft subgrade consisted of a CH or A7-(6) clay, having a liquid limit of 100 % and a plastic limit of

40 %. One hundred percent of the clay material passes the #200 sieve. Specific gravity of the clay is 2.70. Modified Proctor compaction tests resulted in a maximum dry density of 16.0 kN/m$^3$ occurring at an optimum moisture content of 20.0 %. The clay was compacted at a moisture content of approximately 45 % in order to obtain a *CBR* of 1.5.

**Table 3.1.2** Geosynthetic material properties.

| | Geogrid A: Tensar BX-1100 | Geogrid B: Tensar BX-1200 | Geotextile: Amoco 2006 |
|---|---|---|---|
| Material | Polypropylene | Polypropylene | Polypropylene |
| Structure | Punched Drawn, Biaxial | Punched Drawn, Biaxial | Woven |
| Mass/Unit Area (g/m$^2$) | 215[1] | 309[1] | 250[3] |
| Aperature Size (mm) | | | |
| Machine Direction | 25[1] | 25[1] | None |
| Cross-Machine Direction | 33[1] | 33[1] | |
| Wide-Width Tensile Strength at 2 % Strain (kN/m) | | | |
| Machine Direction | 5.06[2] | 7.32[2] | 4.25[4] |
| Cross-Machine Direction | 8.5[2] | 11.9[2] | 13.6[4] |
| Wide-Width Tensile Strength at 5 % Strain (kN/m) | | | |
| Machine Direction | 9.71[2] | 13.4[2] | 11.9[4] |
| Cross-Machine Direction | 16.5[1] | 22.9[2] | 26.4[4] |
| Ultimate Wide-Width Tensile Strength (kN/m) | | | |
| Machine Direction | 13.8[2] | 21.1[2] | 40.2[4] |
| Cross-Machine Direction | 21.2[2] | 31.3[2] | 42.9[4] |

[1] IFAI, 1994; [2] Tensar, 2001; [3] AMOCO, 1996; [4] AMOCO, 2001

The target moisture content of 45 % was established by conducting laboratory, unsoaked *CBR* tests. Figure 3.1.4 shows the variation of *CBR* with compaction moisture content. On this figure, it is noted that only a relatively small change in *CBR* results between a moisture content range of 43 to 46 %.

The hard subgrade (approximate *CBR*=15 at a moisture content of 14 %) consisted of fines trapped from the baghouse of a local batch hot-mix plant. The material is classified as a SM or A-4, with 40 % non-plastic fines and a liquid limit of 18 %. Specific gravity of the silty-sand is 2.68. Modified Proctor tests resulted in a maximum dry density of 18.2 kN/m$^3$ occurring at a

moisture content of 11.5 %. This material was typically compacted at a moisture content of 14.8 % and a dry unit weight of 17.5 kN/m$^3$.

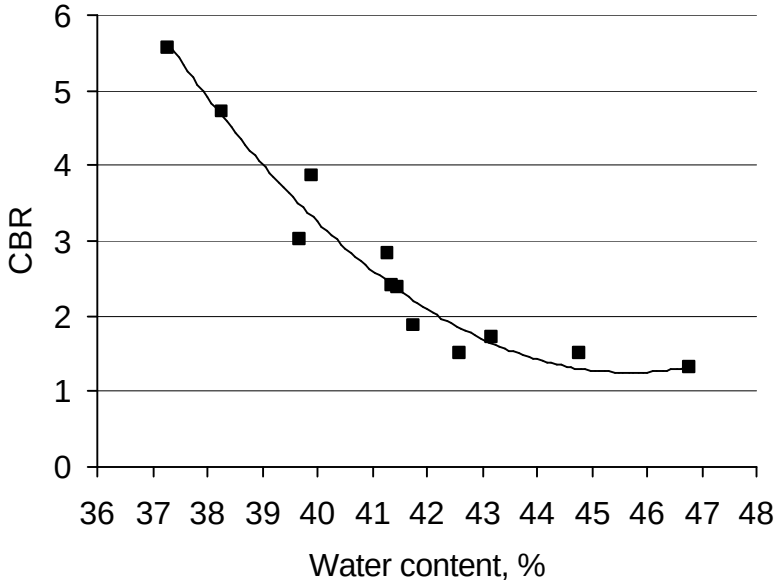


**Figure 3.1.4** *CBR* versus compaction moisture content for the clay subgrade.

As constructed properties of the compacted clay and silty sand subgrade in the test sections are given in Section 3.1.4. Shelby tubes were pushed into the subgrade during excavation of the sections for each test section. Undisturbed samples were used to conduct triaxial tests, with results presented in Section 4.2 where the constitutive model for the subgrade materials is presented and calibrated.

### *3.1.3 Instrumentation*

An extensive array of instrumentation was used in the test sections to quantify the mechanical response of the pavement materials to pavement loading. This data has allowed for the description of reinforcement mechanisms and has provided data to which the models developed in this report have been compared. The test sections contained instruments to measure applied pavement load, surface deflection, and stress and strain in the various pavement layers. Instrumentation has been categorized into sensors measuring applied pavement load, asphalt surface deflection, stress and strain in the base course and subgrade, and strain on the geosynthetic. Data acquisition software was configured to record information on the full time-history of response for prescribed load cycles and maximum and minimum sensor response for

other load cycles. A full description of the type of sensors used, installation techniques and the data acquisition used is given in Perkins (1999a).

### *3.1.4 As-Constructed Pavement Layer Properties*

Perkins (1999a) has described the construction techniques used for the test sections and the quality control measures taken to collect data during and after construction. Quality control measures were taken to provide information on the consistency of the pavement layer materials between test sections. These measures included measurement of in situ water content and dry density in the subgrade and base course layers during construction and during excavation, DCP tests on the compacted subgrade during construction and during excavation, measurement of in-place density of the compacted AC, and measurement of in-place density of the AC from 100 mm and 150 mm diameter AC drill cores. Additional tests were performed on both bulk AC samples and the 100 mm diameter cores. These tests included determination of asphalt cement content, air voids, rice specific gravity, Marshall stability, penetration and kinematic viscosity. A statistical analysis of these measures was provided and discussed in Perkins (1999a) and showed which sections were directly comparable.

As-constructed asphalt concrete properties for the test sections are given in Table 3.1.3. Test section temperature is determined from average room temperature over the course of the test. Thickness, density and air voids were determined from direct measurements on 100 mm and 150 mm diameter cores taken from the test sections. Asphalt content was determined from bulk samples. Marshall stability and flow was determined from 100 mm cores taken from the test sections.

As-constructed measurements of the base aggregate and subgrade are listed in Table 3.1.4 and Table 3.1.5, respectively. Table 3.1.6 provides information on loading conditions for each test section.

**Table 3.1.3** As-constructed asphalt concrete properties.

| Section | Test Section Temperature (°C) | Thickness (mm) | Density (kN/m$^3$) | Air Voids (%) | Asphalt Cement (%) | Marshalls | |
|---|---|---|---|---|---|---|---|
| | | | | | | Stability (lb) | Flow |
| CS2 | 17 | 78 | 23.1 | 3.3 | 6.8 | 2013 | 26 |
| CS5 | 24 | 76 | 22.6 | 5.6 | 6.1 | 2292 | 13 |
| CS6 | 21 | 75 | 23.3 | 3.1 | 6.6 | 2471 | 18 |
| CS7 | 24 | 75 | 22.9 | 4.3 | 6.6 | 1979 | 16 |
| CS8 | 24 | 76 | 23.1 | 3.3 | 6.1 | 2527 | 15 |
| CS9 | 26 | 79 | 22.7 | 5.2 | 6.3 | 2167 | 14 |
| CS10 | 18 | 75 | 22.9 | 4.3 | 6.5 | 2190 | 13 |
| CS11 | 25 | 77 | 23.4 | 1.9 | 6.0 | 2480 | 20 |
| SSS1 | 21 | 78 | 23.0 | 4.1 | 5.4 | 2956 | 17 |
| SSS2 | 26 | 79 | 22.6 | 6.3 | 5.7 | 2043 | 18 |
| SSS3 | 16 | 77 | 22.4 | 6.7 | 6.2 | 1372 | 17 |
| SSS4 | 16 | 78 | 22.8 | 4.4 | 6.1 | 2125 | 17 |

**Table 3.1.4** As-constructed base course properties.

| Section | Thickness (mm) | Dry Density (kN/m$^3$) |
|---|---|---|
| CS2 | 300 | 20.6 |
| CS5 | 300 | 20.6 |
| CS6 | 300 | 21.0 |
| CS7 | 300 | 20.6 |
| CS8 | 300 | 20.7 |
| CS9 | 375 | 20.9 |
| CS10 | 375 | 20.5 |
| CS11 | 300 | 20.5 |
| SSS1 | 210 | 20.6 |
| SSS2 | 205 | 20.7 |
| SSS3 | 200 | 20.8 |
| SSS4 | 200 | 21.1 |

**Table 3.1.5** As-constructed subgrade properties.

| Section | Thickness (mm) | Moisture Content (%) | Dry Density (kN/m$^3$) |
|---|---|---|---|
| CS2 | 1045 | 44.8 | 11.4 |
| CS5 | 1045 | 44.9 | 11.4 |
| CS6 | 1045 | 44.4 | 11.1 |
| CS7 | 1045 | 44.2 | 11.4 |
| CS8 | 1045 | 44.8 | 11.5 |
| CS9 | 970 | 44.9 | 11.4 |
| CS10 | 970 | 44.9 | 11.3 |
| CS11 | 1045 | 45.1 | 11.4 |
| SSS1 | 1128 | 14.7 | 17.0 |
| SSS2 | 1131 | 14.9 | 17.0 |
| SSS3 | 1147 | 14.8 | 17.1 |
| SSS4 | 1145 | 14.8 | 17.1 |

**Table 3.1.6** Test section loading conditions.

| Section | Average Peak Load (kN) | Peak Load Standard Deviation (kN) | Average Minimum Load (kN) |
|---|---|---|---|
| CS2 | 40.1 | 0.27 | 1.0 |
| CS5 | 40.1 | 0.34 | 1.2 |
| CS6 | 39.9 | 0.37 | 1.3 |
| CS7 | 40.0 | 0.22 | 1.3 |
| CS8 | 40.1 | 0.21 | 1.2 |
| CS9 | 39.9 | 0.26 | 1.6 |
| CS10 | 40.1 | 0.32 | 1.2 |
| CS11 | 40.0 | 0.44 | 1.0 |
| SSS1 | 40.1 | 0.89 | 2.2 |
| SSS2 | 40.3 | 0.34 | 1.2 |
| SSS3 | 40.2 | 0.73 | 1.3 |
| SSS4 | 40.5 | 0.47 | 1.0 |

## 3.2 Summary of Results and Data Analysis

Presented in Figures 3.2.1, 3.2.2 and 3.2.3 are results of permanent surface deformation versus load cycle applied to each of the test sections. Sections CS2 and CS8 are duplicate unreinforced test sections with identical pavement layers. Test sections CS5, 6, 7 and 11 can be compared to CS2 and 8 to evaluate *TBR*. Similarly, test section CS10 can be compared to CS9 for evaluation of *TBR*. Test sections SSS1 and 4 are duplicate unreinforced test sections. These test sections showed a better performance, defined in terms of permanent surface deformation, as compared to the corresponding reinforced sections SSS2 and SSS3. As described in Perkins (1999a), the

principal reason for this observation was the lower air voids of the asphalt concrete in test sections SSS1 and 4 as compared to SSS2 and 3 and the resulting reduced stiffness of this layer. Had the asphalt concrete been more comparable between these sections, it is believed that little differences in pavement performance would have been seen between reinforced and unreinforced sections, meaning that reinforcement had little impact for sections with this structural section and subgrade strength.

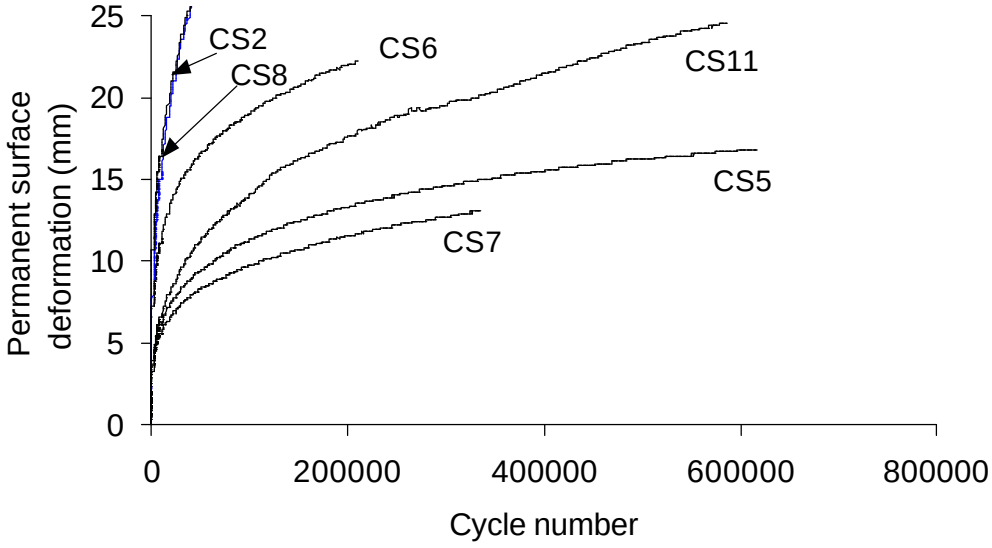


**Figure 3.2.1** Permanent surface deformation versus load cycle (CS2, 5, 6, 7, 8, 11).

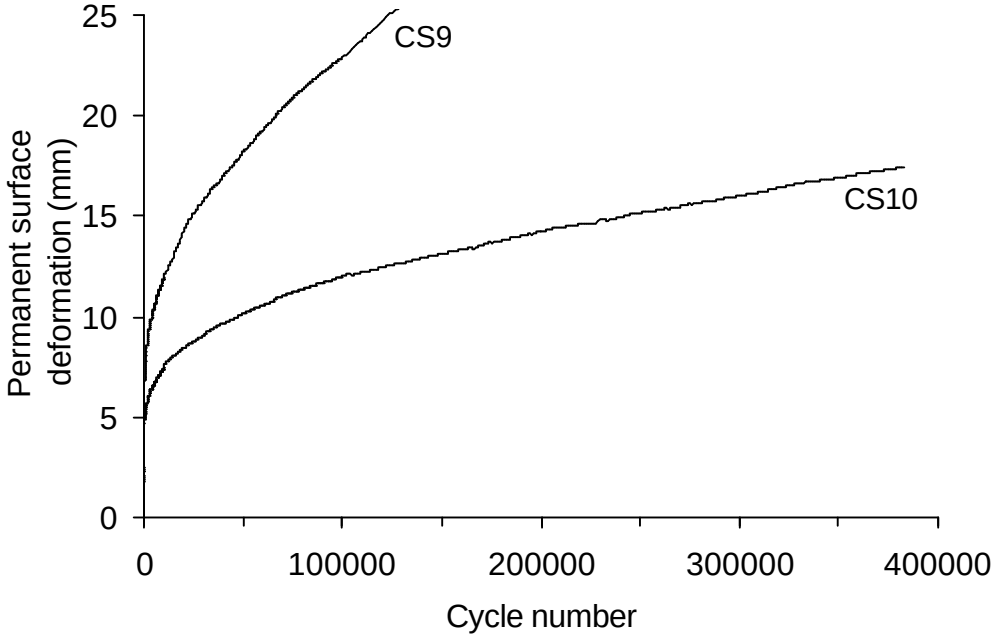


**Figure 3.2.2** Permanent surface deformation versus load cycle (CS9, 10).

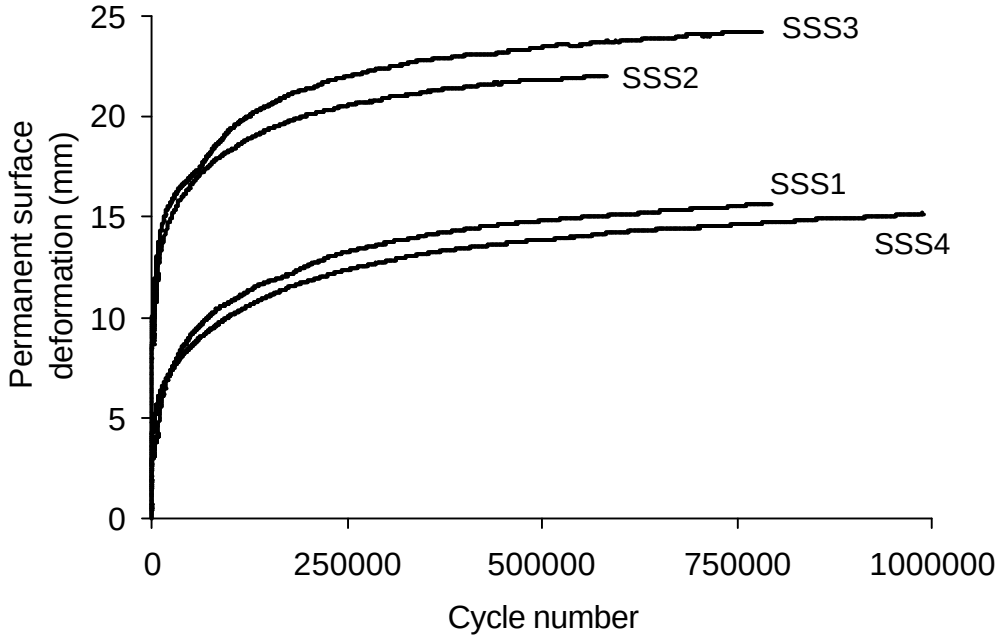


**Figure 3.2.3** Permanent surface deformation versus load cycle (SSS1, 2, 3, 4).

Figures 3.2.4 and 3.2.5 provide values of *TBR* computed at permanent surface deformation values ranging from 1 mm to 25 mm. In Figure 3.2.4, sections CS5, 6, 7 and 11 were compared to section CS2 to calculate *TBR* values. In Figure 3.2.5, section CS10 was compared to CS9.

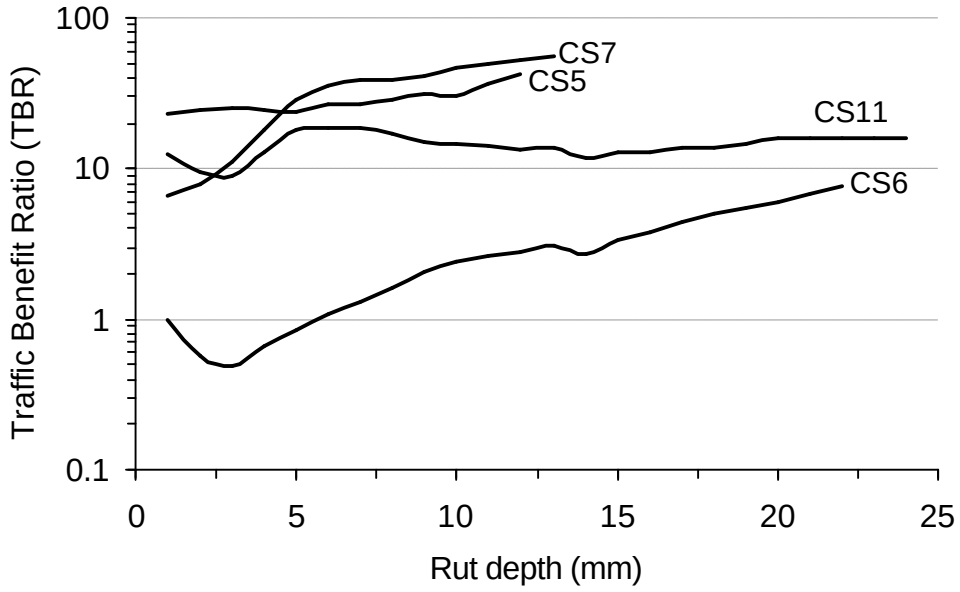


**Figure 3.2.4** *TBR* for sections CS5, 6, 7 and 11 relative to section CS2.

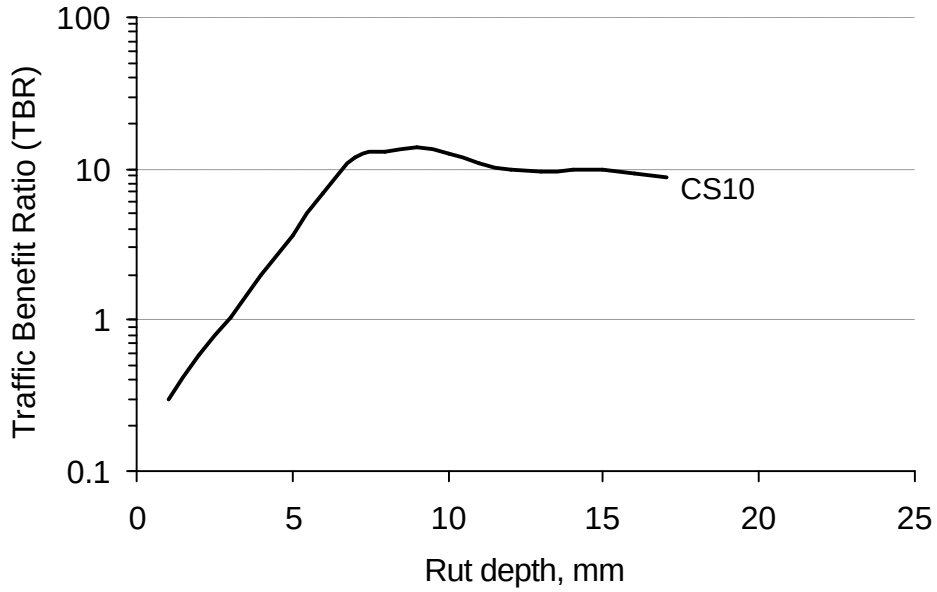


**Figure 3.2.5** *TBR* for section CS10 relative to section CS9.

In Section 5.4, a method is presented for relating reinforcement benefit to strain and stress measures from unreinforced and reinforced pavement section layers. Validation of this method by comparison to results from test sections requires an analysis of the results from the test sections described above. This analysis is presented below.

Each test section contained LVDT's to measure permanent and dynamic strain in the vertical direction at typically four depths in the subgrade layer. Figure 3.2.6 presents data from test section CS2 showing values of permanent strain vs. depth from the top of the subgrade for 6 values of applied load cycle.

The data shown in Figure 3.2.6 plots as a straight line on a semi-log scale according to the equation:

$$\log e_{v-p} = A\, z + B \tag{3.2.1}$$

where $z$ is the depth from the top of the subgrade and $A$ and $B$ are constants for the line. Constants $A$ and $B$ were determined for each load cycle for which data was available for each test section. For test section CS2 for the load cycles given in Figure 3.2.6, the line resulting from Equation 3.2.1 is plotted as the "Equation" line for each data set.

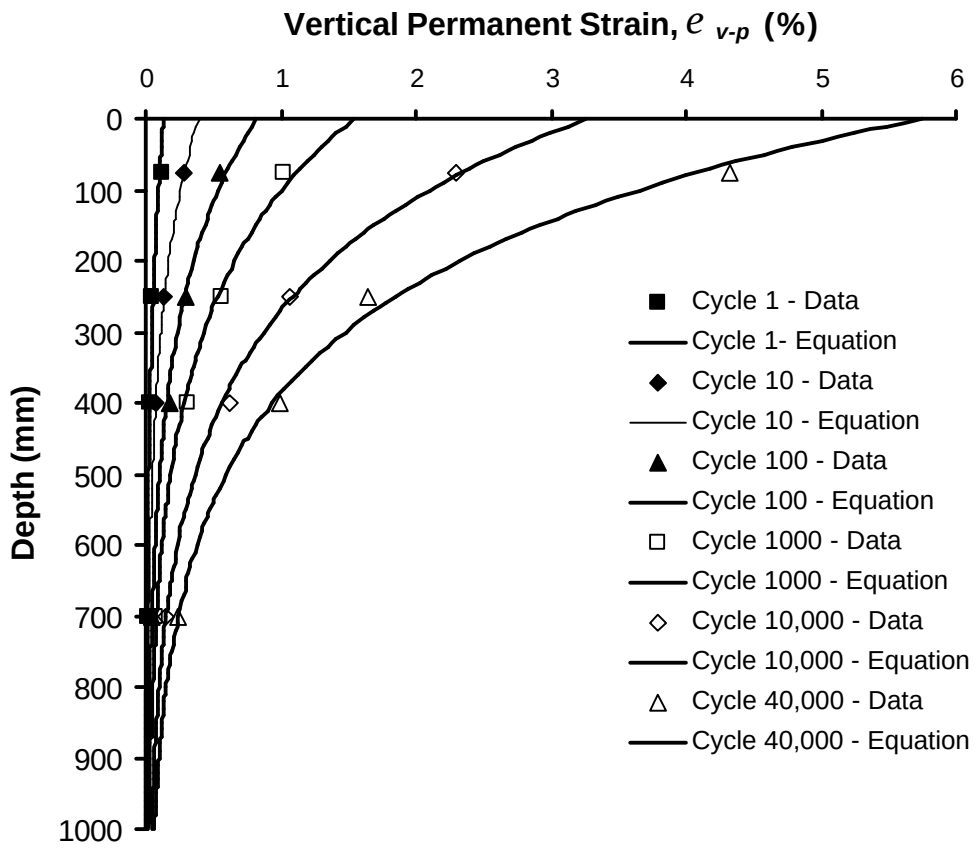


**Figure 3.2.6** Permanent vertical strain vs. depth in the subgrade for test section CS2.

Integration of Equation 3.2.1 over the depth of the subgrade allows for the calculation of permanent deformation of the subgrade for each load cycle for which data is available and for each data set where Equation 3.2.1 is evaluated. Integration of Equation 3.2.1 results in Equation 3.2.2.

$$\Delta_S = \frac{10^{AH+B} - 10^{B}}{A \ln 10} \tag{3.2.2}$$

where $H$ is the height of the subgrade layer. From this procedure, the deformation of the subgrade as a function of load cycle was calculated. The deformation from Equation 3.2.2 is both the total compression or change in thickness of the subgrade, and the deformation of the top of the subgrade. Subtracting the subgrade deformation at each load cycle from the permanent surface deformation, where the later is a measured quantity, yields a deformation that is assumed to be the permanent deformation or change in thickness of the base aggregate, which assumes

that the asphalt concrete thickness does not change appreciably compared to the thickness change of the base and subgrade layers during repetitive loading. This procedure allows for the generation of deformation versus load cycle for the surface, base and subgrade as illustrated in Figure 3.2.7 for an unreinforced section (CS2) where it is seen that surface deformation is shared nearly equally between compression of the base and the subgrade. This procedure was repeated for all test sections where similar results were obtained.

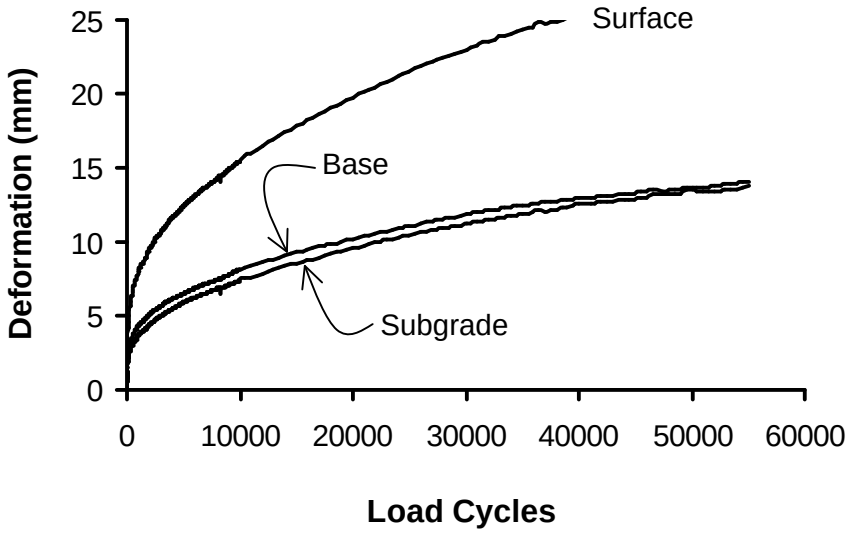


**Figure 3.2.7** Permanent deformation of surface, base and subgrade layers - CS2.

Geosynthetic reinforcement can be thought of as having an effect on reducing permanent strains or deformations in the base and the subgrade. Treating each separately allows for the calculation of a reinforcement benefit due to a reinforcement effect on the base and on the subgrade. From the test sections available, reinforcement benefit can be expressed in terms of a *TBR*. *TBR* was calculated in Figures 3.2.4 and 3.2.5 from surface deformations, where this *TBR* should be viewed as a total reinforcement benefit for all reinforcement effects acting on the pavement system ($TBR_T$). A *TBR* for reinforcement effects on the base and reinforcement effects on the subgrade can be calculated separately for each test section by calculating a surface deformation curve for a reinforced section if improvement in deformation was experienced only by the base and then only by the subgrade. This is accomplished by starting with the surface deformation curve of the unreinforced section and subtracting from this curve either the improvement in deformation of the base or the subgrade for a reinforced section. Subtracting

both the improvement of the base and subgrade from the unreinforced surface deformation curve results in the measured surface deformation curve of the reinforced section. This is accomplished by applying Equations 3.2.3 and 3.2.4 for each load cycle where data is available and using Equation 3.2.5 as a check.

$$\Delta_{R-B} = \Delta_U - \left(\Delta_{B-U} - \Delta_{B-R}\right) \tag{3.2.3}$$

$$\Delta_{R-S} = \Delta_U - \left(\Delta_{S-U} - \Delta_{S-R}\right) \tag{3.2.4}$$

$$\Delta_R = \Delta_U - \left(\Delta_{B-U} - \Delta_{B-R} + \Delta_{S-U} - \Delta_{S-R}\right) \tag{3.2.5}$$

where:

$\Delta_{R\text{-}B}$ = Calculated surface deformation for reinforced pavement assuming reinforcement reduces only deformations in the base layer.

$\Delta_{R\text{-}S}$ = Calculated surface deformation for reinforced pavement assuming reinforcement reduces only deformations in the subgrade layer.

$\Delta_U$ = Measured surface deformation of unreinforced section.

$\Delta_R$ = Measured surface deformation of reinforced section

$\Delta_{B\text{-}U}$ = Deformation of base layer for the unreinforced section.

$\Delta_{B\text{-}R}$ = Deformation of base layer for the reinforced section.

$\Delta_{S\text{-}U}$ = Deformation of subgrade layer for the unreinforced section.

$\Delta_{S\text{-}R}$ = Deformation of subgrade layer for the reinforced section.

Figure 3.2.8 shows an example from a reinforced section (CS11) showing the calculation of these curves. At a given permanent surface deformation level (12.5 mm as in the case of Figure 3.2.8) a partial *TBR* can be computed for reinforcement effects on the base and on the subgrade ($TBR_B$, $TBR_S$) by dividing the number of load cycles necessary to reach 12.5 mm of deformation from the respective calculated curves for base and subgrade reinforcement by the corresponding load cycles for the measured unreinforced curve. For this test section, the following numbers were obtained: $TBR_T$ = 13.5, $TBR_B$ = 3.01, $TBR_S$ = 2.61, where all measurements were made at a level of 12.5 mm. Carrying out these computations for all test sections results in values of *TBR* measured at 12.5 mm of permanent surface deformation given in Table 3.2.1.

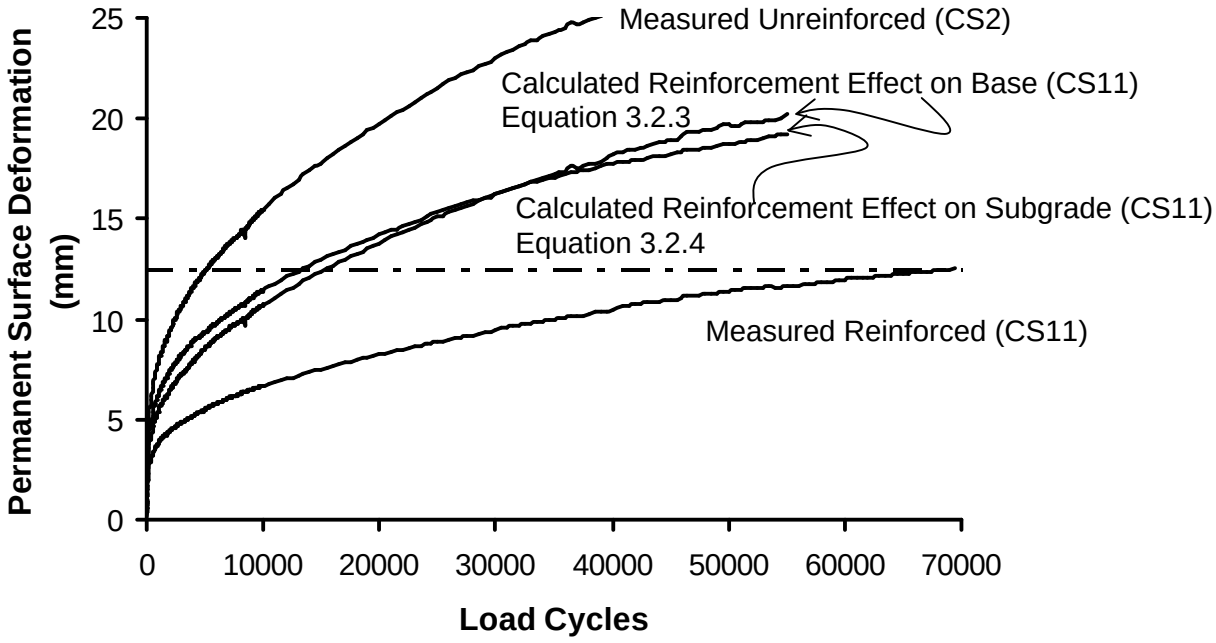


**Figure 3.2.8** Calculated surface deformation curves for isolated reinforcement effects on base and subgrade for test section CS11.

**Table 3.2.1** *TBR*'s for reinforced test sections at 12.5 mm permanent surface deformation.

| Section | $TBR_T$ | $TBR_B$ | $TBR_S$ |
|---|---|---|---|
| CS5 | 29.7 | 7.74 | 2.95 |
| CS6 | 2.90 | 1.43 | 1.66 |
| CS7 | 54.4 | 3.47 | 3.13 |
| CS10 | 9.82 | 2.63 | 2.23 |
| CS11 | 13.5 | 3.01 | 2.61 |

The methods presented later in this report also rely upon the determination of the total vertical strain in and at the top of the subgrade when peak pavement load is applied for the first load cycle. This has been accomplished by the use of Equation 3.2.1 where constants *A* and *B* are determined from data for the first load cycle. Equation 3.2.1 is then evaluated at $z = 0$ to yield the permanent strain in the top of the subgrade for the first load cycle. Data from test sections typically show that the dynamic or recoverable vertical strain in the subgrade, measured as the difference between the strain at peak load minus the permanent strain when the load is released for a given load cycle, is relatively constant over the course of repeated pavement loading. For a given test section, single values of dynamic strain were determined for each depth in the

subgrade where LVDT's were located by averaging the dynamic strain recorded for each load cycle. Plotting these values versus depth showed that an equation of the same form as Equation 3.2.1 fit the data well. Figure 3.2.9 shows an example of this data for test section CS2. Dynamic strain at the top of the subgrade was then added to the permanent strain at the top of the subgrade for the first load cycle to give the total strain at the top of the subgrade for the first load cycle, with results for each test section summarized in Table 3.2.2. Also shown in this table is the number of load cycles necessary to reach 12.5 mm of permanent surface deformation. For the unreinforced test sections (SSS1, SSS4, CS2, CS9) the values reported are directly from measured surface deformation from the test sections. For the reinforced sections, the numbers given are for permanent surface deformations computed for reinforcement effects occurring only within the subgrade layer according to Equation 3.2.4 and as illustrated for reinforced test section CS11 in Figure 3.2.8. This has been done to associate reinforcement benefit on the subgrade with a response measure pertinent to the subgrade. The load cycle numbers shown in Table 3.2.2 were the values used to produce the values for $TBR_S$ given in Table 3.2.1.

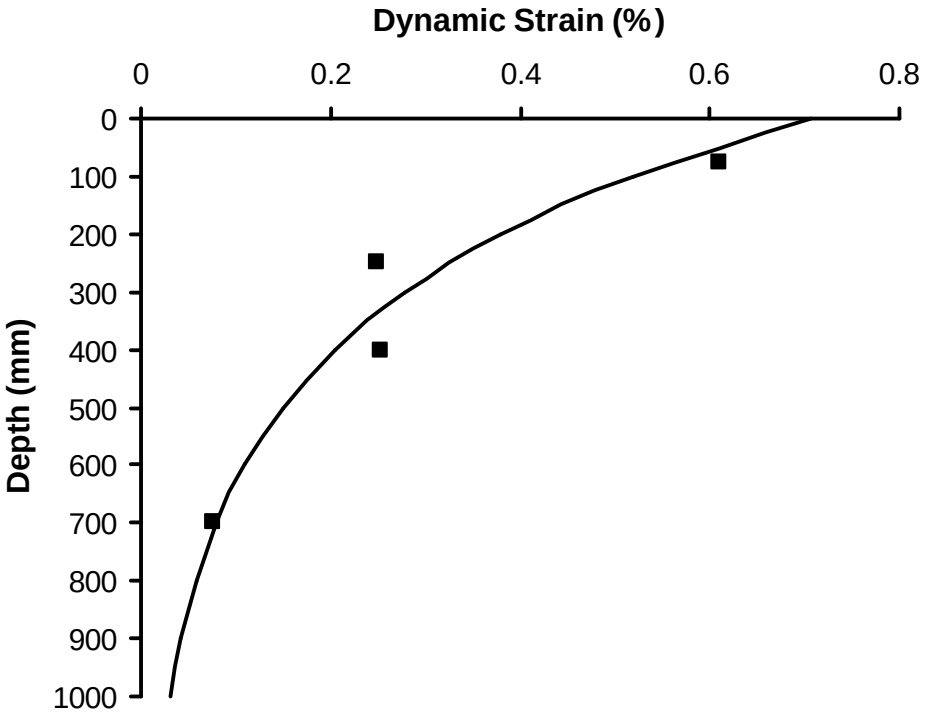


**Figure 3.2.9** Measured dynamic strain versus depth and best fit line per Equation 3.2.1 for test section CS2.

Values of total vertical strain in the top of the subgrade for the first load cycle were plotted against the number of load cycles necessary for 12.5 mm of permanent surface deformation from Table 3.2.2 (Figure 3.2.10). A best fit line of the form given in Equation 3.2.6, where *A* and *B* are constants, and where $e_v$ is in decimal form, produced values of $A = 1.8\times10^{-5}$ and $B = -4.07$.

$$N_{12.5\,mm} = Ae_v^{-B} \tag{3.2.6}$$

Equation 3.2.6 is commonly referred to as a subgrade rutting model for flexible pavements with values for *B* as reported by four agencies ranging from 3.95 to 4.48 and values of *A* ranging from $6.15\times10^{-7}$ to $1.36\times10^{-9}$ (Huang, 1993). Information from Table 3.2.1 and Equation 3.2.6 is used later in Sections 5 and 7 for development of the design model.

**Table 3.2.2** Total vertical strain at peak load for the first load cycle.

| Section | Total Vertical Strain (%) | Load Cycles for 12.5 mm Permanent Surface Deformation |
|---|---|---|
| SSS1 | 0.266 | 195,000 |
| SSS4 | 0.272 | 263,000 |
| CS2 | 0.843 | 5140 |
| CS5 | 0.618 | 15,200 |
| CS6 | 0.753 | 8550 |
| CS7 | 0.584 | 16,100 |
| CS9 | 0.712 | 12,500 |
| CS10 | 0.559 | 27,900 |
| CS11 | 0.680 | 13,400 |

## 4.0 PAVEMENT LAYER MATERIAL MODELS AND CALIBRATION TESTS

As discussed in Section 1.0, the numerical finite element model developed as part of this work was designed to be used for the extraction of key stress and strain measures from the pavement layers when one cycle of pavement load is applied. These mechanistic response measures are then used in empirical distress models to quantify long-term pavement performance and reinforcement benefit. The purpose of this section is to describe the material models developed for the various pavement layers and the laboratory tests used to calibrate these models. The relationship of material properties used in these models to commonly used pavement layer material properties is also presented. It should be recognized that the majority of the material parameters contained in the models for the various pavement materials described below are not

contained in the design model described in Sections 7 and 8, and Appendix B. The properties contained in the material models described in this section were developed for the purposes of establishing the finite element model, which was used in the parametric study to quantify reinforcement benefit as a function of a smaller and easily identifiable subset of pavement and geosynthetic properties and characteristics.

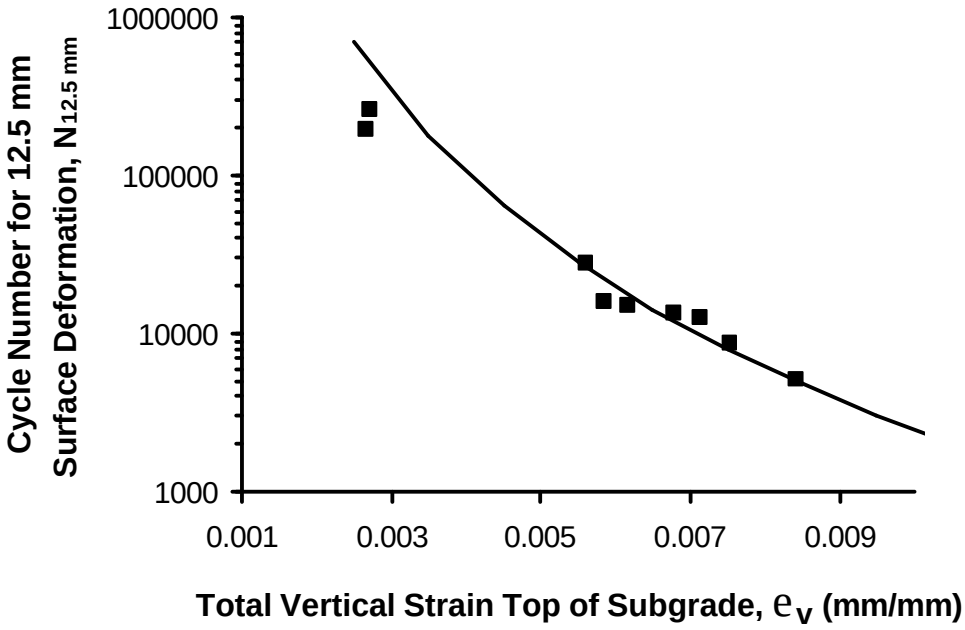


**Figure 3.2.10** Total vertical strain in top of the subgrade for the first load cycle versus number of load cycles to reach 12.5 mm of permanent surface deformation.

## 4.1 Asphalt Concrete

Mechanistic-empirical flexible pavement models commonly use isotropic, linearly-elastic material models for the asphalt concrete. Initially, such a model was adapted for use in this study for sake of simplicity and for ease of comparison to other studies. Given the need to examine permanent strains, however, in the subgrade after one load application, a material model for the asphalt concrete that allowed for the development of permanent strain upon release of the load was required. Otherwise, the elastic rebound of the asphalt concrete layer would create artificial vertical tensile stresses and strains in the top of the aggregate layer. A plasticity component was added to the model to allow for the development of permanent strain. The plasticity was introduced by specification of an ultimate yield stress corresponding to a perfect plasticity hardening law.

Incorporation of this material model into the finite element model described in Section 5 showed that vertical stresses in the subgrade close to the centerline of the load plate tended to be under predicted, while vertical stresses at a radius greater than approximately 300 mm tended to be over predicted. In addition, the predicted deflected shape of the asphalt surface tended to be more flat than that seen from test section results. These findings suggested that the use of isotropic elastic and plastic properties for the asphalt concrete tended to cause this layer to act too much like an elastic slab distributing the stress too broadly. For these reasons, direction dependency, or anisotropy, was added for the elastic and plastic properties. The addition of anisotropy essentially allowed for the reduction of the flexural stiffness of the asphalt layer while maintaining the vertical stiffness in compression.

Direction dependence of elastic properties was prescribed through the use of a linear, orthotropic elastic constitutive matrix. Orthotropic linear elasticity is described by three moduli ($E_{ij}$), three independent Poisson's ratios ($n_{ij}$) and three shear moduli ($G_{ij}$), resulting in the elastic constitutive matrix

$$\begin{Bmatrix} e_x \\ e_y \\ e_z \\ g_{xy} \\ g_{xz} \\ g_{yz} \end{Bmatrix} = \begin{bmatrix} 1/E_x & -n_{yx}/E_y & -n_{zx}/E_z & 0 & 0 & 0 \\ -n_{xy}/E_x & 1/E_y & -n_{zy}/E_z & 0 & 0 & 0 \\ -n_{xz}/E_x & -n_{yz}/E_y & 1/E_y & 0 & 0 & 0 \\ 0 & 0 & 0 & 1/G_{xy} & 0 & 0 \\ 0 & 0 & 0 & 0 & 1/G_{xz} & 0 \\ 0 & 0 & 0 & 0 & 0 & 1/G_{yz} \end{bmatrix} \begin{Bmatrix} s_x \\ s_y \\ s_z \\ t_{xy} \\ t_{xz} \\ t_{yz} \end{Bmatrix} \tag{4.1.1}$$

where the subscripts *x* and *y* denote the in-plane horizontal directions, and *z* denotes the vertical direction. Plasticity was described in terms of an ultimate yield stress, $s^0_{AC}$, and six plastic potential ratios, $R_{ij}$, given in Equation 4.1.2, whose values are typically less than one and describe the reduction in yield stress in each respective direction.

$$\begin{Bmatrix} R_x \\ R_y \\ R_z \\ R_{xy} \\ R_{xz} \\ R_{yz} \end{Bmatrix} = \frac{1}{s^{o}_{AC}} \begin{Bmatrix} \bar{s}_x \\ \bar{s}_y \\ \bar{s}_z \\ \sqrt{3}\,\bar{t}_{xy} \\ \sqrt{3}\,\bar{t}_{xz} \\ \sqrt{3}\,\bar{t}_{yz} \end{Bmatrix} \tag{4.1.2}$$

Values of elastic modulus ($E_z$), Poisson's ratio and yield stress ($s^0_{AC}$) in the principal direction of loading (i.e. the z-direction) were determined by conducting indirect tension (IDT) resilient modulus tests per ASTM D4123 (ASTM, 2001b), where these tests were performed at the Asphalt Institute, Lexington, Kentucky. Tests were performed on 150 mm diameter samples cored from the test sections described in Section 3. Four 150 mm diameter cores were typically taken from each test section upon the completion of the tests and were taken from areas outside the footprint of the load plate. An additional six 100 mm cores were also obtained. Percent air voids was determined for each core with the average air voids computed. Resilient modulus was typically determined for two 150 mm cores from most sections. These cores were chosen to bracket as closely as possible the average air voids for the test section. Resilient modulus tests were performed at the average room temperature existing during the time the corresponding test section was loaded and were performed at three frequencies of loading (0.33, 0.5 and 1 Hz) and at two test positions corresponding to a 90 degree rotation. At the end of resilient modulus testing, the samples were loaded to failure to determine the ultimate strength of each core. Values of resilient modulus and Poisson's ratio are reported in Table 4.1.1 and are average values from each test rotation and testing frequency.

The IDT test results show a strong dependency on test specimen temperature and a lesser dependence on specimen air voids. The dependence on air voids appears to become stronger as the test temperature decreases. Given the consistency between certain sets of results from the test sections, it would appear that the difference in actual temperature in the asphalt concrete during the period over which pavement loading occurred between test sections is less than that implied by the values of room temperature reported in Tables 3.1.3 and 4.1.1. For instance, test sections CS2 and CS8 were identical unreinforced test sections that displayed nearly identical pavement loading performance. The differences in room temperature for the two tests was reported as 7 degrees C. The IDT tests performed at this temperature difference resulted in a significant difference in modulus of the AC, which did not appear to be evident from the test section results. It is believed that the differences in actual AC temperature in the test sections was moderated by the presence of the large body of soil upon which AC rested and is less than that implied by room temperature measurements. Given the relatively small differences in average air voids between the sections and the uncertainty regarding the true temperature of the asphalt concrete during testing, typical values of modulus, Poisson's ratio and ultimate tensile strength were used

for all test section modeling. A value of modulus for $E_z$ of 2500 MPa, a Poisson's ratio of 0.35 and a yield strength of 675 kPa were chosen. A modulus of 2500 MPa corresponds approximately to a structural layer coefficient of 0.4 corresponding to AASHTO (1993). Values of the other parameters in Equations 4.1.1 and 4.1.2 as used in the finite element model for modeling all cases examined are given in Table 4.1.2. The selection of the remaining values shown in Table 4.1.2 was based on matching as closely as possible the vertical stresses observed in the test sections.

**Table 4.1.1** Indirect tension resilient modulus test results.

| Test Section | IDT Test Temperature (degree C) | Specimen Air Voids (%) | Average Resilient Modulus (MPa) | Average Poisson's Ratio | Ultimate Tensile Strength (kPa) |
|---|---|---|---|---|---|
| SSS3-1 | 15 | 2.93 | 4583 | 0.34 | 1273 |
| SSS3-3 | 16 | 4.17 | 3748 | 0.34 | 1009 |
| SSS3-4 | 15 | 5.32 | 3032 | 0.30 | 938 |
| SSS4-1 | 15 | 4.25 | 4519 | 0.26 | 1218 |
| SSS4-2 | 15 | 3.38 | 4596 | 0.31 | 1288 |
| SSS4-4 | 16 | 5.57 | 2826 | 0.15 | 888 |
| CS2-3 | 17 | 1.97 | 3668 | 0.42 | 828 |
| CS2-4 | 17 | 1.97 | 4094 | 0.36 | 901 |
| CS5-3 | 24 | 5.12 | 1150 | 0.22 | 585 |
| CS6-2 | 21 | 2.47 | 1934 | 0.35 | 604 |
| CS7-1 | 24 | 4.46 | 1741 | 0.31 | 538 |
| CS7-3 | 24 | 2.66 | 2049 | 0.41 | 581 |
| CS8-2 | 24 | 2.87 | 1723 | 0.38 | 567 |
| CS9-2 | 26 | 4.09 | 1356 | 0.41 | 447 |
| CS9-4 | 26 | 6.10 | 1188 | 0.33 | 468 |
| CS10-2 | 18 | 2.96 | 2944 | 0.42 | 977 |
| CS11-1 | 25 | 1.23 | 1796 | 0.95 | 449 |
| CS11-4 | 25 | 1.88 | 1538 | 0.32 | 441 |

## 4.2 Base Aggregate and Subgrade

The constitutive model used for both the base aggregate and the subgrade soil is based on the bounding surface concept originally developed by Dafalias (1975) and extended for the description of isotropic cohesive soils by Dafalias and Hermann (1982) and later updated by Dafalias and Hermann (1986). The model was originally selected and incorporated into the finite element model used in this study to provide a material model capable of showing the

accumulation of permanent strain with repeated load. Since the finite element model, as used in the work described in this report, is used for only one load cycle, many of the base aggregate and subgrade material model features are not fully utilized. The model was incorporated into the finite element model as a user defined material model (UMAT).

**Table 4.1.2** Material parameter values used for the asphalt concrete.

| Parameter | Value |
|---|---|
| $E_x$ (MPa) | 1250 |
| $E_y$ (MPa) | 1250 |
| $E_z$ (MPa) | 2500 |
| $G_{xy}$ (MPa) | 463 |
| $G_{xz}$ (MPa) | 63.8 |
| $G_{yz}$ (MPa) | 63.8 |
| $n_{xy}$ | 0.35 |
| $n_{xz}$ | 0.35 |
| $n_{yz}$ | 0.35 |
| $s^0_{AC}$ (kPa) | 675 |
| $R_x$ | 0.4 |
| $R_y$ | 0.4 |
| $R_z$ | 1.0 |
| $R_{xy}$ | 1.0 |
| $R_{xz}$ | 0.4 |
| $R_{yz}$ | 0.4 |

The model is described in terms of two surfaces represented in the stress space shown in Figure 4.2.1. The parameters *I* and *J* represent the first stress invariant and the square root of the second deviatoric stress invariant, respectively, and, in general terms, are reflective of mean normal stress and shear stress, respectively. These surfaces are also a function of the lode angle, $a$, defined in terms of the third deviatoric stress invariant. The lode angle reflects stress paths ranging from triaxial compression to triaxial extension.

The larger surface shown in Figure 4.2.1 represents the bounding surface, which in a conventional plasticity model is equivalent to a yield surface. The second surface shown in Figure 4.2.1 denotes an elastic zone. Stress states within the elastic zone produce purely elastic behavior. Stress states lying between the elastic zone and the bounding surface are capable of producing both elastic and inelastic behavior. As the stress state approaches the bounding surface, the rate of plastic strain increases. In a conventional plasticity model, the surface for the

elastic zone is coincidental with the bounding surface, meaning that stress states lying below the current yield surface always produce purely elastic behavior.

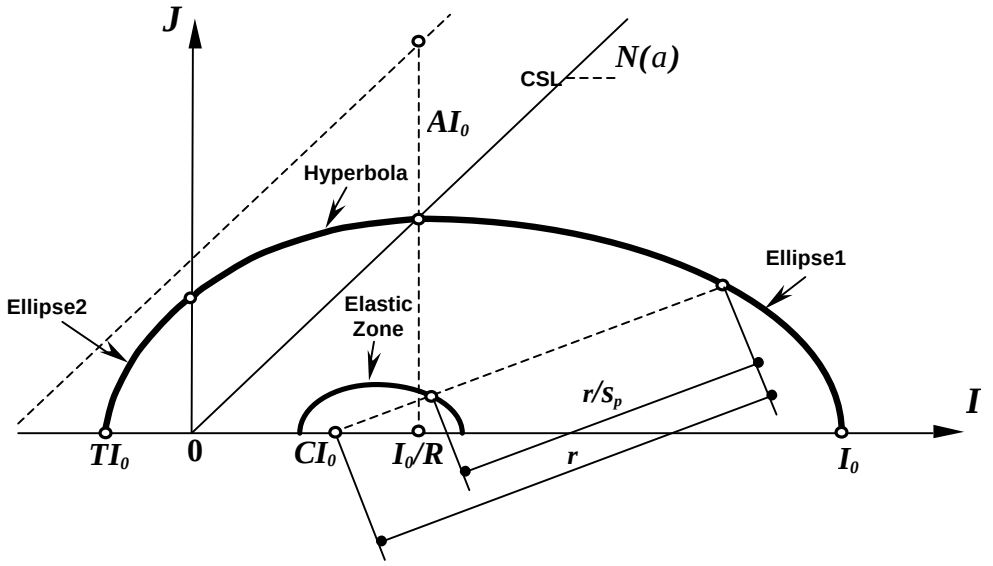


**Figure 4.2.1** Schematic illustration of the bounding surface plasticity model.

A radial mapping rule is used to locate a point on the bounding surface corresponding to some state of stress inside or on the bounding surface. This mapping rule is illustrated by the dashed line in Figure 4.2.1 having an origin on the $I$ axis at the value $CI_o$, where $C$ is a material parameter and $I_o$ is defined below. This mapping rule is necessary to prescribe yielding characteristics determined from the image point on the bounding surface to the current state of stress.

The bounding surface concept is general and permits the inclusion of any type of formulation for a yield surface, which is taken to represent the formulation for the bounding surface. The bounding surface used in the current model consists of three segments, as illustrated in Figure 4.2.1. The adoption of a combined surface allows greater flexibility in assigning behavior within the tension region of the stress space, the importance of which is discussed below. The bounding surface model used for the base aggregate and the subgrade soil uses a yield surface formulation extended from critical state soil mechanics models (Schofield and Wroth, 1968). A critical state line, defining the failure state of the material, is given by a line with a slope of $N$, where $N$ is a function of the lode angle and is related to the slope of the critical

state line, $M$, in $p$-$q$ stress space, and where $M$ is given in terms of the material's drained friction angle as

$$M = \frac{6\sin f}{3 - \sin f} \tag{4.2.1}$$

This formulation specifies the current size of the bounding surface in terms of the parameter $I_o$, the value of which reflects the amount of preloading or preconsolidation of the material. The value of $I_o/R$ represents the value of $I$ at the intersection of the bounding surface and the critical state line. The parameter $R$ defines the ratio of the major to minor axes of ellipse 1 and is a material constant.

The quantity $TI_o$ defines the intersection of ellipse 2 with the $I$ axis in the tension region and dictates the tensile strength of the material, with the tensile strength changing depending on the value of $I_o$ as dictated by overconsolidation. The parameter $T$ is a material constant and can be set to a low value to model materials with little tensile strength, such as base aggregates.

The remaining point defining the shape of the bounding surface is the intersection of the surface with the $J$ axis. This intersection point is governed by the material constant $A$. Small values of $A$ pertain to materials with little cohesion. The parameters $R$, $A$ and $T$ are known as shape factors. The parameter $s_p$ defines the size of the elastic zone. A value of 1 means that the elastic zone shrinks to a point located at the projection center, $CI_o$. As $s_p$ increases to infinity, the elastic zone becomes larger and approaches the bounding surface.

The model contains another five material parameters in addition to those listed above. The first two ($m$ and $h$) are associated with the hardening rule. The next two ($l$ and $k$) are associated with the critical state soil mechanics definition of compression behavior in a void ratio vs. natural logarithm plot and are related to the compression index, $C_c$, and the swelling index, $C_s$, as defined from one-dimensional consolidation tests, by Equations 4.2.2 and 4.2.3.

$$l = \frac{C_c}{2.303} \tag{4.2.2}$$

$$k = \frac{C_s}{2.303} \tag{4.2.3}$$

The last parameter that is specified is either Poisson's ratio, $\nu$, or the shear modulus, $G$. If Poisson's ratio is specified as a constant, then bulk modulus, $K$, shear modulus, $G$, and elastic modulus, $E$ are calculated from Equations 4.2.4 through 4.2.6.

$$K = \frac{(1+e_{in})}{3\kappa}\left(\langle I - I_L \rangle + I_L\right) \tag{4.2.4}$$

$$G = \frac{3(1-2\nu)}{2(1+\nu)}K \tag{4.2.5}$$

$$E = K + \frac{4G}{3} \tag{4.2.6}$$

where $I$ is the current first stress invariant or bulk stress (defined as the sum of the three principal stresses), $I_L$ is a constant typically taken equal to atmospheric pressure and $e_{in}$ is the initial void ratio of the material. The bulk stress, $I$, is defined in the same way as the stress state term, $\theta$, in commonly used $k_1$-$\theta$-$k_2$ expressions (i.e. Equation 4.2.7) used in pavement engineering for computing resilient modulus as a function of stress state.

$$M_R = k_1\theta^{k_2} \tag{4.2.7}$$

In Equation 4.2.4, if $I$ is less than or equal to $I_L$, then the quantity ($\langle I\text{-}I_L\rangle+I_L$) becomes equal to $I_L$. If $I$ is greater than $I_L$, then the quantity ($\langle I\text{-}I_L\rangle+I_L$) becomes equal to $I$. This ensures that the values of the moduli computed from Equations 4.2.4 – 4.2.6 do not become excessively small for small values of $I$ and that the minimum values of modulus computed will correspond to the minimum value obtained from the expression ($\langle I\text{-}I_L\rangle+I_L$), with this minimum value being equal to $I_L$. Otherwise, according to these equations, shear modulus and elastic modulus will increase as the bulk stress increases. If $G$ is specified as a constant rather than Poisson's ratio, then bulk modulus and elastic modulus are calculated from Equations 4.2.4 and 4.2.6, where $G$ in Equation 4.2.6 is equal to the constant value specified.

The model contains the ability to define separate material constants for $M$, $R$, $A$ and $h$ for stress paths in compression and extension. In the absence of data to support a proper selection of

these terms, values of these parameters were taken to be equal in extension and compression, with the exception of the parameter $M$ in extension for the base aggregate. For the base aggregate, the ratio of the parameter $M$ in extension to compression ($M_E/M_C$) was taken as 0.8 to better match results from test sections.

Use of the model also requires the definition of several variables defining the initial state of the material. Namely, the initial void ratio ($e_{in}$) and the preconsolidation pressure ($I_o$) of the material must be specified. A summary of material parameters for the model is given in Table 4.2.1, where all parameters are dimensionless except $I_L$, $I_o$ and $G$, which have dimensions of stress.

**Table 4.2.1** Listing of bounding surface model material parameters.

| Parameter | Name | Typical Range of Values |
|---|---|---|
| $l$ | Virgin compression slope | 0.1-0.2 |
| $k$ | Swell/recompression slope | 0.02-0.08 |
| $M$ | Slope of critical state line in $p$-$q$ stress space | 0.8-1.4 |
| $M_E/M_C$ | Ratio of $M$ in extension to compression | 0.7-1.0 |
| $n$ or $G$ | Poisson's ratio or shear modulus | 0.15-0.3 or 6.5 to 65 MPa |
| $I_L$ | Atmospheric pressure | 101 kPa |
| $R$ | Shape parameter | 2-3 |
| $A$ | Shape parameter | 0.02-0.2 |
| $T$ | Shape parameter | 0.05-0.15 |
| $C$ | Projection center parameter | 0.0-0.5 |
| $s_p$ | Elastic zone parameter | 1-2 |
| $m$ | Hardening parameter | 0.02 |
| $h$ | Hardening parameter | 5-50 |
| $e_{in}$ | Initial void ratio | material dependent |
| $I_o$ | Preconsolidation pressure | material dependent |

The model is not ideally suited for the description of granular soils since it has been formulated in terms of critical state soil mechanics concepts. In particular, the parameters $l$ and $k$ generally do not adequately define the compression behavior of granular soils. While the shape parameters describing the cohesion and tensile strength ($A$ and $T$) can be set low to mimic the lack thereof in granular soils, some finite level of cohesion and tensile strength is always predicted. In addition numerical instabilities can sometimes result when $A$ and $T$ are given low values. The influence of bulk stress on elastic moduli for aggregate materials, as defined from Equations 4.2.4 – 4.2.6, is not as pronounced as that commonly recognized by the use of $k_1$-$q$-$k_2$

expressions. To overcome this limitation, Equation 4.2.4 was modified for only the base aggregate material by adding two additional constants, $C_1$ and $C_2$, as given in Equation 4.2.8.

$$K = C_1 \frac{(1+e_{in})}{3k}\left(\langle I - I_L \rangle + I_L\right)^{C_2} \tag{4.2.8}$$

The constant $C_2$ has the same effect as $k_2$ in Equation 4.2.7, while the constant $C_1$ can be set to a value such that its combination with $e_{in}$ and $k$ produces the same effect as $k_1$ in Equation 4.2.7. The influence on elastic modulus as computed from Equation 4.2.6 by the use of Equation 4.2.8 is discussed later in this section as results of model calibration are presented.

Detailed steps required for calibration of the constants given in Table 4.2.1 are described in Kaliakin et al. (1987). In general, calibration of the model requires that three consolidated-undrained conventional triaxial compression tests be performed at three different levels of overconsolidation ratio. Data from the hydrostatic compression portion of the tests is used to calibrate the compression parameters of the model. Calibration of the model from these tests resulted in the parameters given in Table 4.2.2. For the base aggregate and silty sand subgrade, Poisson's ratio was specified, meaning that shear modulus and the other elastic moduli were a function of bulk stress. For the base aggregate, the parameter $I_L$ was set purposely low in order to provide for a variation of modulus over all bulk stress levels. For the clay subgrade, a constant shear modulus was selected. The value of $I_L$ was set purposely high in this case to ensure that little variation in modulus occurred over the range of bulk stress expected in this layer. This ensured that the values of modulus used by specification of the properties given in Table 4.2.2 were approximately constant for all levels of loading and for all points within the subgrade layer. This is consistent with the manner in which this material was prepared in the test sections described in Section 3 of this report. The value of shear modulus given in Table 4.2.2 was selected, in part, by relating *CBR* for this material to resilient modulus though Equation 4.2.9 (Heukelom and Klomp, 1962), assuming that resilient modulus was equivalent to elastic or Young's modulus (Equation 4.2.10), and then calculating shear modulus from elastic modulus and an assumed Poisson's ratio of 0.5 (Equation 4.2.11), where a Poisson's ratio of 0.5 represents saturated subgrade loaded in an undrained manner. This produces a value of shear modulus of 5170 kPa when *CBR* = 1.5. Further support for the use of these values and their relationship to resilient modulus values is described below.

$$M_R(psi) = 1500\ CBR \tag{4.2.9}$$

$$E(kPa) = 6.89\,M_R(psi) = 10{,}335\ CBR \tag{4.2.10}$$

$$G(kPa) = \frac{E}{2(1+n)} = 3445\ CBR \tag{4.2.11}$$

**Table 4.2.2** Calibrated bounding surface model parameters for test section materials.

| Parameter | Values | | |
|---|---|---|---|
| | Clay Subgrade | Silty Sand Subgrade | Base Aggregate |
| $l$ | 0.225 | 0.022 | 0.007 |
| $k$ | 0.11 | 0.005 | 0.0018 |
| $M$ | 0.65 | 1.6 | 1.8 |
| $M_E/M_C$ | 1.0 | 1.0 | 0.8 |
| $n$ | - | 0.2 | 0.3 |
| $G$ (kPa) | 5170 | - | - |
| $I_L$ (kPa) | 600.0 | 101.4 | 0.3 |
| $R$ | 2.0 | 1.4 | 2.3 |
| $A$ | 0.02 | 0.02 | 0.02 |
| $T$ | 0.05 | 0.01 | 0.01 |
| $C$ | 0.3 | 0.0 | 0.3 |
| $s_p$ | 1.75 | 1.1 | 1.0 |
| $m$ | 0.02 | 0.02 | 0.02 |
| $h$ | 50.0 | 15 | 50.0 |
| $C_1$ | 1 | 1 | 40 |
| $C_2$ | 1 | 1 | 0.6 |
| $e_{in}$ | 1.30 – 1.39 | 0.537 – 0.547 | 0.223 – 0.259 |
| $I_o$ (kPa) | 225 | 750 | 450 |

Since the use of resilient modulus for the characterization of base aggregate and subgrade materials is commonly used in pavement engineering, additional work was performed to evaluate the range of resilient modulus values predicted by the model described above using the parameters for the different materials given in Table 4.2.2. This was accomplished by using the model to simulate the loading sequence, measurement of strains and calculation of resilient modulus as used in the test specification for resilient modulus tests for aggregate and subgrade soils per AASHTO T 292-91 (AASHTO, 1991). For the base aggregate material, the calculation of resilient modulus from the model simulation results is plotted against bulk stress, $q$, in Figure 4.2.2. The best-fit line in this Figure is from the use of Equation 4.2.7 with values of $k_1$ = 4460

and $k_2$ = 0.63, when $q$ and $M_R$ are in units of psi. According to AASHTO (1993), these values represent a typical base aggregate that would be in a damp condition. Assuming a typical value of $q$ of 20 psi in the base aggregate layer, a layer coefficient for the aggregate of 0.14 is obtained from the AASHTO (1993) equations.

A similar simulation of the resilient modulus test was performed using model parameters for the clay subgrade and silty-sand subgrade where an undrained simulation was performed for the clay subgrade. For the clay subgrade, resilient modulus did not change appreciably with bulk stress, as a result of the high value of $I_L$ used, and changed only moderately for the range of deviatoric stress values used, giving an average value of resilient modulus of approximately 15.5 MPa (2260 psi). According to the Equation 4.2.9, commonly used for cohesive subgrades, this corresponds to a *CBR* of 1.5, whereas the measured *CBR* for the clay subgrade from the test sections was also 1.5. A similar simulation using the silty-sand subgrade parameters resulted in a range of resilient modulus values from 18 to 29 MPa (2600 to 4200 psi) when following the subgrade testing protocol and 14 to 140 MPa (2000 to 20,000 psi) when following the unbound aggregate testing protocol. These results indicate that the bounding surface plasticity model used for the base aggregate and subgrade soils provides a comparable description of elastic properties commonly used in conventional pavement engineering practice.

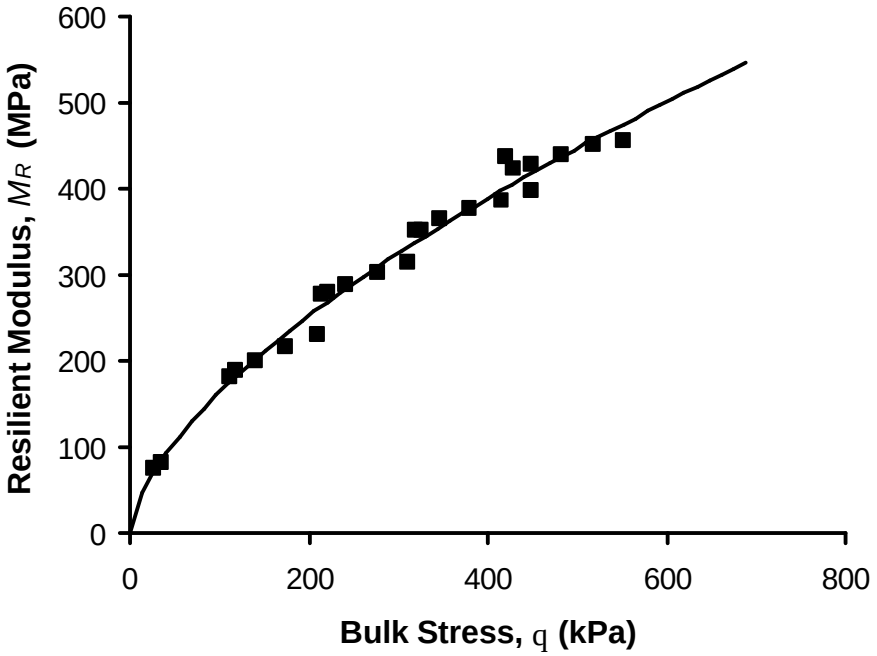


**Figure 4.2.2** Predicted resilient modulus values from base aggregate bounding surface model.

## 4.3 Geosynthetics

A linear elastic, anisotropic model was used for the geosynthetic material. This type of model was chosen for several reasons. The finite element model described in Section 5 was developed to provide stress and strain response measures for one cycle of pavement load. Results from test sections have indicated that the dynamic strain, or the strain for one load cycle, induced in the geosynthetic is relatively small and is most likely within the elastic range for most geosynthetic products. In addition, tension testing and data analysis protocols are not readily available for the identification of material properties for more complex material models involving plasticity or creep.

The finite element model described in Section 5 incorporates membrane elements for the geosynthetic. These elements possess the property of having load carrying capacity in tension but no capacity in compression and no resistance to bending. These elements are ideally suited for describing the behavior of flexible sheets with little to no out-of-plane flexural stiffness. Membrane elements with a thickness of 1 mm were used.

The anisotropic linear elastic model developed is given by Equation 4.3.1, where *xm*, *m* and *n* correspond to the cross-machine, machine and normal directions, respectively, of the geosynthetic. The model contains an elastic modulus for each principal material direction. Response normal to the geosynthetic does not impact the material's behavior, meaning that $E_n$ is chosen only to ensure stability of the elastic matrix. Values of elastic modulus are based on the assumed 1 mm thickness of the material.

$$\begin{Bmatrix} e_{xm} \\ e_{m} \\ e_{n} \\ g_{xm-m} \\ g_{xm-n} \\ g_{m-n} \end{Bmatrix} = \begin{bmatrix} 1/E_{xm} & -n_{m-xm}/E_m & -n_{n-xm}/E_n & 0 & 0 & 0 \\ -n_{xm-m}/E_{xm} & 1/E_m & -n_{n-m}/E_n & 0 & 0 & 0 \\ -n_{xm-n}/E_{xm} & -n_{m-n}/E_m & 1/E_n & 0 & 0 & 0 \\ 0 & 0 & 0 & 1/G_{xm-m} & 0 & 0 \\ 0 & 0 & 0 & 0 & 1/G_{xm-n} & 0 \\ 0 & 0 & 0 & 0 & 0 & 1/G_{m-n} \end{bmatrix} \begin{Bmatrix} s_{xm} \\ s_{m} \\ s_{n} \\ t_{xm-m} \\ t_{xm-n} \\ t_{m-n} \end{Bmatrix} \quad (4.3.1)$$

Three independent Poisson's ratios ($n_{ij}$) and three shear moduli ($G_{ij}$) are contained in the model. The three values of *G* are set equal to one another. The three Poisson's ratios specified are $n_{xm\text{-}m}$, $n_{xm\text{-}n}$ and $n_{m\text{-}n}$, where these are set equal to one another. The remaining three are

calculated from the relationship given in Equation 4.3.2, which is necessary for stability of the elastic matrix.

$$n_{ij} = n_{ji} \frac{E_i}{E_j} \tag{4.3.2}$$

The importance and practical significance of the elastic constants contained in Equation 4.3.1 was examined by creating a finite element model of the geosynthetic consisting of a one element model to which a biaxial load was applied. This type of loading is comparable to that which would be experienced by the geosynthetic in base reinforcement applications. Axial displacement in each material direction of the applied load allowed for an apparent or effective tensile stiffness or modulus to be calculated for each direction. This value was computed by dividing the applied load in each direction by the original sample width and then by the axial strain in the direction of the load. The effect of the ratio of specified modulus in the machine and cross-machine directions (i.e. $E_m/E_{xm}$) was examined by using the material parameter sets for cases 1-5 shown in Table 4.3.1. The effect of reducing Poisson's ratio from 0.5 to 0 is seen from cases 1 and 6. Results of apparent stiffness are given in Table 4.3.2. These results show that the effect of modulus anisotropy is to reduce the effective tensile stiffness of the material in each material direction. A decrease of the effective modulus results in greater lateral movement of the base aggregate and greater shear strain induced in the top of the subgrade. The effect of reducing Poisson's ratio is also seen to result in a reduction of the effective tensile stiffness in each material direction. Poisson's ratio describes the ability of the material to transmit load between the two principal material directions.

**Table 4.3.1** Geosynthetic material properties for biaxial loading.

| Case | $E_{xm}$ (MPa) | $E_m$ (MPa) | $E_n$ (MPa) | $n_{xm-m}$ | $n_{xm-n}$ | $n_{m-n}$ | $G_{xm-m}$ (MPa) | $G_{xm-n}$ (MPa) | $G_{m-n}$ (MPa) |
|---|---|---|---|---|---|---|---|---|---|
| 1 | 100 | 100 | 100 | 0.5 | 0.5 | 0.49 | 33 | 33 | 33 |
| 2 | 100 | 75 | 75 | 0.5 | 0.5 | 0.49 | 33 | 33 | 33 |
| 3 | 100 | 50 | 50 | 0.5 | 0.5 | 0.49 | 33 | 33 | 33 |
| 4 | 100 | 25 | 25 | 0.5 | 0.5 | 0.49 | 33 | 33 | 33 |
| 5 | 100 | 10 | 10 | 0.5 | 0.5 | 0.49 | 33 | 33 | 33 |
| 6 | 100 | 100 | 100 | 0 | 0 | 0 | 33 | 33 | 33 |

**Table 4.3.2** Geosynthetic apparent stiffness for biaxial loading.

| Case | Apparent stiffness in *xm* direction (kN/m) | Apparent stiffness in *m* direction (kN/m) |
|---|---|---|
| 1 | 200 | 200 |
| 2 | 169 | 138 |
| 3 | 143 | 86 |
| 4 | 120 | 40 |
| 5 | 108 | 15 |
| 6 | 100 | 100 |

Variations in the shear modulus do not result in changes in apparent stiffness for this type of loading where shear stresses are not introduced. For pavement loading applications, however, it is anticipated that radial loading of the geosynthetic as base aggregate spreads laterally in all radial directions will result in in-plane shear stresses being introduced in the geosynthetic. For this case, reduction of the shear modulus results in greater movement of the geosynthetic in radial directions off the principal axes of the material and a corresponding reduction in reinforcement benefit, as illustrated in Section 7.4.

Material discussed in Section 2.1 indicated that tensile modulus has a significant impact on reinforcement benefit derived from the geosynthetic. Use of the material model described above allows for the influence of the isotropic elastic modulus to be examined. The introduction of anisotropy of the elastic modulus allows for this effect on pavement response to be examined, where the results presented above suggest that this material effect is important. Use of an anisotropic model also allows the shear modulus to be reduced.

The selection of values for the geosynthetic material model is based partly on information that can be extracted from wide-width tensile tests, ASTM 4595 (ASTM, 2001a), and partly on the assignment of typical values anticipated for various classes of geosynthetics. In particular, values of elastic modulus in the machine and cross machine directions, $E_{m,}\, E_{xm}$, can be estimated from ASTM 4595 while values of Poisson's ratio and shear modulus need to be assigned by other means.

Values for elastic modulus in the machine and cross-machine directions ($E_{m,}\, E_{xm}$) are derived from values of secant tensile modulus in these material directions from wide-width tension tests. It should not necessarily be expected that a one-to-one correspondence exists between elastic modulus used in the material model described above and secant tensile modulus determined from wide-width tension tests. As described in Section 7.6, the relationship between

these two parameters is established by comparison of predictions from the mechanistic-empirical model to results from test sections.

The ratio between secant modulus from the two principal directions of the geosynthetic as seen from wide-width tensile tests is maintained in the material model described above, but the magnitude of the modulus values is not necessarily the same. Differences in magnitude are expected for several reasons. The material model described above assumes a certain thickness for the geosynthetic, which then governs the selection of elastic modulus. The finite element response model using the geosynthetic material model described above is based on one load application and is pertinent to a small strain response of the geosynthetic. Secant tensile modulus from ASTM 4595 at values of axial strain less than 2 % are not commonly reported. Strains of 2 % in the geosynthetic for the first load application of a pavement are significantly higher than what would normally be expected. Finally, the rate of load application is as much as 100 times faster in the pavement application than in a wide-width tension test. The combination of these effects suggests that the values of elastic modulus as used in Equation 4.3.1 should be expected to be greater than values of secant tensile modulus determined from ASTM 4595.

Test methods for the definition of Poisson's ratio and shear modulus, as defined in Equation 4.3.1, do not currently exist. In addition, values for these two material properties for various geosynthetics have not been reported. The design model, however, indicates that reinforcement benefit is moderately sensitive to variations of these two parameters, as is demonstrated in Section 7.4. Given the absence of test methods and typical values for these properties, the design model described in Section 7 defines reinforcement benefit (or more specifically a reduction factor applied to reinforcement benefit) in terms of two values for Poisson's ratio and two values for shear modulus, where these two values describe either good or poor conditions for benefit.

The design model has been calibrated from test section results using two extruded geogrids of the same manufacturing process and one woven geotextile. The calibration process involved the assignment of either good or poor values for these properties such that benefit from the test section results could be matched. As such, it is suggested that these two properties be related to the geosynthetic type and structure. Additional results from test sections using a wider range of geosynthetic products is necessary prior to being able to develop specific guidelines for selection of these two properties. In the absence of these results, the values used for the two types of

products used in test sections for which the design model was calibrated should be used as a starting point. The qualitative application guidelines for geosynthetic type given in Table 2.1.2 derived from the GMA WPII (Berg et al., 2000) may also be used in the assignment of these values.

Differences in interface shear properties may also be responsible for the differences in pavement performance seen between various geosynthetics. As discussed in Section 2.1 and 2.6, small displacement shear stiffness of the interface is most likely the key material parameter for this component of the reinforced pavement system. Existing test protocols and test data are, however, not currently available to explicitly define this property. The design model presented in Section 7 uses a reduction factor for interface shearing resistance that has been calibrated for the two types of geosynthetics used in previously constructed test sections. These values serve as a starting point for geogrid and geotextile type materials. Further definition of this reduction factor for other geosynthetic materials should come from additional test section results or from further laboratory interface testing.

## 5.0 PAVEMENT TEST FACILITY FINITE ELEMENT MODEL

A finite element model was created to simulate the pavement layer thicknesses, boundary conditions and loading present in the pavement test sections described in Section 3. All modeling was done using the commercial program ABAQUS (Hibbitt, Karlson and Sorensen, 1998). Three types of models were created. The first is a model of pavement test sections without reinforcement and is described in Section 5.1. The second is a model where reinforcement is described in such a way that it represents the maximum amount of reinforcement benefit that could be expected with a “perfect” reinforcement product. Since effects of the reinforcement are ultimately expressed in terms of prevention of lateral movement of the base aggregate at the level of the geosynthetic, perfect reinforcement is simulated by modifying the unreinforced model by preventing all in-plane or lateral motions of the base aggregate element nodes at the level of the geosynthetic. This in effect simulates reinforcement with an infinitely stiff geosynthetic and an infinitely stiff contact shear interface between the geosynthetic and the aggregate. This model is described in Section 5.2. The third type of model created is one where a separate material layer corresponding to the geosynthetic is added to the unreinforced model and is described in Section 5.3.

This approach of creating three types of finite element models was taken to describe the effects of reinforcement in a systematic way that isolates the effects of each variable or group of variables on the system. The unreinforced models provide response parameters for pavements without any type of reinforcement, where these response parameters are described in Section 5.4. The perfect reinforced models do not contain parameters associated with the geosynthetic. Any benefit from the effect of the perfect reinforcement model is then a function of the remaining pavement system variables, which include AC and base aggregate thickness, and subgrade stiffness. From these results, conclusions can be made regarding the combinations of structural section thickness and subgrade stiffness for which perfect reinforcement provides benefit. The third type of model contains a reinforcement layer with corresponding material properties. Variation of these properties allows for conclusions to be made regarding how those properties modify or reduce the maximum benefit seen from the corresponding perfect reinforcement case. Execution of models according to this approach minimizes the number of cases that need to be analyzed and provides for a systematic method for interpreting the results.

## 5.1 Unreinforced FE Model

The finite element model of unreinforced pavements is a 3-dimensional model created to match the nominal conditions for the pavement test facility described in Section 3. A two-dimensional axi-symmetric model was not used because of the potential influence of the box's square corners and for the later inclusion of a layer of geosynthetic reinforcement that has direction dependent material properties. Symmetry of the box was recognized such that a model of one-quarter of the box was created. Figure 5.1.1 illustrates the geometry and boundary conditions used for the development of the model. Actual layer thicknesses for the AC and base aggregate are described in Section 6.

The width in the *x* and *y* directions of the ¼ box modeled was 1 m. The pavement load was applied as a pressure equal to 550 kPa over one-quarter of a circular plate having a radius of 152 mm. The load plate and rubber pad used in the pavement test sections described in Section 3 were modeled by plates having a radius of 152 mm. The load plate had a thickness of 25 mm and was given isotropic elastic properties with a Young's modulus of $2\times10^8$ kPa and a Poisson's ratio of 0.33. The rubber pad had a thickness of 4 mm and was also given elastic properties with a Young's modulus of 400 kPa and a Poisson's ratio of 0. The pavement load was applied in a

ramp step up to its maximum pressure of 550 kPa. Given that the material models used for the three pavement layers were independent of time, it was not necessary to match the exact time-history of the pavement load.

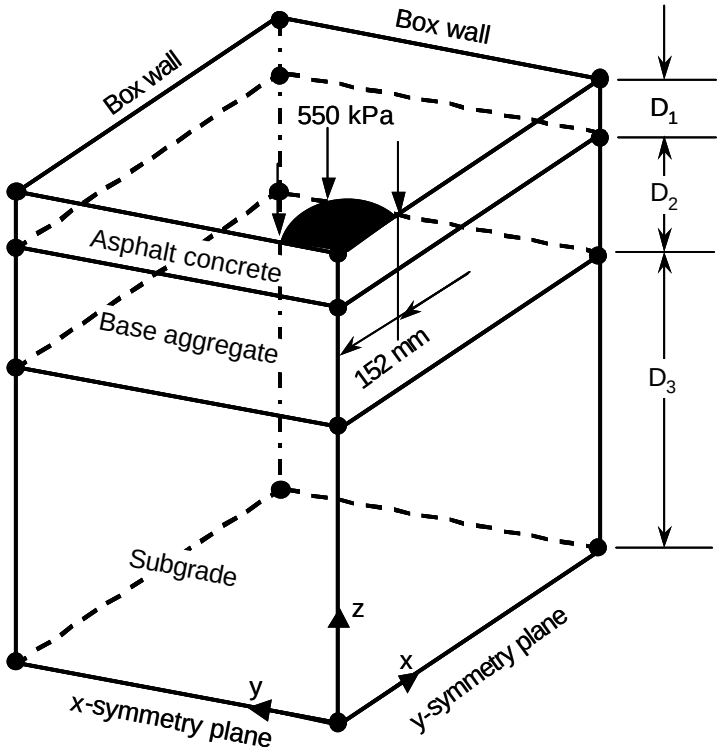


**Figure 5.1.1** Finite element model of unreinforced pavement test sections.

The vertical edge directly beneath the load plate centerline was a symmetry line and was therefore constrained from motion in the *x* and *y* dimensions and free from constraints in the *z* direction. The four faces of the box were constrained in a direction perpendicular to the box face and in the second horizontal direction parallel to the box wall, and otherwise free of constraint in the *z* direction. The nodes along the perimeter of the asphalt concrete layer directly adjacent to the box walls were free of all constraints such that the nodes were free to move in from the box wall as pavement load was applied. This boundary condition removed an artificial attachment of the asphalt concrete to the walls of the box and thereby prevented tensile loads from developing in the asphalt concrete. The symmetry planes of the model were unconstrained in the *z* direction and in the horizontal direction parallel to the plane. Motion in the horizontal direction perpendicular to the plane was constrained.

Eight-noded hexagonal solid elements were used for all material layers. Approximately 42 elements were used for each of the load plate and rubber pad while 230, 570 and 1710 elements were used for the asphalt concrete, base aggregate and subgrade layers, respectively. The nodes between the material layers were equivalenced and therefore connected.

## 5.2 Perfect Reinforced FE Model

In order to reduce the number of model cases analyzed under the parametric study described in Section 6 and to provide for a systematic approach to interpreting results, a series of model cases were analyzed where the reinforcement was modeled in such a way as to provide for the maximum effect on pavement performance. Within the context of the material and finite element models developed for this project, the principal effect of reinforcement on the performance of the pavement is the prevention of lateral strain or displacement of the base aggregate at the interface with the geosynthetic. Maximum effect of a reinforcement layer could thereby be simulated by preventing all lateral motion of the base course aggregate at the level where it would be in contact with the geosynthetic. This was accomplished by modifying the unreinforced model described in Section 5.1 by prescribing boundary conditions to the nodes at the bottom of the base aggregate, where these boundary conditions prevented all $x$ and $y$ motion of the nodes. According to this approach, a geosynthetic layer was not explicitly included in this type of finite element model.

For these models, the simulated reinforcement effectively has an infinite tensile stiffness and an infinitely stiff contact interface with the base aggregate. The observation of reinforcement benefit, or the lack thereof, was then due to the influence of pavement variables other than geosynthetic properties. The variables associated with the pavement that are believed to have the most significant influence on reinforcement benefit are thickness of the AC and base aggregate layer and the properties of the subgrade dictating its stiffness and strength. This is a relatively small number of variables in comparison to that which would be introduced if an actual layer of reinforcement with its own set of material properties was introduced. Results from model cases using the perfect reinforced model are used to make conclusions regarding the influence of the structural section thickness and subgrade properties on reinforcement benefit. Additional work with the model described in Section 5.3 is then used to modify and reduce reinforcement benefit

observed for cases of perfect reinforcement by the influence of specific properties pertinent to geosynthetics.

## 5.3 Geosynthetic Reinforced FE Model

A third type of finite element model was created where a sheet of geosynthetic reinforcement was included as part of the pavement cross-section. The geosynthetic was modeled by 4 noded membrane elements that have the property of containing tensile load carrying capacity, but have no resistance in bending or compression. Membrane elements are two-dimensional elements that are commonly used for describing flexible sheets having tensile load carrying capacity. The material model described in Section 4.3 was used for the geosynthetic. In all cases, the geosynthetic was placed between the base aggregate and the subgrade. The nodes of the geosynthetic were equivalenced with the nodes in the base aggregate above and the subgrade material below such that the three materials moved together as a unit. This approach isolates the effect of geosynthetic material properties from those of interface properties. The effect of contact interface properties is accounted for by comparison of model predictions where all other properties have been accounted for to test section results. Remaining reductions in benefit are then due to the influence of contract properties.

## 5.4 Response Parameters and Extension to Reinforcement Benefit

The types of models described in Sections 5.1 – 5.3 were executed with two response measures extracted from the models to characterize pavement performance and eventually used to describe reinforcement benefit. From material presented in Section 3.2, it was seen that reinforcement benefit, defined in terms of an extension of life of the pavement, could be broken into reinforcement effects on the base aggregate layer and on the subgrade layer. Partial traffic benefit ratios for the base and subgrade ($TBR_B$ and $TBR_S$) were defined and determined directly from test section data for the various test sections available.

Test section data indicated that vertical strain in the top of the subgrade at peak load for the first load cycle could be related to the number of load cycles necessary to reach 12.5 mm of permanent surface deformation through a well-recognized subgrade rutting model (Huang, 1993). This model is given again in Equation 5.4.1, where the constants $A$ and $B$ were found to be equal to $1.8\times10^{-5}$ and 4.07, respectively, from the test sections reported in Section 3.

$$N_{12.5\,mm} = Ae_v^{-B} \tag{5.4.1}$$

If the vertical strain in Equation 5.4.1 is evaluated for comparison reinforced and unreinforced pavement sections, then the ratio of the number of load cycles necessary to reach 12.5 mm of permanent surface deformation will be given by Equation 5.4.2.

$$\frac{N_{12.5mm-R}}{N_{12.5mm-U}} = \left(\frac{e_{v-R}}{e_{v-U}}\right)^{-B} \tag{5.4.2}$$

where the symbols *R* and *U* denote reinforced and unreinforced pavement sections. The ratio of load cycles or vehicle passes necessary to reach 12.5 mm of surface deformation provides a direct definition of *TBR* at this rut depth. Since this definition of *TBR* involves an effect of the reinforcement only on the subgrade, the value is viewed as a partial *TBR* describing only subgrade effects and is taken as the same $TBR_S$ defined in Section 3.2. According to this formulation, the first response measure extracted from the models is the vertical compressive strain in the top of the subgrade directly beneath the load plate centerline when the pavement load has been fully applied for comparison reinforced and unreinforced test sections. Values of vertical compressive strain are extrapolated from integration points within the first element in the subgrade in order to extrapolate back to a value at the top of the subgrade. $TBR_S$ is then defined from model response parameters by Equation 5.4.2

$$TBR_S = \left(\frac{e_{v-R}}{e_{v-U}}\right)^{-B} \tag{5.4.2}$$

where *B* was calibrated from test section data and found to equal 4.07. The use of Equation 5.4.2 with the vertical strain results for the test sections given in Table 3.2.2 results in the values given in Table 5.4.1, which are compared to the values of $TBR_S$ defined directly from load cycle numbers reported in Table 3.2.2. Any discrepancies between the two values for a given test section are due to the inability of Equation 5.4.2 to fully describe results seen from test sections, where these discrepancies were shown previously in Figure 3.2.10.

**Table 5.4.1** $TBR_S$ for reinforced test sections.

| Section | $TBR_S$ (Table 3.2.1) | $TBR_S$ (Equation 5.4.2) |
|---|---|---|
| CS5 | 2.95 | 3.54 |
| CS6 | 1.66 | 1.59 |
| CS7 | 3.13 | 4.45 |
| CS10 | 2.23 | 2.67 |
| CS11 | 2.61 | 2.40 |

The second response measure extracted from the finite element models is a measure that describes reinforcement effects on the base aggregate. It has been speculated that reinforcement has the effect of providing confinement to the aggregate and thereby increasing bulk stress. An increase in bulk stress has the effect of increasing stiffness of the base aggregate layer. Due to the difficulties in measuring lateral stress and the difficulty of measuring stress components at more than just several points within the base layer of test sections, this reinforcement mechanism has not been verified experimentally but the direct effects of the mechanism have.

In the finite element models, bulk stress is extracted from a number of integration points within the base aggregate layer when the full pavement load has been applied. Since bulk stress changes from point to point within the aggregate layer, it is necessary to define a representative or average value of bulk stress for the layer. The volume of aggregate used to define the average is concentrated around and under the applied load since this is the material that is responsible for spreading the load to the underlying subgrade. The geometry used to define the volume of aggregate over which the bulk stress is averaged corresponds to a right frustum shown in Figure 5.4.1. Also shown on this figure are curves of normalized vertical stress at three depths in the aggregate caused by a uniform pressure on the circular plate shown. The volume used is seen to be an approximation of the zone of most significant stress intensity. It should be noted that typical recommendations for the selection of bulk stress for use in the determination of resilient modulus from laboratory tests rely upon input only from stresses along the load centerline. Within the volume shown in Figure 5.4.1, greater weight is given to values along the load plate centerline and towards the bottom of the base layer according to the averaging and weighting Equation 5.4.3, where $q_{avg}$ is the average bulk stress for the volume of base, $q_i$ is the value of bulk stress at each integration point within the volume, $V_i$ is the material volume associated with each integration point, $r_i$ is the radius from the load centerline to the integration point, $z_i$ is the

vertical distance from the bottom of the base to the integration point, and $n$ is the number of integration points within the volume for which values of $q_i$ are collected.

$$q_{avg} = \frac{\sum_{i=1}^{n} q_i \left( \frac{V_i}{r_i \; z_i} \right)^2}{\sum_{i=1}^{n} \left( \frac{V_i}{r_i \; z_i} \right)^2} \tag{5.4.3}$$

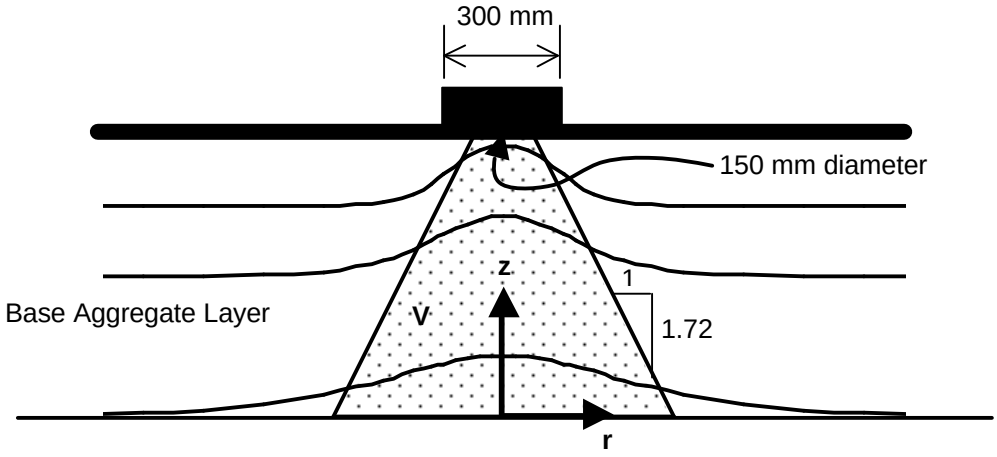


**Figure 5.4.1** Volume used for averaging bulk stress in the base aggregate layer.

To account for the effect of differences in bulk stress between reinforced and unreinforced pavement sections, Equation 4.2.7 (repeated below as Equation 5.4.4) is used to relate bulk stress to resilient modulus of the base aggregate layer. Reinforcement has, in general, the effect of increasing bulk stress for the base course layer; Equation 5.4.4 thereby accounts for reinforcement effects in the base layer by an increase in the layer's resilient modulus.

$$M_R = k_1 q^{\,k_2} \tag{5.4.4}$$

From Section 4.2, it was demonstrated that the constants $k_1$ and $k_2$ take on values of 4460 and 0.63 (when $q$ and $M_R$ are in units of psi) using the bounding surface plasticity model and model parameters given in Section 4.2. These values are used below to account for bulk stress effects in the base aggregate layer.

The 1993 AASHTO pavement design equation (Equation 5.4.5) is used to calculate the number of ESAL's ($W_{18}$) for a reinforced and an unreinforced pavement section for which $q$ has been individually evaluated and $M_R$ determined from Equation 5.4.4.

$$W_{18} = 10\text{^}\left[ Z_R\ S_o + 9.36\log(SN+1) - 0.2 + \frac{\log\left(\frac{\Delta PSI}{4.2-1.5}\right)}{0.4 + \frac{1094}{(SN+1)^{5.19}}} + 2.32\log(M_S) - 8.07 \right] \qquad (5.4.5)$$

In Equation 5.4.5, $Z_R$ is the standard normal deviate, $S_o$ is the combined standard error and *DPSI* is the loss of design serviceability. Values of $Z_R$, $S_o$ *DPSI* have been taken as constants for all pavement geometries analyzed and have been given values of -1.645, 0.35 and 1.9, respectively, where the value of $Z_R$ used corresponds to a reliability of 95 %. In Equation 5.4.5, $M_S$ is the effective roadbed (subgrade) resilient modulus where values are assigned according to Equation 4.2.9 for the different subgrades modeled. The structural number (*SN*) in Equation 5.4.5 is given by

$$SN = a_1 D_1 + a_2 D_2 m_2 \qquad (5.4.6)$$

where $a_1$ and $a_2$ are the layer coefficients of the asphalt concrete and base aggregate layers, respectively, $D_1$ and $D_2$ are the thicknesses of the AC and base layers, respectively, and $m_2$ is the drainage coefficient of the base layer. The layer coefficient $a_1$ is taken as 0.4, which was shown in Section 4.1 to be comparable with the modulus values used for this layer in the finite element models. The drainage coefficient is taken as 1.0. The base layer coefficient, $a_2$, is given in terms of resilient modulus by Equation 5.4.7 (AASHTO, 1993).

$$a_2 = 0.249(\log M_R) - 0.977 \qquad (5.4.7)$$

Based on a particular pavement geometry, defining values of $D_1$ and $D_2$, and a value for $M_S$, the finite element model is analyzed for the reinforced and unreinforced case with values of mean stress extracted from each. Equations 5.4.5 – 5.4.7 are used to evaluate $W_{18}$ for the reinforced and unreinforced pavements. The ratio of $W_{18}$ for the reinforced and unreinforced pavements

then defines a *TBR* for reinforcement of the base, with this *TBR* viewed as a partial *TBR* and written as:

$$TBR_B = \frac{W_{18-R}}{W_{18-U}} \tag{5.4.8}$$

The two partial *TBR*'s need to be combined together to define a total *TBR* for the pavement. An explicit expression between partial and total *TBR* that involves only load cycle and rut depth parameters is not possible without making significant assumptions regarding the shape of the surface deformation versus load cycle curves. It is possible, however, to compute a total *TBR* through the use of the AASHTO 1993 pavement design equation (Equation 5.4.5). This is done by using Equation 5.4.5 to determine an increased resilient modulus for the subgrade that produces a *TBR* for the subgrade as defined from Equation 5.4.2, while the base layer coefficients are equal for reinforced and unreinforced cases. Base and subgrade effects are then combined together in Equation 5.4.5 by keeping the higher resilient modulus for the subgrade and including the mean stress effect of the higher resilient modulus for the base layer. Because of the log nature of Equation 5.4.5 and the effect of increases in resilient modulus of the subgrade and increases in structural number due to an increase in base layer modulus, this approach is the same as defining the total *TBR* from the product of the partial *TBR*'s (Equation 5.4.9).

$$TBR_T = TBR_B \times TBR_S \tag{5.4.9}$$

The use of Equation 5.4.9 is conservative in comparison to that which has been observed from test sections described in Section 3. Examination of Table 3.2.1 shows that the use of Equation 5.4.9 to compute $TBR_T$ from $TBR_B$ and $TBR_S$ yields values that are in all cases less than the values of $TBR_T$ observed directly from test section results. It should be noted that all *TBR*'s discussed above pertain to values for the condition where *BCR* = 0.

## 6.0 PARAMETRIC STUDY AND RESULTS

Material presented in Section 2.1 indicated that current research work shows that the benefit derived from geosynthetic reinforcement is strongly dependent on design parameters associated with the pavement system and on material properties and characteristics associated with the geosynthetic. Reinforcement benefit is generally seen to be dependent on the strength and/or

stiffness of the subgrade layer. Reinforcement benefit generally increases as subgrade *CBR* decreases. Reinforcement benefit is generally thought to be negligible above a subgrade *CBR* of 8. Reinforcement benefit is also dependent on the thickness of the structural section of the pavement, including the AC and base aggregate. For very thin sections with low structural numbers, base reinforcement does not appear to offer significant benefit. As structural sections become very thick, reinforcement benefit is seen to diminish. As described in Section 5, a finite element model simulating perfect reinforcement was created to examine the effect of these pavement variables (AC and base thickness, and subgrade properties) on reinforcement benefit. Results from this model involving cases where these parameters are varied are described in Section 6.1.

Material presented in Section 2.1 indicated that tensile modulus of the geosynthetic is an important design parameter, suggesting also that the ratio of modulus in the weak and strong directions of the material should be important. The definition of other material properties related to the type and structure of the geosynthetic that can be used directly in a structural analysis of a reinforced pavement is not as clear. Material presented in Section 4.3 indicated that certain properties within the context of an anisotropic linear elastic model for the geosynthetic could be varied and shown to affect the apparent or effective stiffness of the material under biaxial loading. These parameters (Poisson's ratio and shear modulus) are shown here and in Section 7 to have a seconday influence on reinforcement benefit.

## 6.1 Variation of Parameters for Perfect Reinforced Models

All models examined under the parametric study used the same properties for the asphalt concrete and base aggregate layer as described in Sections 4.1 and 4.2, respectively. Material parameters for the asphalt concrete and base aggregate were given in Tables 4.1.2 and 4.2.2, respectively. As discussed previously, the values of modulus used for the asphalt concrete approximate a material with a layer coefficient of 0.4 (AASHTO, 1993). The resilient modulus values that were inferred from the use of the material model for the base aggregate represented an aggregate in a damp state with a layer coefficient ranging from 0.08 to 0.12.

For the perfect reinforced models, AC thickness, base thickness and subgrade properties were varied. The values of AC thickness and base thickness used, along with corresponding case names, are given in Table 6.1.1 and 6.1.2.

**Table 6.1.1** AC thickness in parametric study.

| AC Thickness Case Name | AC1 | AC2 | AC3 | AC4 | AC5 |
|---|---|---|---|---|---|
| AC Thickness (mm) | 50 | 75 | 100 | 125 | 150 |

**Table 6.1.2** Base thickness in parametric study.

| Base Thickness Case Name | B1 | B2 | B3 | B4 | B5 | B6 |
|---|---|---|---|---|---|---|
| Base Thickness (mm) | 150 | 200 | 250 | 300 | 400 | 600 |

Parameters contained in the bounding surface model for the subgrade were varied to represent subgrades of varying stiffness and strength. Six different subgrade types were modeled where the target *CBR* ranged from 0.5 to 15. The parameters in the bounding surface model most responsible for overall stiffness and strength for situations where one load cycle is applied are $G$, $M$, $l$, $k$, $I_o$ and $e_{in}$. Values of each parameter for the 6 different subgrade cases are given in Table 6.1.3. Values of $G$ were estimated for different values of *CBR* from Equation 4.2.11, which was previously shown in Section 4.2 to simulate a resilient modulus value comparable to that which would be predicted by the use of Equations 4.2.9 – 4.2.11. Values of $M$ were assumed to vary linearly between a value of $M$ of 0.62 for a *CBR* of 0.5 and a value of 1.0 for a *CBR* of 15. Values of compression index, $l$, were estimated from Equation 6.1.1 (Holtz and Kovacs, 1981), which represents remolded clays. The liquid limit used in Equation 6.1.1 was assumed to vary linearly between 85 and 44 for values of *CBR* of 0.5 to 15. Values of $k$ were assumed to be one-half the values of $l$. Values of preconsolidation pressure, $I_o$, were estimated from critical state soil mechanics concepts and were dependent on values of $M$, $l$, $k$. Values of $e_{in}$ were assumed to vary linearly between 1.35 and 0.57 for values of *CBR* of 0.5 and 15. All other parameters in the model were kept identical to those of the clay subgrade as given in Table 4.2.2.

$$l = 0.003(LL - 7) \tag{6.1.1}$$

Each set of material properties for the subgrade was used in the subgrade material model to simulate a resilient modulus test for cohesive materials per AASHTO (1991), as previously described in Section 4.2. Measurement of strain from the resilient modulus test simulation allowed for the resilient modulus to be computed, which is listed in Table 6.1.3. Equation 4.2.9 was then used to estimate *CBR*, where it is seen that the target *CBR* used to estimate the model

properties $G$, $M$, $l$, $k$, $I_o$ and $e_{in}$ is nearly identical to that estimated from the simulation of the resilient modulus test.

**Table 6.1.3** Subgrade properties in parametric study.

| Subgrade Case Name | Target *CBR* | $G$ (MPa) | $M$ | $l$ | $k$ | $I_o$ (kPa) | $e_{in}$ | $M_R$ (MPa) | *CBR* Equation 4.2.9 |
|---|---|---|---|---|---|---|---|---|---|
| S1 | 0.5 | 1.72 | 0.62 | 0.233 | 0.117 | 303 | 1.35 | 5.26 | 0.509 |
| S2 | 1 | 3.45 | 0.64 | 0.229 | 0.115 | 615 | 1.33 | 10.3 | 0.998 |
| S3 | 2 | 6.89 | 0.66 | 0.220 | 0.110 | 1520 | 1.27 | 20.4 | 1.98 |
| S4 | 4 | 13.8 | 0.72 | 0.204 | 0.102 | 4560 | 1.16 | 42.1 | 4.08 |
| S5 | 8 | 27.6 | 0.84 | 0.170 | 0.085 | 15,200 | 0.95 | 83.6 | 8.08 |
| S6 | 15 | 51.7 | 1.0 | 0.111 | 0.056 | 43,500 | 0.57 | 154 | 15.0 |

The combination of the 5 AC thickness values, 6 base course thickness values and 6 subgrade types resulted in 180 runs. Identical runs were performed for unreinforced models and reinforcement modeled by perfect reinforcement, resulting in 360 individual runs. Table 6.1.4 presents the case names and values of the two response measures collected for each model run. Values of $TBR_S$ and $TBR_B$ computed according to the material presented in Section 5.4 are also presented. Results from Table 6.1.4 are used in Section 7.1.1 for the development of equations describing general trends in the data.

From Table 6.1.4, it is seen that values of *TBR* decrease as the subgrade *CBR* increases, which is consistent with experimental observations. For a subgrade with a CBR of 15, values of *TBR* are seen to be nearly equal to one in comparison to values seen for lower strength subgrades. Variations of *TBR* with structural section thickness indicate lower values of benefit for very thin sections and for sections that are thicker than some critical value. These trends are made clearer in Section 7.1. Values of $TBR_B$ are generally small in comparison to $TBR_S$, with the exception of cases with the thickest base section used. These results are taken as not being representative of the model and are treated in Section 7 in such a way that these high values are ignored. The relatively high values of $TBR_S$ are expected and are reduced for actual geosynthetic modulus values in later sections.

Results from the parametric study for the 180 perfect reinforcement cases analyzed can also be used to assess *BCR*, or more specifically combinations of *BCR* and *TBR* for certain comparison sets. For each unreinforced case where reinforced runs were made for the same AC thickness, the same subgrade condition and for reduced base thickness, a value of *BCR* is known

or presumed from the established base thickness of the unreinforced and reinforced models. For instance, if case AC1-B6-S1 for an unreinforced pavement is compared to AC1-B5-S1 for a reinforced case, a *BCR* of 33 % is presumed as the two models are established. From the 360 model runs, 75 sets of unreinforced and reinforced comparison runs, where a *BCR* was presumed, were available for each of the 6 subgrade conditions, giving 450 comparisons for the 6 subgrade conditions. The response measures of vertical subgrade strain and bulk stress in the base aggregate were compared between these comparison runs to assess $TBR_S$ and $TBR_B$. Values greater than one indicate a remaining *TBR* for the assumed *BCR*. Values less than one indicate that the assumed *BCR* resulted in a reduction of life of the reinforced pavement as compared to the reinforced section.

**Table 6.1.4a** Response measures from unreinforced and perfect reinforced models (subgrade $CBR = 0.5$).

| Model Name | Unreinforced | | Perfect Reinforcement | | $TBR_S$ | $TBR_B$ |
|---|---|---|---|---|---|---|
| | $e_v$ (%) | $q$ (kPa) | $e_v$ (%) | $q$ (kPa) | | |
| AC 1 - B 1 - S 1 | 8.160 | 175.21 | 3.451 | 417.95 | 33.2 | 3.0 |
| AC 2 - B 1 - S 1 | 4.632 | 148.94 | 2.041 | 338.53 | 28.1 | 2.5 |
| AC 3 - B 1 - S 1 | 3.403 | 128.91 | 1.441 | 289.94 | 33.0 | 2.2 |
| AC 4 - B 1 - S 1 | 2.400 | 107.78 | 0.909 | 230.16 | 52.0 | 2.0 |
| AC 5 - B 1 - S 1 | 1.269 | 93.47 | 0.584 | 177.77 | 23.6 | 1.7 |
| AC 1 - B 2 - S 1 | 6.616 | 153.81 | 2.654 | 357.46 | 41.2 | 3.6 |
| AC 2 - B 2 - S 1 | 3.240 | 127.85 | 1.463 | 288.51 | 25.5 | 3.0 |
| AC 3 - B 2 - S 1 | 2.296 | 115.72 | 0.958 | 237.70 | 35.0 | 2.4 |
| AC 4 - B 2 - S 1 | 1.555 | 277.48 | 0.599 | 402.81 | 48.5 | 1.4 |
| AC 5 - B 2 - S 1 | 1.048 | 84.44 | 0.370 | 145.86 | 69.1 | 1.8 |
| AC 1 - B 3 - S 1 | 4.851 | 138.68 | 1.955 | 321.92 | 40.3 | 4.2 |
| AC 2 - B 3 - S 1 | 2.218 | 114.74 | 0.936 | 238.51 | 33.5 | 3.2 |
| AC 3 - B 3 - S 1 | 1.525 | 102.44 | 0.578 | 175.79 | 51.7 | 2.2 |
| AC 4 - B 3 - S 1 | 1.110 | 85.66 | 0.332 | 144.85 | 135.3 | 2.0 |
| AC 5 - B 3 - S 1 | 0.787 | 77.21 | 0.230 | 101.01 | 150.2 | 1.4 |
| AC 1 - B 4 - S 1 | 2.790 | 120.85 | 1.105 | 265.59 | 43.3 | 4.5 |
| AC 2 - B 4 - S 1 | 1.447 | 102.10 | 0.496 | 165.65 | 77.9 | 2.4 |
| AC 3 - B 4 - S 1 | 1.064 | 85.81 | 0.289 | 131.28 | 202.0 | 2.1 |
| AC 4 - B 4 - S 1 | 0.792 | 297.82 | 0.215 | 361.12 | 203.4 | 1.3 |
| AC 5 - B 4 - S 1 | 0.558 | 64.33 | 0.191 | 87.53 | 77.8 | 1.6 |
| AC 1 - B 5 - S 1 | 0.994 | 84.63 | 0.252 | 117.60 | 266.4 | 2.3 |
| AC 2 - B 5 - S 1 | 0.668 | 73.24 | 0.186 | 91.62 | 180.9 | 1.7 |
| AC 3 - B 5 - S 1 | 0.495 | 59.04 | 0.164 | 84.49 | 89.7 | 2.2 |
| AC 4 - B 5 - S 1 | 0.392 | 47.38 | 0.158 | 82.87 | 39.7 | 3.2 |
| AC 5 - B 5 - S 1 | 0.323 | 39.34 | 0.160 | 83.81 | 17.5 | 4.3 |
| AC 1 - B 6 - S 1 | 0.257 | 36.19 | 0.146 | 86.40 | 9.9 | 32.0 |
| AC 2 - B 6 - S 1 | 0.209 | 32.15 | 0.129 | 85.79 | 7.2 | 35.0 |
| AC 3 - B 6 - S 1 | 0.186 | 30.99 | 0.127 | 87.26 | 4.8 | 28.6 |
| AC 4 - B 6 - S 1 | 0.179 | 32.08 | 0.132 | 89.76 | 3.4 | 19.7 |
| AC 5 - B 6 - S 1 | 0.170 | 34.46 | 0.145 | 93.25 | 1.9 | 13.7 |

**Table 6.1.4b** Response measures from unreinforced and perfect reinforced models (subgrade $CBR = 1$).

| Model Name | Unreinforced | | Perfect Reinforcement | | $TBR_S$ | $TBR_B$ |
|---|---|---|---|---|---|---|
| | $e_v$ (%) | $q$ (kPa) | $e_v$ (%) | $q$ (kPa) | | |
| AC 1 - B 1 - S 2 | 4.882 | 203.77 | 2.501 | 487.38 | 15.2 | 2.9 |
| AC 2 - B 1 - S 2 | 2.809 | 184.22 | 1.601 | 376.17 | 9.9 | 2.2 |
| AC 3 - B 1 - S 2 | 2.247 | 165.82 | 1.210 | 325.56 | 12.4 | 1.9 |
| AC 4 - B 1 - S 2 | 1.705 | 139.48 | 0.808 | 272.18 | 20.8 | 1.8 |
| AC 5 - B 1 - S 2 | 1.113 | 119.29 | 0.528 | 216.65 | 20.8 | 1.6 |
| AC 1 - B 2 - S 2 | 3.545 | 193.11 | 1.900 | 399.06 | 12.7 | 2.9 |
| AC 2 - B 2 - S 2 | 2.145 | 162.74 | 1.182 | 315.78 | 11.3 | 2.4 |
| AC 3 - B 2 - S 2 | 1.681 | 143.35 | 0.828 | 267.71 | 17.9 | 2.1 |
| AC 4 - B 2 - S 2 | 1.265 | 312.76 | 0.517 | 431.76 | 38.2 | 1.4 |
| AC 5 - B 2 - S 2 | 0.896 | 101.72 | 0.319 | 160.42 | 66.5 | 1.6 |
| AC 1 - B 3 - S 2 | 2.423 | 168.87 | 1.324 | 329.25 | 11.7 | 3.0 |
| AC 2 - B 3 - S 2 | 1.592 | 140.82 | 0.758 | 264.61 | 20.5 | 2.6 |
| AC 3 - B 3 - S 2 | 1.217 | 120.29 | 0.467 | 202.28 | 49.3 | 2.1 |
| AC 4 - B 3 - S 2 | 0.920 | 100.68 | 0.291 | 150.84 | 107.6 | 1.7 |
| AC 5 - B 3 - S 2 | 0.646 | 89.02 | 0.220 | 107.56 | 80.2 | 1.3 |
| AC 1 - B 4 - S 2 | 1.659 | 143.46 | 0.793 | 271.75 | 20.2 | 3.3 |
| AC 2 - B 4 - S 2 | 1.136 | 116.53 | 0.394 | 179.42 | 74.7 | 2.2 |
| AC 3 - B 4 - S 2 | 0.857 | 94.70 | 0.260 | 134.76 | 127.9 | 1.8 |
| AC 4 - B 4 - S 2 | 0.641 | 308.76 | 0.205 | 360.74 | 104.3 | 1.2 |
| AC 5 - B 4 - S 2 | 0.455 | 69.83 | 0.183 | 94.05 | 41.0 | 1.5 |
| AC 1 - B 5 - S 2 | 0.771 | 90.50 | 0.226 | 118.37 | 148.3 | 2.0 |
| AC 2 - B 5 - S 2 | 0.525 | 78.15 | 0.177 | 96.55 | 84.1 | 1.7 |
| AC 3 - B 5 - S 2 | 0.396 | 63.54 | 0.156 | 89.47 | 44.6 | 2.1 |
| AC 4 - B 5 - S 2 | 0.319 | 52.61 | 0.148 | 87.54 | 22.8 | 2.8 |
| AC 5 - B 5 - S 2 | 0.268 | 45.03 | 0.145 | 88.06 | 12.0 | 3.6 |
| AC 1 - B 6 - S 2 | 0.207 | 40.06 | 0.126 | 89.06 | 7.7 | 21.3 |
| AC 2 - B 6 - S 2 | 0.173 | 36.15 | 0.114 | 88.73 | 5.4 | 22.6 |
| AC 3 - B 6 - S 2 | 0.156 | 35.12 | 0.112 | 90.11 | 3.8 | 18.9 |
| AC 4 - B 6 - S 2 | 0.149 | 36.86 | 0.114 | 92.30 | 3.0 | 13.1 |
| AC 5 - B 6 - S 2 | 0.143 | 39.93 | 0.119 | 95.17 | 2.1 | 9.3 |

**Table 6.1.4c** Response measures from unreinforced and perfect reinforced models (subgrade *CBR* = 2).

| Model Name | Unreinforced | | Perfect Reinforcement | | $TBR_S$ | $TBR_B$ |
|---|---|---|---|---|---|---|
| | $e_v$ (%) | $q$ (kPa) | $e_v$ (%) | $q$ (kPa) | | |
| AC 1 - B 1 - S 3 | 2.626 | 270.66 | 1.874 | 498.77 | 4.0 | 2.1 |
| AC 2 - B 1 - S 3 | 1.966 | 231.33 | 1.357 | 394.96 | 4.5 | 1.8 |
| AC 3 - B 1 - S 3 | 1.629 | 208.76 | 1.028 | 351.08 | 6.5 | 1.6 |
| AC 4 - B 1 - S 3 | 1.253 | 172.76 | 0.686 | 313.81 | 11.6 | 1.7 |
| AC 5 - B 1 - S 3 | 0.866 | 154.58 | 0.441 | 221.17 | 15.6 | 1.3 |
| AC 1 - B 2 - S 3 | 2.080 | 234.02 | 1.435 | 392.81 | 4.5 | 2.1 |
| AC 2 - B 2 - S 3 | 1.528 | 201.29 | 0.945 | 331.59 | 7.1 | 1.9 |
| AC 3 - B 2 - S 3 | 1.214 | 176.27 | 0.649 | 291.39 | 12.8 | 1.8 |
| AC 4 - B 2 - S 3 | 0.918 | 366.50 | 0.416 | 457.07 | 25.1 | 1.2 |
| AC 5 - B 2 - S 3 | 0.626 | 123.06 | 0.265 | 164.84 | 33.2 | 1.3 |
| AC 1 - B 3 - S 3 | 1.536 | 202.64 | 0.950 | 333.27 | 7.1 | 2.2 |
| AC 2 - B 3 - S 3 | 1.104 | 170.18 | 0.553 | 284.03 | 16.7 | 2.1 |
| AC 3 - B 3 - S 3 | 0.836 | 146.64 | 0.358 | 219.36 | 31.7 | 1.7 |
| AC 4 - B 3 - S 3 | 0.620 | 120.84 | 0.244 | 152.25 | 44.9 | 1.3 |
| AC 5 - B 3 - S 3 | 0.439 | 102.28 | 0.196 | 118.58 | 26.7 | 1.2 |
| AC 1 - B 4 - S 3 | 1.064 | 168.76 | 0.527 | 267.36 | 17.4 | 2.3 |
| AC 2 - B 4 - S 3 | 0.747 | 133.56 | 0.303 | 186.91 | 39.3 | 1.8 |
| AC 3 - B 4 - S 3 | 0.561 | 111.01 | 0.220 | 138.41 | 45.0 | 1.4 |
| AC 4 - B 4 - S 3 | 0.423 | 320.34 | 0.180 | 360.59 | 32.3 | 1.2 |
| AC 5 - B 4 - S 3 | 0.324 | 77.89 | 0.161 | 103.51 | 17.3 | 1.5 |
| AC 1 - B 5 - S 3 | 0.483 | 104.36 | 0.190 | 121.99 | 44.6 | 1.5 |
| AC 2 - B 5 - S 3 | 0.352 | 83.67 | 0.154 | 103.70 | 28.6 | 1.6 |
| AC 3 - B 5 - S 3 | 0.278 | 69.98 | 0.136 | 96.70 | 18.3 | 2.0 |
| AC 4 - B 5 - S 3 | 0.231 | 59.91 | 0.127 | 94.27 | 11.5 | 2.5 |
| AC 5 - B 5 - S 3 | 0.200 | 52.98 | 0.122 | 94.27 | 7.4 | 2.9 |
| AC 1 - B 6 - S 3 | 0.151 | 45.61 | 0.100 | 92.99 | 5.2 | 13.4 |
| AC 2 - B 6 - S 3 | 0.131 | 42.34 | 0.094 | 92.97 | 3.8 | 13.3 |
| AC 3 - B 6 - S 3 | 0.119 | 42.75 | 0.091 | 93.98 | 3.1 | 10.3 |
| AC 4 - B 6 - S 3 | 0.114 | 45.77 | 0.090 | 95.77 | 2.6 | 7.3 |
| AC 5 - B 6 - S 3 | 0.110 | 49.16 | 0.091 | 98.08 | 2.2 | 5.6 |

**Table 6.1.4d** Response measures from unreinforced and perfect reinforced models (subgrade $CBR = 4$).

| Model Name | Unreinforced | | Perfect Reinforcement | | $TBR_S$ | $TBR_B$ |
|---|---|---|---|---|---|---|
| | $e_v$ (%) | $q$ (kPa) | $e_v$ (%) | $q$ (kPa) | | |
| AC 1 - B 1 - S 4 | 1.523 | 376.25 | 1.322 | 519.35 | 1.8 | 1.5 |
| AC 2 - B 1 - S 4 | 1.163 | 340.90 | 0.960 | 434.30 | 2.2 | 1.3 |
| AC 3 - B 1 - S 4 | 0.920 | 311.52 | 0.713 | 387.01 | 2.8 | 1.2 |
| AC 4 - B 1 - S 4 | 0.693 | 277.37 | 0.484 | 347.49 | 4.3 | 1.2 |
| AC 5 - B 1 - S 4 | 0.468 | 207.15 | 0.308 | 267.69 | 5.5 | 1.2 |
| AC 1 - B 2 - S 4 | 1.098 | 326.02 | 0.918 | 405.50 | 2.1 | 1.4 |
| AC 2 - B 2 - S 4 | 0.801 | 284.41 | 0.612 | 353.90 | 3.0 | 1.3 |
| AC 3 - B 2 - S 4 | 0.624 | 243.48 | 0.432 | 312.13 | 4.5 | 1.3 |
| AC 4 - B 2 - S 4 | 0.462 | 412.99 | 0.290 | 470.74 | 6.6 | 1.1 |
| AC 5 - B 2 - S 4 | 0.337 | 144.89 | 0.209 | 174.90 | 7.0 | 1.2 |
| AC 1 - B 3 - S 4 | 0.743 | 273.71 | 0.558 | 348.14 | 3.2 | 1.5 |
| AC 2 - B 3 - S 4 | 0.532 | 225.31 | 0.358 | 297.30 | 5.0 | 1.5 |
| AC 3 - B 3 - S 4 | 0.409 | 180.23 | 0.253 | 224.82 | 7.1 | 1.3 |
| AC 4 - B 3 - S 4 | 0.320 | 140.30 | 0.190 | 160.99 | 8.3 | 1.2 |
| AC 5 - B 3 - S 4 | 0.256 | 113.75 | 0.161 | 135.11 | 6.7 | 1.2 |
| AC 1 - B 4 - S 4 | 0.489 | 206.12 | 0.324 | 267.66 | 5.4 | 1.6 |
| AC 2 - B 4 - S 4 | 0.363 | 155.86 | 0.221 | 191.49 | 7.5 | 1.4 |
| AC 3 - B 4 - S 4 | 0.290 | 127.89 | 0.171 | 145.97 | 8.5 | 1.2 |
| AC 4 - B 4 - S 4 | 0.239 | 331.66 | 0.145 | 360.18 | 7.6 | 1.1 |
| AC 5 - B 4 - S 4 | 0.203 | 90.06 | 0.131 | 117.20 | 5.9 | 1.4 |
| AC 1 - B 5 - S 4 | 0.252 | 110.47 | 0.147 | 129.63 | 8.9 | 1.5 |
| AC 2 - B 5 - S 4 | 0.203 | 91.21 | 0.123 | 113.66 | 7.6 | 1.6 |
| AC 3 - B 5 - S 4 | 0.170 | 78.08 | 0.109 | 106.67 | 6.2 | 1.9 |
| AC 4 - B 5 - S 4 | 0.149 | 68.84 | 0.101 | 103.86 | 4.9 | 2.2 |
| AC 5 - B 5 - S 4 | 0.134 | 62.69 | 0.097 | 103.45 | 3.8 | 2.5 |
| AC 1 - B 6 - S 4 | 0.100 | 54.20 | 0.075 | 98.75 | 3.1 | 7.8 |
| AC 2 - B 6 - S 4 | 0.090 | 54.64 | 0.070 | 98.43 | 2.7 | 6.0 |
| AC 3 - B 6 - S 4 | 0.084 | 57.28 | 0.068 | 99.25 | 2.4 | 4.6 |
| AC 4 - B 6 - S 4 | 0.080 | 60.43 | 0.066 | 100.68 | 2.2 | 3.7 |
| AC 5 - B 6 - S 4 | 0.077 | 63.47 | 0.066 | 102.56 | 1.9 | 3.2 |

**Table 6.1.4e** Response measures from unreinforced and perfect reinforced models (subgrade $CBR = 8$).

| Model Name | Unreinforced | | Perfect Reinforcement | | $TBR_S$ | $TBR_B$ |
|---|---|---|---|---|---|---|
| | $e_v$ (%) | $q$ (kPa) | $e_v$ (%) | $q$ (kPa) | | |
| AC 1 - B 1 - S 5 | 0.661 | 563.93 | 0.675 | 574.42 | 0.9 | 1.0 |
| AC 2 - B 1 - S 5 | 0.531 | 491.42 | 0.531 | 495.91 | 1.0 | 1.0 |
| AC 3 - B 1 - S 5 | 0.423 | 420.18 | 0.414 | 426.73 | 1.1 | 1.0 |
| AC 4 - B 1 - S 5 | 0.326 | 340.51 | 0.302 | 368.89 | 1.4 | 1.1 |
| AC 5 - B 1 - S 5 | 0.251 | 242.63 | 0.214 | 288.44 | 1.9 | 1.1 |
| AC 1 - B 2 - S 5 | 0.468 | 436.83 | 0.476 | 439.19 | 0.9 | 1.0 |
| AC 2 - B 2 - S 5 | 0.365 | 367.84 | 0.358 | 380.26 | 1.1 | 1.0 |
| AC 3 - B 2 - S 5 | 0.294 | 291.22 | 0.269 | 324.40 | 1.4 | 1.1 |
| AC 4 - B 2 - S 5 | 0.232 | 441.35 | 0.196 | 472.33 | 2.0 | 1.1 |
| AC 5 - B 2 - S 5 | 0.192 | 166.31 | 0.156 | 201.33 | 2.3 | 1.2 |
| AC 1 - B 3 - S 5 | 0.325 | 333.76 | 0.316 | 356.81 | 1.1 | 1.1 |
| AC 2 - B 3 - S 5 | 0.256 | 262.45 | 0.228 | 301.41 | 1.6 | 1.2 |
| AC 3 - B 3 - S 5 | 0.206 | 195.28 | 0.171 | 227.90 | 2.1 | 1.2 |
| AC 4 - B 3 - S 5 | 0.173 | 151.47 | 0.137 | 176.86 | 2.5 | 1.2 |
| AC 5 - B 3 - S 5 | 0.152 | 128.56 | 0.121 | 157.25 | 2.5 | 1.3 |
| AC 1 - B 4 - S 5 | 0.232 | 225.65 | 0.203 | 267.13 | 1.7 | 1.3 |
| AC 2 - B 4 - S 5 | 0.186 | 168.13 | 0.152 | 197.63 | 2.3 | 1.3 |
| AC 3 - B 4 - S 5 | 0.156 | 134.78 | 0.123 | 158.87 | 2.6 | 1.3 |
| AC 4 - B 4 - S 5 | 0.136 | 342.53 | 0.108 | 360.25 | 2.6 | 1.1 |
| AC 5 - B 4 - S 5 | 0.123 | 103.26 | 0.100 | 135.81 | 2.4 | 1.5 |
| AC 1 - B 5 - S 5 | 0.135 | 115.63 | 0.105 | 140.56 | 2.8 | 1.6 |
| AC 2 - B 5 - S 5 | 0.115 | 98.54 | 0.090 | 126.62 | 2.7 | 1.7 |
| AC 3 - B 5 - S 5 | 0.101 | 86.95 | 0.081 | 120.00 | 2.5 | 1.9 |
| AC 4 - B 5 - S 5 | 0.091 | 80.19 | 0.076 | 117.22 | 2.2 | 2.0 |
| AC 5 - B 5 - S 5 | 0.085 | 78.41 | 0.072 | 116.66 | 2.0 | 2.0 |
| AC 1 - B 6 - S 5 | 0.063 | 73.83 | 0.054 | 106.82 | 1.9 | 3.2 |
| AC 2 - B 6 - S 5 | 0.058 | 75.50 | 0.051 | 106.28 | 1.8 | 2.6 |
| AC 3 - B 6 - S 5 | 0.055 | 77.76 | 0.048 | 106.75 | 1.7 | 2.3 |
| AC 4 - B 6 - S 5 | 0.053 | 80.22 | 0.047 | 107.82 | 1.6 | 2.1 |
| AC 5 - B 6 - S 5 | 0.051 | 82.54 | 0.046 | 109.28 | 1.6 | 1.9 |

**Table 6.1.4f** Response measures from unreinforced and perfect reinforced models (subgrade $CBR = 15$).

| Model Name | Unreinforced | | Perfect Reinforcement | | $TBR_S$ | $TBR_B$ |
|---|---|---|---|---|---|---|
| | $e_v$ (%) | $q$ (kPa) | $e_v$ (%) | $q$ (kPa) | | |
| AC 1 - B 1 - S 6 | 0.329 | 658.87 | 0.341 | 626.27 | 0.9 | 0.9 |
| AC 2 - B 1 - S 6 | 0.274 | 566.63 | 0.287 | 543.58 | 0.8 | 1.0 |
| AC 3 - B 1 - S 6 | 0.222 | 470.59 | 0.234 | 459.47 | 0.8 | 1.0 |
| AC 4 - B 1 - S 6 | 0.177 | 376.07 | 0.184 | 384.58 | 0.8 | 1.0 |
| AC 5 - B 1 - S 6 | 0.149 | 287.12 | 0.149 | 319.50 | 1.0 | 1.1 |
| AC 1 - B 2 - S 6 | 0.239 | 488.82 | 0.255 | 469.18 | 0.8 | 0.9 |
| AC 2 - B 2 - S 6 | 0.192 | 410.88 | 0.207 | 403.94 | 0.7 | 1.0 |
| AC 3 - B 2 - S 6 | 0.158 | 317.60 | 0.166 | 333.49 | 0.8 | 1.1 |
| AC 4 - B 2 - S 6 | 0.131 | 457.67 | 0.130 | 472.02 | 1.0 | 1.0 |
| AC 5 - B 2 - S 6 | 0.116 | 188.39 | 0.112 | 231.19 | 1.2 | 1.2 |
| AC 1 - B 3 - S 6 | 0.169 | 364.20 | 0.185 | 365.92 | 0.7 | 1.0 |
| AC 2 - B 3 - S 6 | 0.138 | 282.65 | 0.144 | 306.57 | 0.9 | 1.1 |
| AC 3 - B 3 - S 6 | 0.115 | 205.87 | 0.114 | 238.24 | 1.1 | 1.2 |
| AC 4 - B 3 - S 6 | 0.101 | 161.16 | 0.096 | 196.56 | 1.3 | 1.3 |
| AC 5 - B 3 - S 6 | 0.093 | 144.47 | 0.087 | 180.94 | 1.3 | 1.3 |
| AC 1 - B 4 - S 6 | 0.125 | 235.83 | 0.127 | 266.76 | 0.9 | 1.2 |
| AC 2 - B 4 - S 6 | 0.104 | 175.67 | 0.100 | 207.23 | 1.2 | 1.3 |
| AC 3 - B 4 - S 6 | 0.090 | 142.50 | 0.084 | 173.84 | 1.3 | 1.4 |
| AC 4 - B 4 - S 6 | 0.082 | 353.30 | 0.076 | 362.88 | 1.3 | 1.0 |
| AC 5 - B 4 - S 6 | 0.077 | 123.11 | 0.072 | 155.32 | 1.3 | 1.4 |
| AC 1 - B 5 - S 6 | 0.077 | 121.44 | 0.071 | 151.39 | 1.4 | 1.7 |
| AC 2 - B 5 - S 6 | 0.068 | 109.23 | 0.063 | 139.64 | 1.4 | 1.7 |
| AC 3 - B 5 - S 6 | 0.062 | 104.92 | 0.057 | 133.98 | 1.3 | 1.6 |
| AC 4 - B 5 - S 6 | 0.058 | 105.23 | 0.054 | 131.83 | 1.3 | 1.5 |
| AC 5 - B 5 - S 6 | 0.056 | 106.56 | 0.052 | 131.36 | 1.3 | 1.4 |
| AC 1 - B 6 - S 6 | 0.040 | 95.12 | 0.038 | 115.63 | 1.3 | 1.8 |
| AC 2 - B 6 - S 6 | 0.038 | 96.26 | 0.036 | 115.11 | 1.3 | 1.6 |
| AC 3 - B 6 - S 6 | 0.036 | 97.86 | 0.034 | 115.34 | 1.3 | 1.5 |
| AC 4 - B 6 - S 6 | 0.035 | 99.56 | 0.033 | 116.12 | 1.2 | 1.4 |
| AC 5 - B 6 - S 6 | 0.034 | 101.26 | 0.032 | 117.12 | 1.2 | 1.4 |

## 6.2 Variation of Parameters for Geosynthetic Reinforced Models

Results shown in Table 6.1.4 for model cases simulating perfect reinforcement gave relatively high values of *TBR* for many cases. Since these models simulate a geosynthetic with an infinite tensile stiffness and an infinitely stiff contact shear interface between the geosynthetic and the base aggregate, high values of *TBR* were expected. Model cases were analyzed in this way to isolate the effects of AC and base aggregate thickness, and subgrade properties. As discussed in Section 4.3, the anisotropic elastic model used for the geosynthetic allows for the variation of certain properties that are related to physical material properties and possibly material characteristics related to the structure of the geosynthetic. These properties are the in-plane elastic modulus, the ratio between the elastic modulus in the strong and weak directions of the material, Poisson's ratio, and in-plane shear modulus.

The effect of modulus was first examined by using the finite element model described in Section 5.3 with isotropic material properties used for the geosynthetic. Comparison of results to those from similar cases with perfect reinforcement allowed for an assessment of the influence of modulus on reinforcement benefit. Additional cases were created where an anisotropic model was used to examine the effect of the ratio of the modulus in the strong and weak directions of the material. Further cases were created to examine the effect of Poisson's ratio and shear modulus.

### *6.2.1 Parameters to Examine Effect of Reinforcement Modulus*

The finite model described in Section 5.3 was used to examine the influence of the isotropic value of elastic modulus of the geosynthetic on reinforcement benefit. The material model described in Section 4.3 was used for the geosynthetic. All other material layers used the material models previously described with specific properties as summarized below. The material model for the geosynthetic was given elastic properties that represented an isotropic material. In particular, the three elastic moduli were given the same value, the three Poisson's ratios were given the same value and the shear modulus was computed from the elastic modulus and Poisson's ratio as for an isotropic material. Five different values of geosynthetic isotropic elastic modulus were used. Table 6.2.1 gives the values for each of the nine elastic constants contained in the material model for the geosynthetic.

**Table 6.2.1** Parameters for geosynthetic material model to examine effect of reinforcement modulus.

| Case Name | $E_{xm}$ (MPa) | $E_m$ (MPa) | $E_n$ (MPa) | $n_{xm-m}$ | $n_{xm-n}$ | $n_{m-n}$ | $G_{xm-m}$ (MPa) | $G_{xm-n}$ (MPa) | $G_{m-n}$ (MPa) |
|---|---|---|---|---|---|---|---|---|---|
| GM1 | 400 | 400 | 400 | 0.5 | 0.5 | 0.5 | 133 | 133 | 133 |
| GM2 | 1000 | 1000 | 1000 | 0.5 | 0.5 | 0.5 | 333 | 333 | 333 |
| GM3 | 2000 | 2000 | 2000 | 0.5 | 0.5 | 0.5 | 667 | 667 | 667 |
| GM4 | 4000 | 4000 | 4000 | 0.5 | 0.5 | 0.5 | 1333 | 1333 | 1333 |
| GM5 | 8000 | 8000 | 8000 | 0.5 | 0.5 | 0.5 | 2667 | 2667 | 2667 |

Values of Poisson's ratio were set equal to 0.5 since those values produce the stiffest response of the material, as indicated in Section 4.3. The reduction of reinforcement benefit produced by reducing Poisson's ratio is examined in Section 6.2.3. Similarly, values of shear modulus were set relatively high in order to produce maximum values of benefit. The effect of reducing shear modulus is also examined in Section 6.2.3.

Ten pavement sections were analyzed with the case name for the AC and base thickness given in Table 6.2.2. These cases were analyzed for the subgrade cases and geosynthetic material property cases shown in Table 6.2.2, resulting in 250 additional model runs. The three groups of pavement sections distinguished in Table 6.2.2 correspond to relatively thin, medium and thick sections. As discussed in Section 7.2, results were run in these groups in order to provide a means of modifying general trends in the data seen from the model runs for perfect reinforcement described in Section 6.1 for the effect of reinforcement modulus.

**Table 6.2.2** Pavement sections used to evaluate effect of reinforcement modulus.

| Pavement Section | Subgrade Cases | Geosynthetic Cases |
|---|---|---|
| AC1-B1<br>AC1-B2<br>AC2-B1 | S1, S2, S3, S4, S5 | GM1, GM2, GM3, GM4, GM5 |
| AC3-B4<br>AC4-B4<br>AC1-B5<br>AC2-B5 | | |
| AC5-B5<br>AC3-B6<br>AC4-B6 | | |

### *6.2.2 Parameters to Examine Effect of Reinforcement Modulus Anisotropy*

The finite element model described in Section 5.3 was used to examine the influence of direction dependent geosynthetic elastic modulus values on reinforcement benefit. The material model described in Section 4.3 was used for the geosynthetic. The model differed from that described in Section 6.2.1 in that different values of elastic modulus were used in the machine and cross machine directions. Values in the direction normal to the geosynthetic were also changed to provide stability of the elastic matrix. All other material layers used the material models previously described with specific properties as summarized below. Five different values of geosynthetic modulus ratio, defined as the ratio of the minimum to maximum elastic modulus values between the machine and cross machine directions, were used. These ratios were used for two different values of maximum elastic modulus value. Table 6.2.3 gives the values for each of the nine elastic constants contained in the material model for the geosynthetic.

**Table 6.2.3** Parameters for geosynthetic material model to examine effect of reinforcement modulus anisotropy.

| Case Name | $E_{xm}$ (MPa) | $E_m$ (MPa) | $E_n$ (MPa) | Geosynthetic Modulus Ratio ($G_{MR}$) | $n_{xm-m}$ | $n_{xm-n}$ | $n_{m-n}$ | $G_{xm-m}$ (MPa) | $G_{xm-n}$ (MPa) | $G_{m-n}$ (MPa) |
|---|---|---|---|---|---|---|---|---|---|---|
| GA1 | 400 | 400 | 400 | 1 | 0.5 | 0.5 | 0.5 | 133 | 133 | 133 |
| GA2 | 400 | 300 | 300 | 0.75 | 0.5 | 0.5 | 0.5 | 133 | 133 | 133 |
| GA3 | 400 | 200 | 200 | 0.5 | 0.5 | 0.5 | 0.5 | 133 | 133 | 133 |
| GA4 | 400 | 100 | 100 | 0.25 | 0.5 | 0.5 | 0.5 | 133 | 133 | 133 |
| GA5 | 400 | 40 | 40 | 0.1 | 0.5 | 0.5 | 0.5 | 133 | 133 | 133 |
| GA6 | 8000 | 8000 | 8000 | 1 | 0.5 | 0.5 | 0.5 | 2667 | 2667 | 2667 |
| GA7 | 800 | 6000 | 6000 | 0.75 | 0.5 | 0.5 | 0.5 | 2667 | 2667 | 2667 |
| GA8 | 800 | 4000 | 4000 | 0.5 | 0.5 | 0.5 | 0.5 | 2667 | 2667 | 2667 |
| GA9 | 800 | 2000 | 2000 | 0.25 | 0.5 | 0.5 | 0.5 | 2667 | 2667 | 2667 |
| GA10 | 800 | 800 | 800 | 0.1 | 0.5 | 0.5 | 0.5 | 2667 | 2667 | 2667 |

Values of Poisson's ratio were set equal to 0.5 since those values produce the stiffest response of the material. The reduction of reinforcement benefit produced by reducing Poisson's ratio is examined in Section 6.2.3. Similarly, values of shear modulus were set high in order to produce maximum values of benefit. The effect of reducing shear modulus is also examined in Section 6.2.3.

Three pavement sections were analyzed with the case name for the AC, base thickness and subgrade *CBR* given in Table 6.2.4. These cases were analyzed for the geosynthetic material property cases shown in Table 6.2.3, resulting in 30 additional model runs.

**Table 6.2.4** Pavement sections used to evaluate effect of reinforcement modulus anisotropy.

| Pavement Section | Geosynthetic Cases |
|---|---|
| AC2-B5-S1<br>AC1-B2-S3<br>AC5-B6-S5 | GA1-GA10 |

### *6.2.3 Parameters to Examine Effect of Poisson's Ratio and Shear Modulus*

All finite element model cases previously examined used values for Poisson's ratio and shear modulus that would produce optimal values of reinforcement benefit with respect to these two parameters. This was done such that the effects of reinforcement isotropic modulus and reinforcement modulus anisotropy could be systematically accounted for. Additional finite element model cases were created to examine the effect of reducing Poisson's ratio and shear modulus to their lowest possible values. Table 6.2.5 shows values of the elastic properties used for the geosynthetic material model to examine the effect of reducing Poisson's ratio and shear modulus. These properties were used for each of the three pavement sections listed in Table 6.2.6, resulting in an additional 24 cases created to examine these effects.

**Table 6.2.5** Parameters for geosynthetic material model to examine effect of reinforcement Poisson's ratio and shear modulus.

| Case Name | $E_{xm}$ (MPa) | $E_m$ (MPa) | $E_n$ (MPa) | $n_{xm\text{-}m}$ | $n_{xm\text{-}n}$ | $n_{m\text{-}n}$ | $G_{xm\text{-}m}$ (MPa) | $G_{xm\text{-}n}$ (MPa) | $G_{m\text{-}n}$ (MPa) |
|---|---|---|---|---|---|---|---|---|---|
| G*n*G1 | 400 | 400 | 400 | 0.5 | 0.5 | 0.5 | 133 | 133 | 133 |
| G*n*G2 | 8000 | 8000 | 8000 | 0.5 | 0.5 | 0.5 | 2667 | 2667 | 2667 |
| G*n*G3 | 400 | 400 | 400 | 0 | 0 | 0 | 133 | 133 | 133 |
| G*n*G4 | 8000 | 8000 | 8000 | 0 | 0 | 0 | 2667 | 2667 | 2667 |
| G*n*G5 | 400 | 400 | 400 | 0.5 | 0.5 | 0.5 | 0 | 0 | 0 |
| G*n*G6 | 8000 | 8000 | 8000 | 0.5 | 0.5 | 0.5 | 0 | 0 | 0 |
| G*n*G7 | 400 | 400 | 400 | 0 | 0 | 0 | 0 | 0 | 0 |
| G*n*G8 | 8000 | 8000 | 8000 | 0 | 0 | 0 | 0 | 0 | 0 |

**Table 6.2.6** Pavement sections used to evaluate effect of reinforcement Poisson's ratio and shear modulus.

| Pavement Section | Geosynthetic Cases |
|---|---|
| AC2-B5-S1<br>AC1-B2-S3<br>AC5-B6-S5 | G*nG*1- G*nG*8 |

All cases described in Section 6 used equivalenced nodes between the geosynthetic and the surrounding base aggregate and subgrade and thereby simulates a perfectly tied contact interface. As such, the effect of interface properties is not addressed in the above cases. The influence of interface properties is addressed by comparison of design model predictions to test section results in Section 7.6.

## 7.0 DESIGN MODEL DEVELOPMENT

The purpose of this section is to summarize, interpret and synthesize the results from the parametric study cases described in Section 6. Through this process, a design model is developed.

## 7.1 Design Equations for Perfect Reinforcement

### *7.1.1 Equations for TBR for Perfect Reinforcement*

To simplify the interpretation of the results presented in Table 6.1.4 such that general design guidelines and equations could be developed, AC thickness and base aggregate thickness were combined by computing a structural number (*SN*) for each pavement section using Equation 7.1.1.

$$SN = 0.4\ D_1 + 0.14\ D_2 \tag{7.1.1}$$

Equation 7.1.1 uses a layer coefficient of 0.4 for the AC and 0.14 for the base aggregate when the layer thicknesses for the AC and aggregate ($D_1$ and $D_2$, respectively) are in inches. These values for layer coefficients follow from the model calibration and resilient modulus test simulation work described in Section 4.2. Equation 7.1.1 implies a base layer drainage coefficient, $m_2$, of 1.0. The resulting *SN* was then plotted against $TBR_S$ and grouped together for different subgrade types, with the results shown in Figure 7.1.1. $TBR_S$ is labeled as $TBR_{S\text{-}PR}$ to denote values pertaining to the case of perfect reinforcement. While some scatter in the results is

seen, reasonable and consistent trends of $TBR_S$ with *SN* between different subgrade types is observed. The results indicate that reinforcement benefit decreases as subgrade *CBR* increases, with very little improvement for a subgrade *CBR* of 8 and essentially no improvement for a subgrade *CBR* of 15. Reinforcement benefit is seen to increase from low values of *SN* and reaches a maximum around a *SN* of 3.3 and then decreases with no benefit seen after a *SN* of 6. A summary of existing test section work in Section 2.1 indicated that these types of results should be expected and appear to be reasonable in light of currently available information. As discussed earlier, the high values of *TBR* noted in Figure 7.1.1 are expected since these runs represent a geosynthetic material with an infinite modulus and an infinitely stiff shear interface between the geosynthetic and the base aggregate.

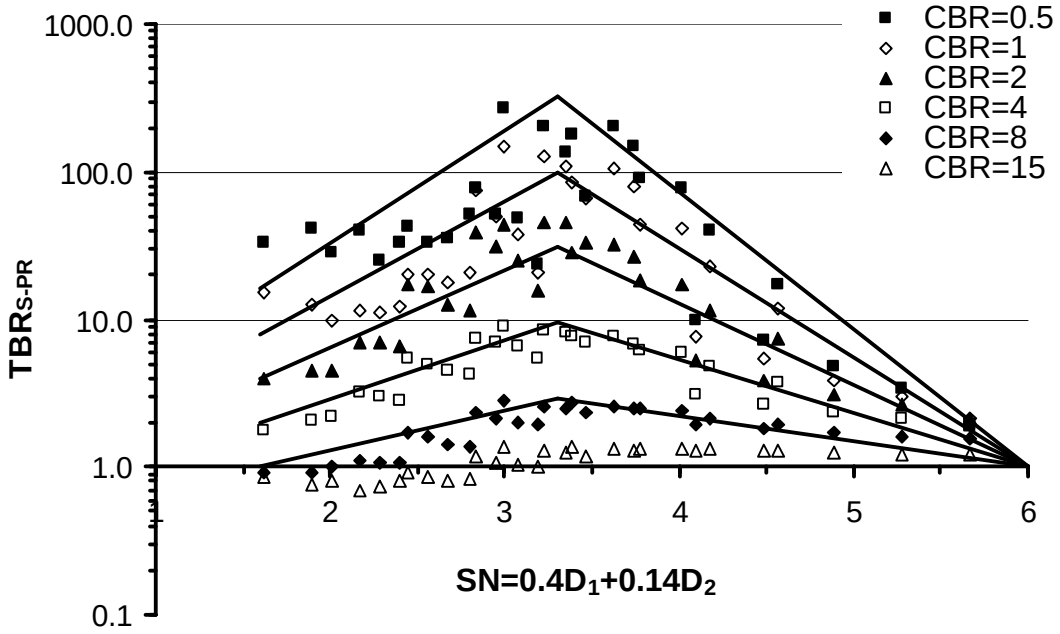


**Figure 7.1.1** $TBR_{S\text{-}PR}$ versus *SN* for perfect reinforcement model cases.

Straight-line equations in the semi-log plot of $TBR_{S\text{-}PR}$ versus *SN* were used to approximate the trend in the data for each subgrade *CBR*. For a subgrade *CBR* of 15, $TBR_{S\text{-}PR}$ was taken as equal to one for all values of *SN*. The equations of each straight-line portion of the curve is given by Equations 7.1.2-7.1.7, where the parameters used in this equation are identified in Figure 7.1.2.

$1.6 \le SN \le 3.3$

$$TBR_{S-PR} = 10^{(m_1 SN + \log y_{o1})} \tag{7.1.2}$$

$$m_1 = \frac{\log \frac{y_2}{y_1}}{1.7} \tag{7.1.3}$$

$$y_{o1} = \frac{y_1}{10^{(1.6 m_1)}} \tag{7.1.4}$$

$3.3 \le SN \le 6.0$

$$TBR_{S-PR} = 10^{(m_2 SN + \log y_{o2})} \tag{7.1.5}$$

$$m_2 = \frac{-\log y_2}{SN_{(TBR_{S-PR}=1)} - 3.3} \tag{7.1.6}$$

$$y_{o2} = \frac{y_2}{10^{(3.3 m_2)}} \tag{7.1.7}$$

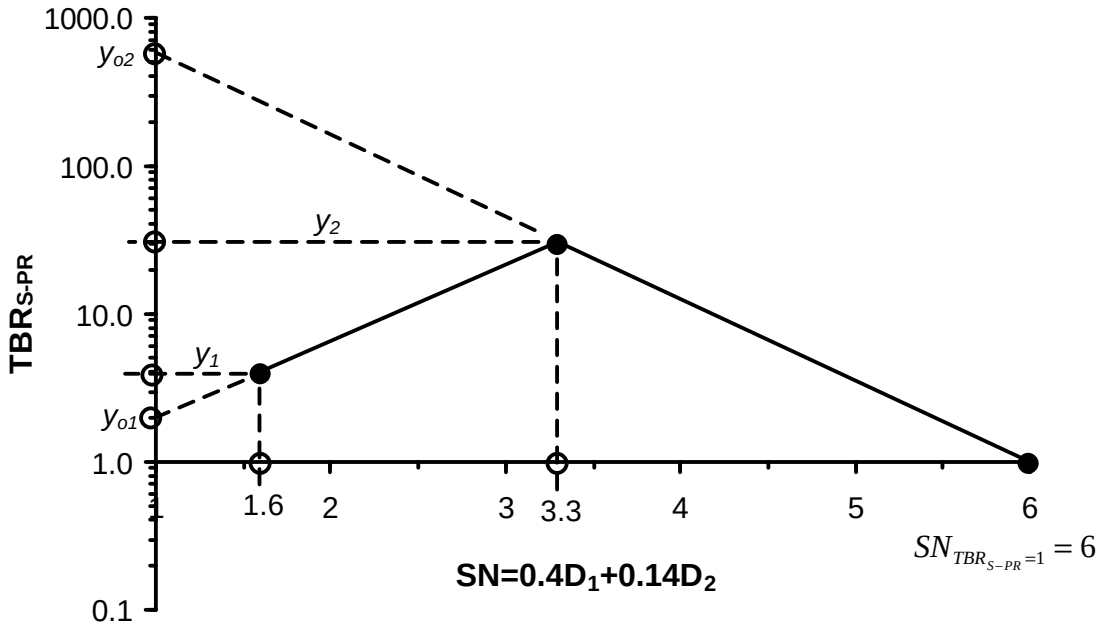


**Figure 7.1.2** Identification of constants for Equations 7.1.2-7.1.9.

With Equations 7.1.2-7.1.7 used to describe the lines seen in Figure 7.1.1, values of $y_1$ and $y_2$ were then related to the subgrade *CBR* with the following expressions derived. The lines shown in Figure 7.1.1 are plotted according to Equations 7.1.2-7.1.9.

$$y_1 = 10^{(\log 8 - \log CBR)} \tag{7.1.8}$$

$$y_2 = 10^{(\log 100 - 1.7 \log CBR)} \tag{7.1.9}$$

A similar assessment of the data in Table 6.1.4 was made to relate $TBR_{B\text{-}PR}$ for the case of perfect reinforcement to AC and base thickness and subgrade *CBR*. In this case, changes in $TBR_{B\text{-}PR}$ were most appreciable for changes in subgrade *CBR* and AC thickness. Changes in base thickness were not seen to appreciably affect $TBR_{B\text{-}PR}$. Figure 7.1.3 shows values from Table 6.1.4 of $TBR_{B\text{-}PR}$ versus AC thickness for various subgrade *CBR* values. Data from a given subgrade *CBR* and a given AC thickness is plotted for each base thickness with the exception of the base thickness of 600 mm. From Table 6.1.4, it is seen that the finite element model produced comparatively high values of $TBR_{B\text{-}PR}$ for most cases where the base thickness was 600 mm. These results appear to be inconsistent with the other data and no experimental data is available in the literature that supports this observation. As will be seen below, the design equations formulated from the data in Figure 7.1.3 excludes these results and thereby avoids what would most likely be unconservative estimates of benefit.

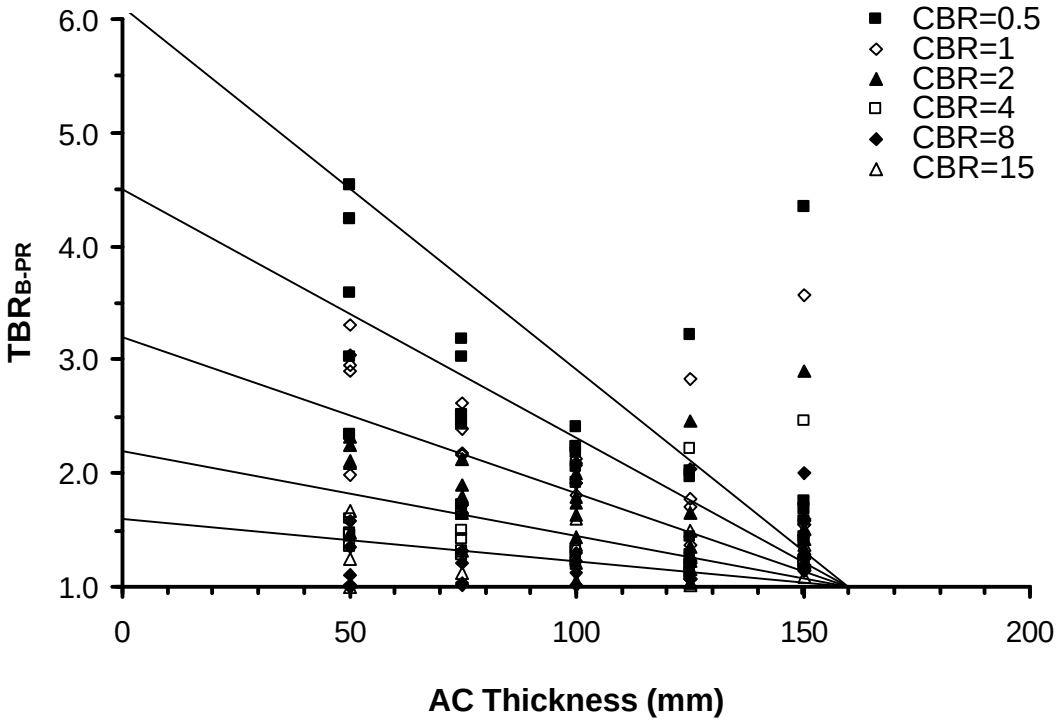


**Figure 7.1.3** $TBR_{B\text{-}PR}$ versus AC thickness ($D_1$) for perfect reinforcement model cases.

From Figure 7.1.3 it is seen that more scatter is observed for results of $TBR_{B\text{-}PR}$ as compared to those observed in Figure 7.1.1 for $TBR_{S\text{-}PR}$. The values of $TBR_{B\text{-}PR}$ are, however, relatively modest in comparison to $TBR_{S\text{-}PR}$. Due to this scatter, relatively simple and conservative estimates of the data were developed by straight-lines in an arithmetic plot of $TBR_{B\text{-}PR}$ versus AC thickness for various subgrade *CBR*'s. The equation of these lines is given by:

$$TBR_{B-PR} = (1-b)\frac{D_1}{160} + b \tag{7.1.10}$$

where $D_1$ is the AC thickness in units of mm and $b$ is the y-intercept of the lines. Values of $b$ were related to subgrade *CBR* through Equation 7.1.11. The lines shown in Figure 7.1.3 result from the use of Equations 7.1.10 and 7.1.11.

$$b = 4.45\, CBR^{-0.522} \tag{7.1.11}$$

### *7.1.2 Equations for BCR and TBR/BCR Combinations for Perfect Reinforcement*

In Section 6.1, 450 comparisons between unreinforced and perfect reinforced models with a reduced base course thickness were available. For each comparison run, a combination of *BCR* and *TBR* was available, where *TBR* was broken into components of $TBR_B$ and $TBR_S$ for each case. The introduction of a new input variable (base course thickness reduction) made it difficult to develop regression equations that reasonably described the results obtained. A simple method was therefore sought for relating combinations of *BCR* and *TBR* to pavement design parameters. The method chosen is described below and is based on existing pavement design principles and methodologies. The method has not been validated against results from test sections, but is compared to results obtained from the finite element model cases described in Section 6.1 in order to assess its reasonableness and degree of safety.

The method relies upon the use of design equations contained in the AASHTO '93 pavement design guide (AASHTO, 1993). The approach was outlined in Berg et al. (2000) and is developed in greater detail below. The method relies upon the knowledge of a *TBR* for equivalent unreinforced and reinforced sections (i.e. *TBR* for *BCR* = 0). The AASHTO '93 pavement design equation is then used to calculate an increased structural layer coefficient for the base course aggregate for the reinforced section that gives the increased number of ESAL's

that this section can carry for the case where no base course thickness reduction is used. The new base layer coefficient is then used to determine the base course thickness reduction such that equal life or ESAL's is predicted for the reinforced and unreinforced pavement (i.e. *BCR* when *TBR* = 1). The method can also be used to calculate the remaining *BCR* for an assumed *TBR* or to calculate the remaining *TBR* for an assumed *BCR*.

An unreinforced pavement design cross section is first presumed to be known. The AC and base thickness and layer coefficients, and the subgrade *CBR* or resilient modulus is required. With these parameters, the 1993 AASHTO pavement design equation is used to calculate the number of ESAL's for the unreinforced pavement ($W_{18\text{-}U}$) from Equations 7.1.12 and 7.1.13.

$$W_{18-U} = 10\wedge\left[ Z_R\ S_o + 9.36\log(SN+1) - 0.2 + \frac{\log\left(\frac{\Delta PSI}{4.2-1.5}\right)}{0.4+\frac{1094}{(SN+1)^{5.19}}} + 2.32\log(M_S) - 8.07 \right] \quad (7.1.12)$$

$$SN = a_1 D_1 + a_2 D_2 m_2 \quad (7.1.13)$$

In Equations 7.1.12 and 7.1.13, $Z_R$ is the standard normal deviate, $S_o$ is the combined standard error, *DPSI* is the loss of design serviceability, $M_S$ is the effective roadbed (subgrade) resilient modulus in units of psi, $a_1$ and $a_2$ are the layer coefficients of the asphalt concrete and base aggregate layers, respectively, $D_1$ and $D_2$ are the thicknesses of the AC and base layers, respectively, and $m_2$ is the drainage coefficient of the base layer. Values of $Z_R$, $S_o$, *DPSI*, $a_1$, $a_2$ and $m_2$ have been taken as constants for the development of this method and have been given values of –1.645, 0.35 and 1.9, 0.4, 0.14 and 1.0, respectively, where the value of $Z_R$ corresponds to a reliability of 95 %. Values of $M_S$ in units of psi are related to subgrade *CBR* through Equation 7.1.14.

$$M_S = 1500\ CBR \quad (7.1.14)$$

A known value of *TBR* when *BCR* = 0 then allows $W_{18}$ to be calculated from Equation 7.1.15 for a reinforced pavement having identical pavement layer thicknesses and properties. In Equation 7.1.15, the *TBR* used may correspond to $TBR_B$, $TBR_S$ or $TBR_T$.

$$W_{18-R} = W_{18-U}\ TBR \tag{7.1.15}$$

The value of $W_{18\text{-}R}$ from Equation 7.1.15 is then used in Equation 7.1.12 to calculate a value of *SN* for the reinforced pavement, with this value used in Equation 7.1.13 to determine a new value of $a_2$ for the reinforced pavement, with all other parameters in Equations 7.1.12 and 7.1.13 being equal to those used for the unreinforced pavement. This approach assumes that the *TBR* seen for the comparative reinforced and unreinforced pavments can be accounted for by an increased structural base layer coefficient. This calculation requires an iterative solution for *SN* in Equation 7.1.12. Once a value of $a_2$ for the reinforced pavement is obtained ($a_{2\text{-}R}$), this value is used in Equation 7.1.13 along with a reduced base thickness for the reinforced pavement ($D_{2\text{-}R}$) such that a *SN* identical to the unreinforced pavement is obtained. The reduced base thickness is calculated from

$$D_{2-R} = \frac{SN_U - a_1 D_1}{a_{2-R}\, m_2} \tag{7.1.16}$$

This allows for the determination of a value of *BCR* when *TBR* = 1 from Equation 7.1.17. Depending on the value of *TBR* used in Equation 7.1.15 ($TBR_B$, $TBR_S$ or $TBR_T$), the computed *BCR* then pertains to reinforcement effects on the base, subgrade or total system.

$$BCR = 100\frac{D_{2-U} - D_{2-R}}{D_{2-U}} \tag{7.1.17}$$

With this approach, values of *TBR* when *BCR*=0 and *BCR* when *TBR*=1 are known. If a value of *TBR* less than $TBR_{BCR=0}$ is used, it should be expected that the remaining benefit can be expressed in terms of a *BCR*. Conversely, if a value of *BCR* less than $BCR_{TBR=1}$ is used, remaining benefit can be expressed in terms of a *TBR*. The same general approach described above is used to determine combinations of *BCR* and *TBR*. Each approach uses the predetermined value of $TBR_{BCR=0}$ to determine the increased structural base layer coefficient of the reinforced pavement. For the case where a desired *BCR* is specified, the reinforced base layer thickness is determined from Equation 7.1.18.

$$D_{2-R} = \left(1 - \frac{BCR}{100}\right) D_{2-U} \tag{7.1.18}$$

Structural number of the reinforced pavement is then determined from Equation 7.1.19.

$$SN_R = a_1 D_1 + a_{2-R} D_{2-R} m_2 \tag{7.1.19}$$

where $a_{2\text{-}R}$ is determined from the method described above and by knowing the value of $TBR_{BCR=0}$. A value of $W_{18\text{-}R}$ is then determined using Equation 7.1.12 using the value of *SN* from Equation 7.1.19. A value of remaining *TBR* is then computed by Equation 7.1.20, where this value should lie between 1 and $TBR_{BCR=0}$, provided the desired value of *BCR* used was less than or equal to $BCR_{TBR=1}$.

$$TBR = \frac{W_{18-R}}{W_{18-U}} \tag{7.1.20}$$

For the case where a desired *TBR* is specified, Equation 7.1.15 is used to calculate the number of ESAL's required of the reinforced section. Equation 7.1.12 is then solved iteratively to give the required *SN* for the reinforced section ($SN_R$). Equation 7.1.21 is then used to determine the base layer thickness necessary to produce this *SN*, where the reinforced structural base layer coefficient is used in this equation.

$$D_{2-R} = \frac{SN_R - a_1 D_1}{a_{2-R} m_2} \tag{7.1.21}$$

The remaining *BCR* is then determined from Equation 7.1.17, where the value obtained should lie between 0 and $BCR_{TBR=1}$, provided the desired value of *TBR* was less than $TBR_{BCR=0}$.

The above approach has not been validated previously by either test section results or comparisons to numerical models. To evaluate the reasonableness of this approach, the above method was compared to results from the parametric study for the case of perfect reinforcement. As described in Section 6.1, 450 comparisons of finite element cases were made to assess combinations of *TBR* and *BCR* from the response measures derived from the models. For these comparisons, an assumed or desired value of *BCR* was used to create the models. The response measures were then used to define the remaining *TBR*. As described previously, the response measures were used to define partial *TBR*'s for the subgrade ($TBR_S$) and base ($TBR_B$) with the product of the two defining the total *TBR* ($TBR_T$). Combinations of *BCR* and *TBR* for each of the

three values of *TBR* were then known from the 450 finite element comparative cases, as summarized in Section 6.1.

The method described above using the AASHTO ’93 pavement design equation was then used to assess remaining *TBR* for the corresponding *BCR* presumed. The value of $TBR_{BCR=0}$ used in the method corresponded to that which was obtained from the finite element model comparison cases of unreinforced and perfect reinforced sections of equivalent thickness. Since three values of *TBR* ($TBR_S$, $TBR_B$, $TBR_T$) are available when *BCR* = 0, the above described method was used to evaluate combinations of *BCR* and *TBR* for each of the three reinforcement effects for each case. In many cases, both the finite element cases and the AASHTO equations gave remaining *TBR*’s less than one because the presumed *BCR* was too great. For cases where remaining *TBR* was greater than one for either method, diagrams of remaining $TBR_S$, $TBR_B$ and $TBR_T$ from the finite element model were plotted against those from the AASHTO equations. These plots are shown in Figures 7.1.4, where results are given separately for each subgrade condition and all cases for presumed values of *BCR* are shown.

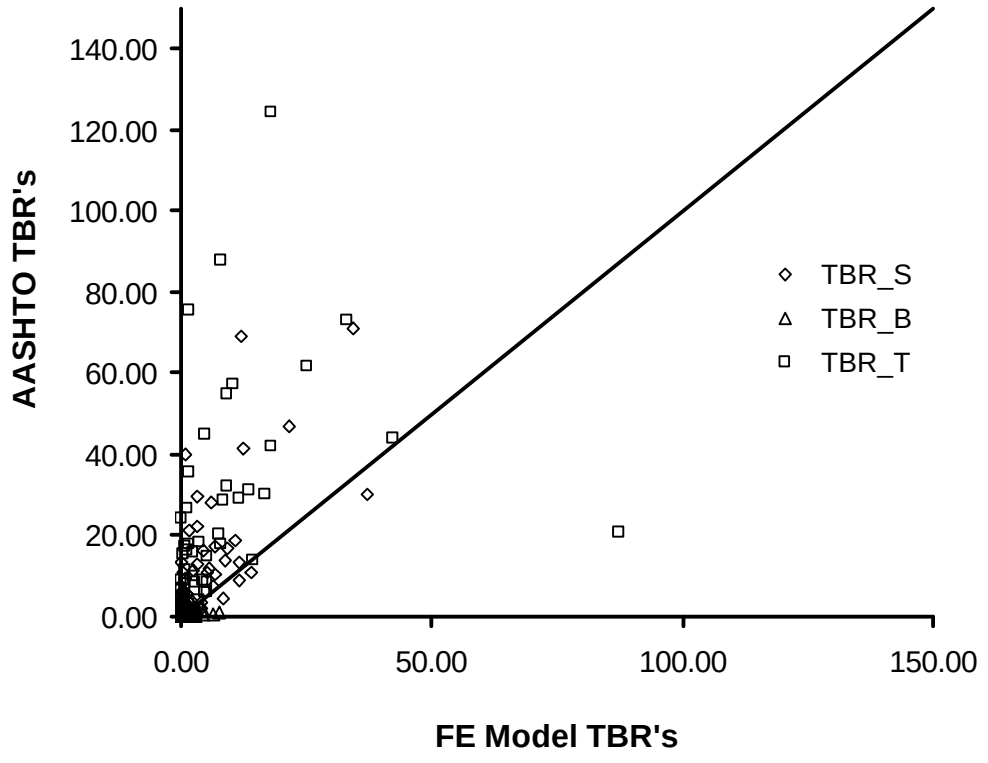


**Figure 7.1.4a** Remaining $TBR_S$, $TBR_B$, $TBR_T$ from finite element model and AASHTO equations (subgrade *CBR* = 0.5).

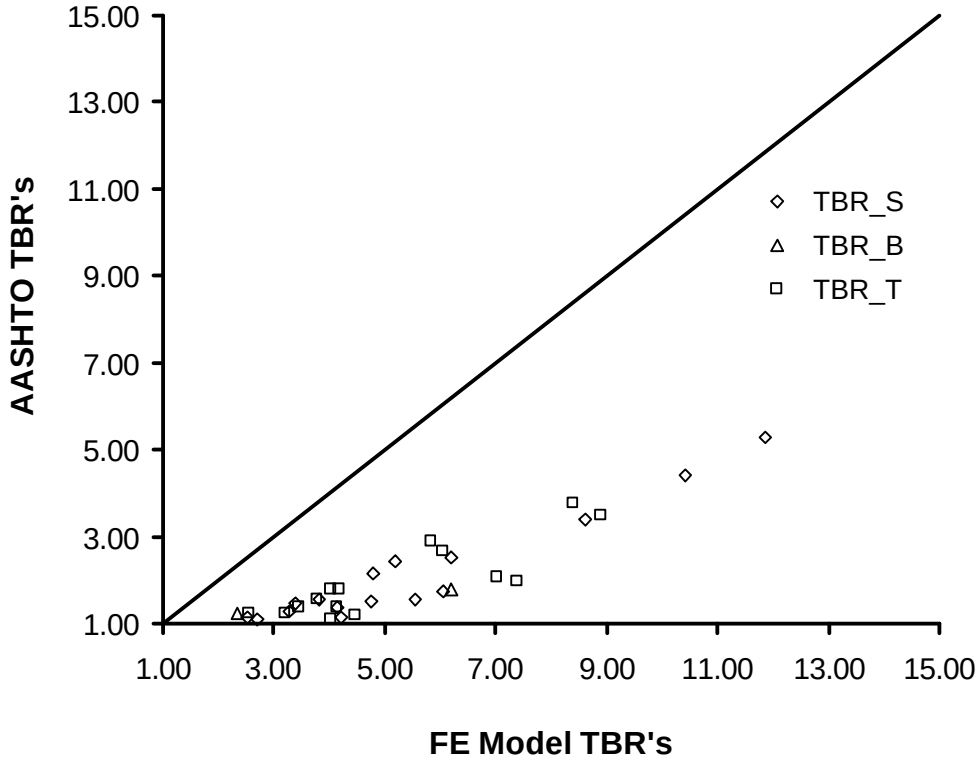


**Figure 7.1.4b** Remaining $TBR_S$, $TBR_B$, $TBR_T$ from finite element model and AASHTO equations (subgrade $CBR$ = 1).

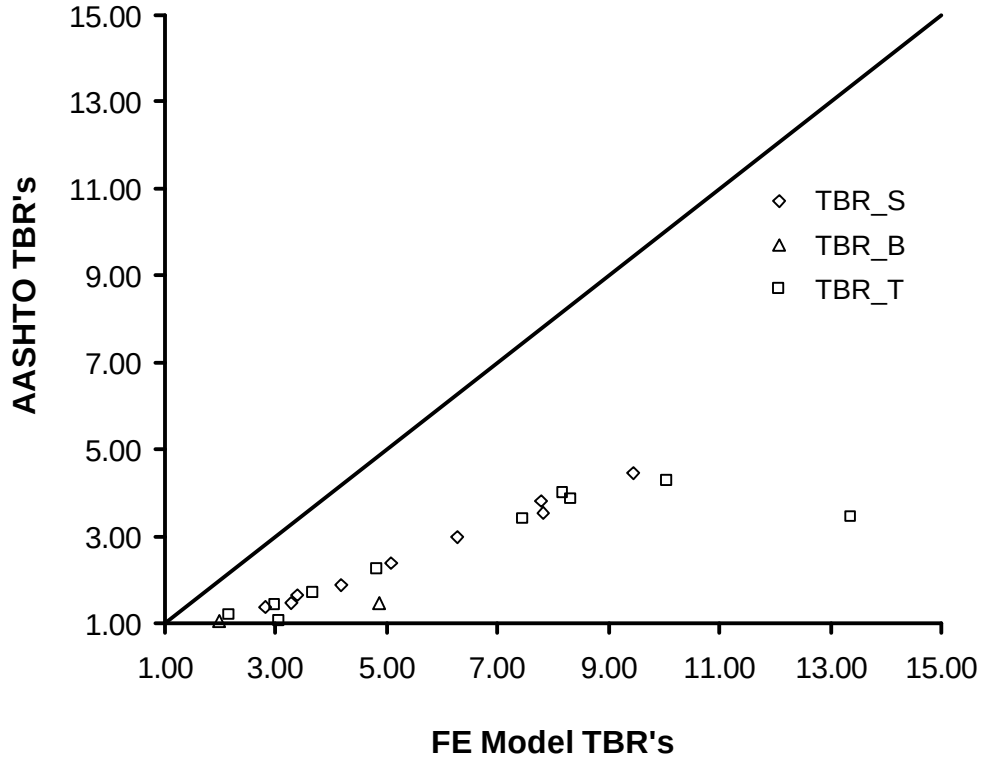


**Figure 7.1.4c** Remaining $TBR_S$, $TBR_B$, $TBR_T$ from finite element model and AASHTO equations (subgrade $CBR$ = 2).

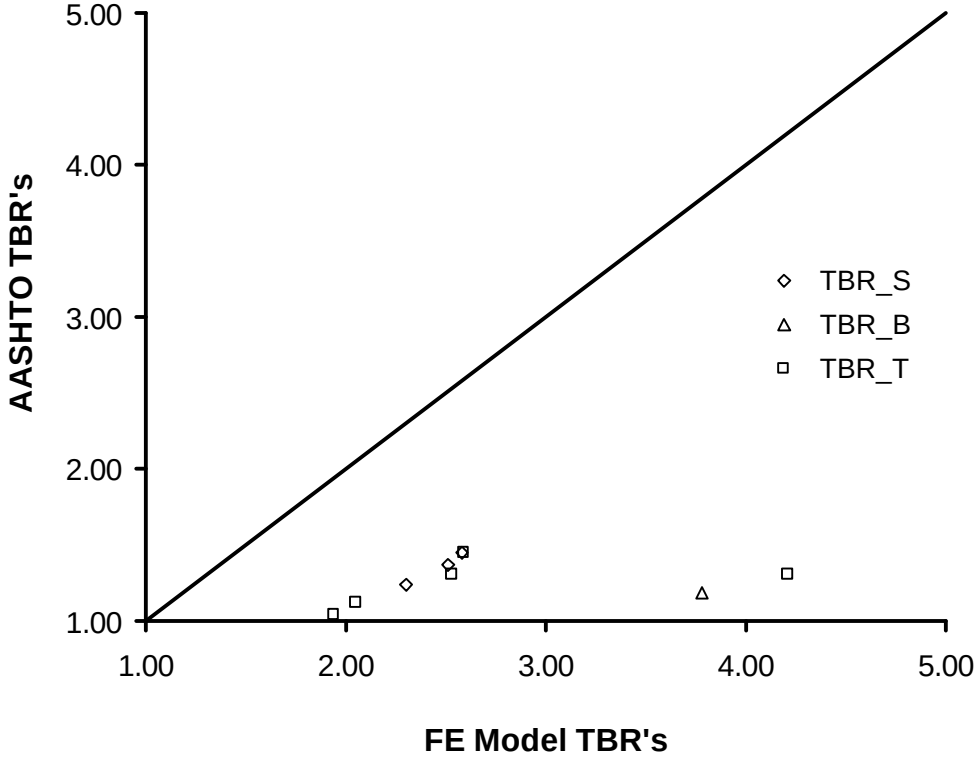


**Figure 7.1.4d** Remaining $TBR_S$, $TBR_B$, $TBR_T$ from finite element model and AASHTO equations (subgrade $CBR$ = 4).

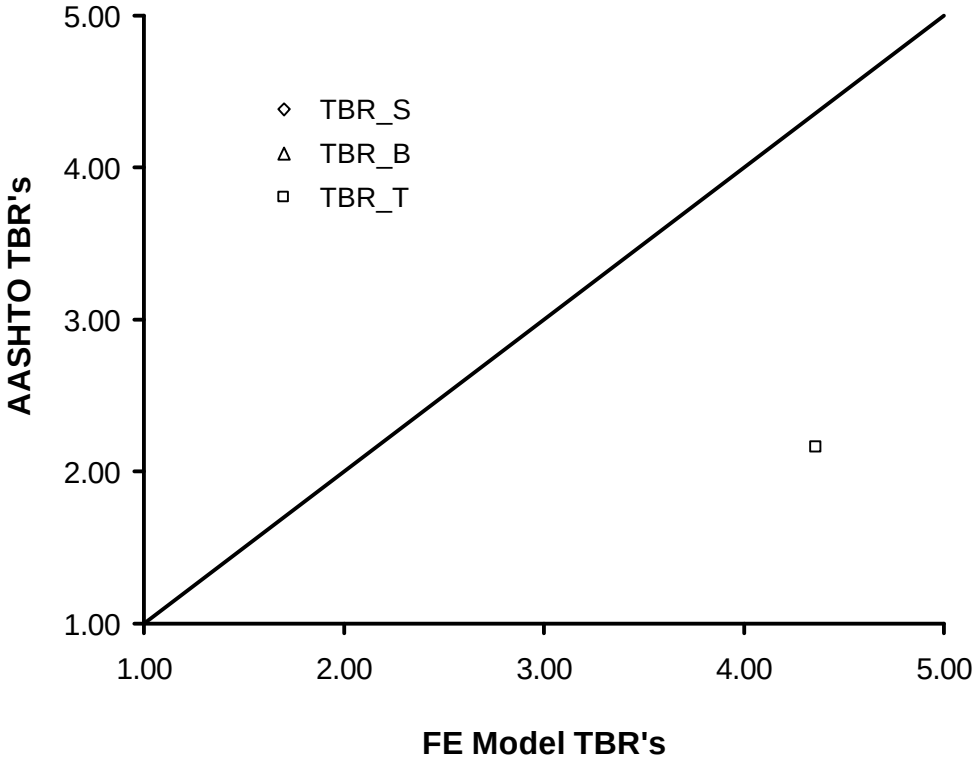


**Figure 7.1.4e** Remaining $TBR_S$, $TBR_B$, $TBR_T$ from finite element model and AASHTO equations (subgrade $CBR$ = 8).

The results seen in Figure 7.1.4 indicate that the use of the AASHTO equations is conservative with respect to that obtained from the finite element model for all *TBR* measures and for all subgrade cases except for the *CBR* = 0.5 case. Due to the apparent unconservative nature of this method for *CBR* = 0.5 and the decreased margin of safety when designing for a BCR at low values of subgrade CBR, it is recommended that this method described above for calculating *BCR* or *TBR*/*BCR* combinations be used only for designs with a subgrade *CBR* $ 1.

## 7.2 Influence of Geosynthetic Isotropic Elastic Modulus on *TBR*

Section 7.1 presented equations for determination of partial and total values of *TBR* ($TBR_S$, $TBR_B$, $TBR_T$) when *BCR* = 0 and a method for calculating either $BCR_{TBR=0}$ or combinations of *BCR* and *TBR* for the condition of perfect reinforcement. The addition of a new variable, namely geosynthetic isotropic modulus, precluded evaluating all 180 cases previously examined for the case of perfect reinforcement for each of the five values of reinforcement elastic modulus given in Section 6.2.1. Particular model cases were chosen for evaluation of each of the five reinforcement elastic modulus values. Section 6.2.1 described 250 additional finite element model cases created to examine the effect of the elastic modulus of the reinforcement on *TBR*. These cases were chosen to provide information on how values of geosynthetic isotropic elastic modulus reduced the *TBR* seen for the case of perfect reinforcement for critical cases.

The equations developed in Section 7.1 for the determination of $TBR_{S\text{-}PR}$, and as shown in Figure 7.1.1, showed that two straight lines in a semi-log plot of $TBR_{S\text{-}PR}$ versus section *SN* could approximate values of $TBR_{S\text{-}PR}$ for perfect reinforcement, where the equations for these lines was a function of the subgrade *CBR*. Key points along these curves correspond to values of *SN* of 1.6, 3.3 and for larger values of *SN* where $TBR_{S\text{-}PR}$ is seen to return to a value of 1. The three sets of model cases shown in Table 6.2.2 were chosen to provide results for sections with values of *SN* close to each of these three values. Three sections within each set were chosen to provide redundancy.

The effect of geosynthetic isotropic elastic modulus was expressed in terms of a reduction factor applied to the value of $TBR_{S\text{-}PR}$ obtained for the corresponding case of perfect reinforcement, where this reduction factor for geosynthetic isotropic modulus ($RF_{GM}$) is given by Equation 7.2.1. The reduction factor is expressed as a percentage and is relative to a *TBR* baseline value of 1.

$$RF_{GM} = 100 \times \frac{TBR_{S-GM} - 1}{TBR_{S-PR} - 1} \tag{7.2.1}$$

### *7.2.1 Equations for $TBR_S$*

Rather than attempting to evaluate the influence of *SN*, subgrade *CBR* and geosynthetic isotropic elastic modulus ($E_G$) on $RF_{GM}$ for all values of *SN*, it was decided to evaluate $RF_{GM}$ for specific values of *SN* for each subgrade *CBR* and geosynthetic isotropic modulus. In particular, a relationship between $RF_{GM}$, subgrade *CBR* and $E_G$ was sought for values of *SN* approximately equal to 1.6, 3.3 and for values between 4.8 and 6, where values of $E_G$ correspond to those used in the material model described in Section 4.3. Since $TBR_{S\text{-}PR}$ is equal to $y_1$, as used in Equations 7.1.3, 7.1.4 and 7.1.8 and shown in Figure 7.1.2, when $SN \approx 1.6$, evaluation of $RF_{GM}$ allows for a new expression to be developed for $y_1$ that accounts for the effect of geosynthetic elastic modulus. A similar approach is used to develop new expressions for $y_2$ and $SN_{TBR=1}$, as used in Equations 7.1.6, 7.1.7 and 7.1.9. In effect, values of geosynthetic isotropic elastic modulus cause the curves shown in Figure 7.1.1 to shift down by shifting points for $y_1$ and $y_2$ down and by shifting the point where the second curve passes through a value for *TBR* of 1 to the left. This is shown schematically in Figure 7.2.1.

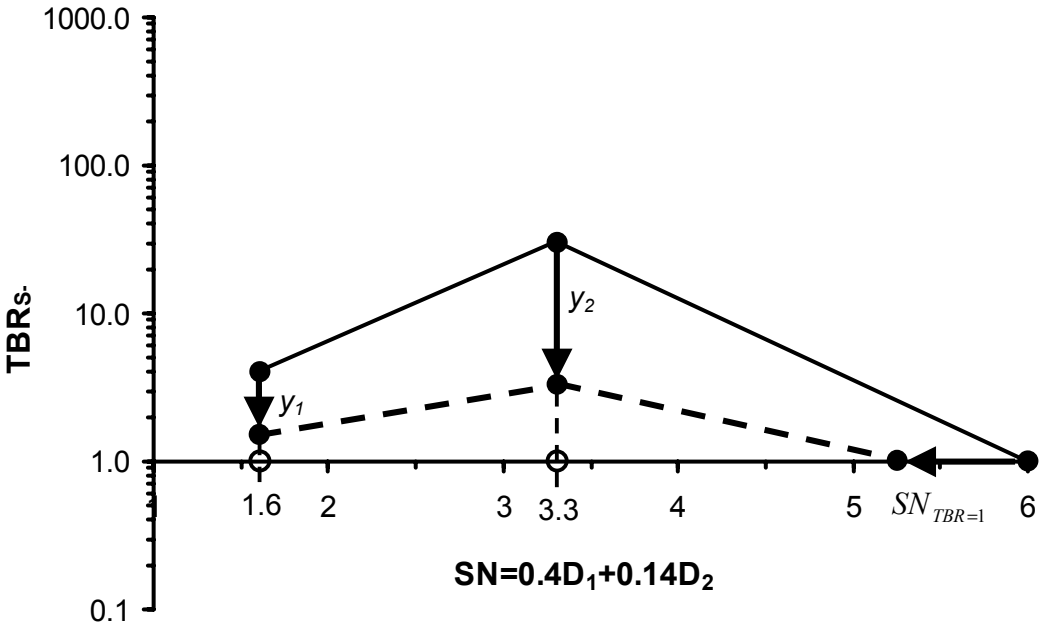


**Figure 7.2.1** Effect of geosynthetic isotropic elastic modulus on curves for $TBR_{S\text{-}PR}$.

The reduction factor for geosynthetic isotropic modulus (Equation 7.2.1) was evaluated for results from AC1-B1 cases, where $SN$ = 1.61, for all six subgrade types and all geosynthetic reinforcement values. Figure 7.2.2 shows the results for $RF_{GM}$ plotted against $E_G$. From these results, $RF_{GM}$ is seen to be strongly dependent on $E_G$ but not on the subgrade $CBR$. A regression equation fitting the data shown in Figure 7.2.2 yields the following equation for $RF_{GM}$, where $E_G$ is in units of kPa. Additional guidance will be provided on how values of $E_G$ are related to secant tensile modulus values from wide-width tensile data in Section 7.6. Equation 7.2.2 is valid for values of $E_G$ from 172,000 to 17,500,000 kPa.

$$RF_{GM} = 49.8 \log(E_G) - 261 \tag{7.2.2}$$

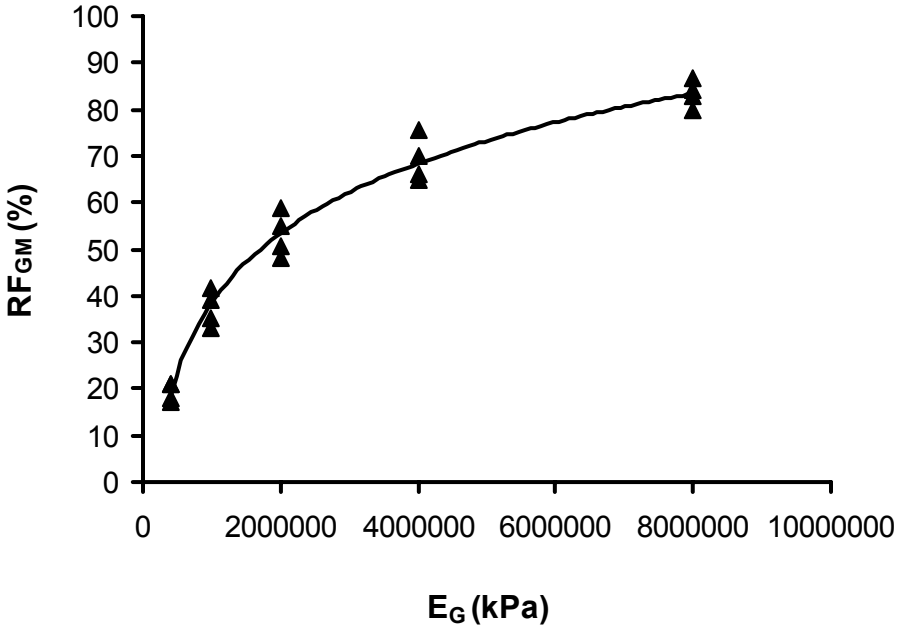


**Figure 7.2.2** Reduction factor for geosynthetic isotropic elastic modulus ($RF_{GM}$) for $SN \approx 1.6$.

Equation 7.2.3 is produced by combining Equations 7.2.1, 7.2.2 and 7.1.8, while recognizing that $TBR_{S\text{-}PR}$ is equal to $y_1$ in Equation 7.1.8 and $TBR_{S\text{-}GM}$ in Equation 7.2.1 is equal to the value of $y_1$ when geosynthetic isotropic elastic modulus is accounted for ($y_{1\text{-}GM}$). From this equation, the value of $y_1$ shown in Figure 7.1.2 can be computed and accounts for the subgrade $CBR$ and the geosynthetic isotropic elastic modulus.

$$y_{1-GM} = \frac{49.8 \log(E_G)}{100}\left(10^{(\log 8 - \log CBR)} - 1\right) + 1 \tag{7.2.3}$$

Finite element models corresponding to the second set listed in Table 6.2.2, where values of *SN* ranged between 2.99 and 3.62, were used to evaluate the influence of reinforcement isotropic elastic modulus on values of $y_2$. A reduction factor for isotropic elastic modulus was defined for these results according to Equation 7.2.1, where for these cases it is recognized that $TBR_{S\text{-}PR}$ is equal to $y_2$ in Equation 7.1.9 and $TBR_{S\text{-}GM}$ is equal to the value of $y_2$ when geosynthetic isotropic modulus is accounted for ($y_{2\text{-}GM}$). Figure 7.2.3 shows $RF_{GM}$ plotted against $E_G$. For these results, it is seen that $RF_{GM}$ is influenced by both reinforcement isotropic elastic modulus and subgrade *CBR*. Reduction factors become more significant as reinforcement modulus decreases and as subgrade *CBR* decreases. Straight lines were used to approximate the trends seen in the data, as shown in Figure 7.2.3, where each line extends through the origin and is given by Equation 7.2.4. The slope of the lines, *m*, was plotted against the subgrade *CBR*, as shown in Figure 7.2.4, with Equation 7.2.5 providing the best fit curve shown. Combination of Equations 7.2.4, 7.2.5, 7.2.2 and 7.1.9 yields a new equation for $y_2$ that accounts for reinforcement isotropic elastic modulus and subgrade *CBR*, where $E_G$ is in units of kPa.

$$RF_{GM} = m\, E_G \tag{7.2.4}$$

$$m = 1.8\times10^{-6}\log(CBR) + 1.57\times10^{-6} \tag{7.2.5}$$

$$y_{2-GM} = \frac{1.8\times10^{-6}\log(CBR) + 1.57\times10^{-6}}{100} E_G \left(10^{(\log 100 - 1.7\log CBR)} - 1\right) + 1 \tag{7.2.6}$$

The effect of reinforcement isotropic elastic modulus on values of $SN_{TBR=1}$ were evaluated by first using Equation 7.2.6 to calculate the value of $y_{2\text{-}GM}$ for each value of isotropic elastic modulus and subgrade *CBR* given in Table 6.2.2. Each value of $y_{2\text{-}GM}$ corresponds to $TBR_{S\text{-}GM}$ for a *SN*=3.3. For the corresponding finite element cases for AC5-B5 where *SN*=4.57, a value of $TBR_{S\text{-}GM}$ is known. Based on these two points, a straight line in a semi-log plot of $TBR_{S\text{-}GM}$ versus *SN* is used to estimate a value for *SN* when $TBR_{S\text{-}GM}$ = 1. Regression equations between these values and $E_G$ and subgrade *CBR* were then developed, with Equation 7.2.7 being the result.

$$SN_{TBR_{S-GM}=1} = 2.54\,(CBR - 0.28)^{0.028}\; E_G{}^{0.0504} \tag{7.2.7}$$

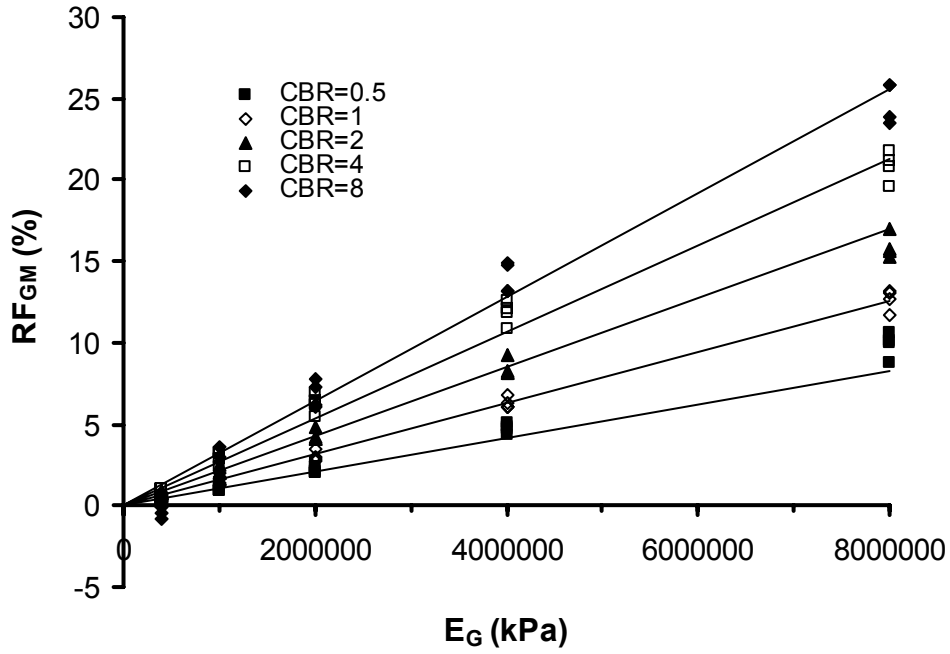


**Figure 7.2.3** Reduction factor for geosynthetic isotropic elastic modulus ($RF_{GM}$) for $SN \approx 3.3$.

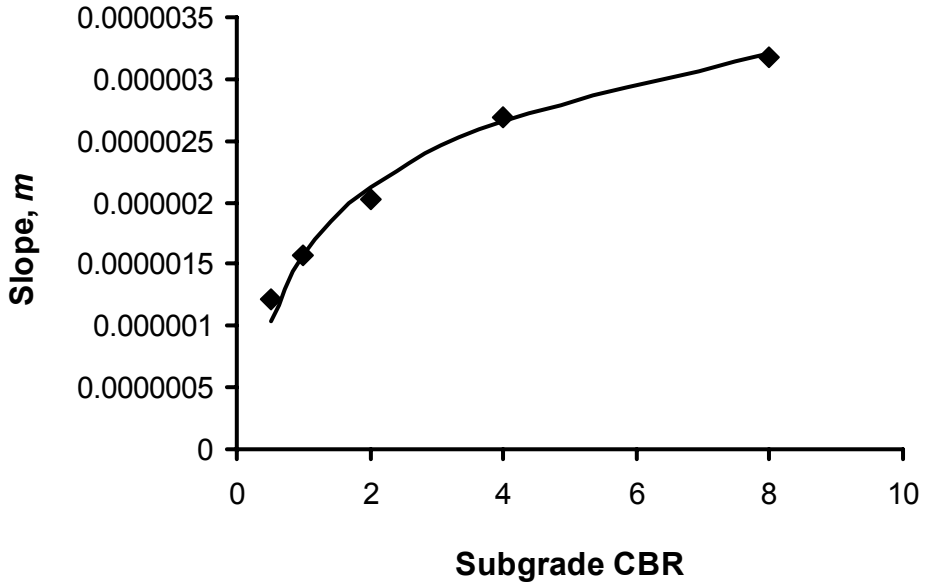


**Figure 7.2.4** Slope *m* versus subgrade *CBR*.

With Equations 7.2.3, 7.2.6 and 7.2.7 used to compute new values of $y_1$, $y_2$ and $SN_{TBR=1}$, the same general equations defined for the case of perfect reinforcement (Equations 7.1.2-7.1.7) are assumed to govern the relationship between $TBR_{S\text{-}GM}$ and *SN*. These equations then become Equations 7.2.8-7.2.13 when the effect of reinforcement isotropic elastic modulus is accounted for.

$1.6 \le SN \le 3.3$

$$TBR_{S-GM} = 10^{(m_1 SN + \log y_{o1})} \tag{7.2.8}$$

$$m_1 = \frac{\log \frac{y_{2-GM}}{y_{1-GM}}}{1.7} \tag{7.2.9}$$

$$y_{o1} = \frac{y_{1-GM}}{10^{(1.6 m_1)}} \tag{7.2.10}$$

$3.3 \le SN \le 6.0$

$$TBR_{S-GM} = 10^{(m_2 SN + \log y_{o2})} \tag{7.2.11}$$

$$m_2 = \frac{-\log y_{2-GM}}{SN_{(TBR_{S-GM}=1)} - 3.3} \tag{7.2.12}$$

$$y_{o2} = \frac{y_{2-GM}}{10^{(3.3 m_2)}} \tag{7.2.13}$$

### *7.2.2 Equations for $TBR_B$*

Reduction factors were also developed to modify values of $TBR_{B\text{-}PR}$ for the case of perfect reinforcement to account for values of geosynthetic isotropic elastic modulus. Evaluation of all cases contained in Table 6.2.2 indicated that the reduction factor for modulus was dependent most strongly on only the reinforcement modulus. The reduction factor developed, having the same general definition as that given in Equation 7.2.1, is given by Equation 7.2.14, where this equation is valid for values of $E_G$ between 143,000 and 8,835,000 kPa.

$$RF_{GM} = 55.8 \log(E_G) - 288 \tag{7.2.14}$$

Combination of Equations 7.2.14, 7.2.1, 7.1.10 and 7.1.11 yields Equation 7.2.15 for determination of $TBR_{B\text{-}GM}$ accounting for the influences of subgrade *CBR*, AC thickness and reinforcement isotropic modulus. The use of Equation 7.2.15 for the conditions present in the finite element cases given in Table 6.2.2 is compared in Figure 7.2.5 to the values of $TBR_B$ computed directly from the finite element results. From this figure it is seen that the combination of the equation used for the $TBR_{B\text{-}PR}$ (Equations 7.1.10 and 7.1.11) and the equation used for the reduction factor (Equation 7.2.14) results in conservative estimates of $TBR_B$ when compared to

results obtained directly from the finite element model and is also seen to eliminate some of the high values predicted for certain sections with a large base thickness.

$$TBR_{B-GM} = \frac{55.8\log(E_G) - 288}{100}\left[\left(1 - 4.45\,CBR^{-0.522}\right)\frac{D_1}{160} + 4.45\,CBR^{-0.522} - 1\right] + 1 \quad (7.2.15)$$

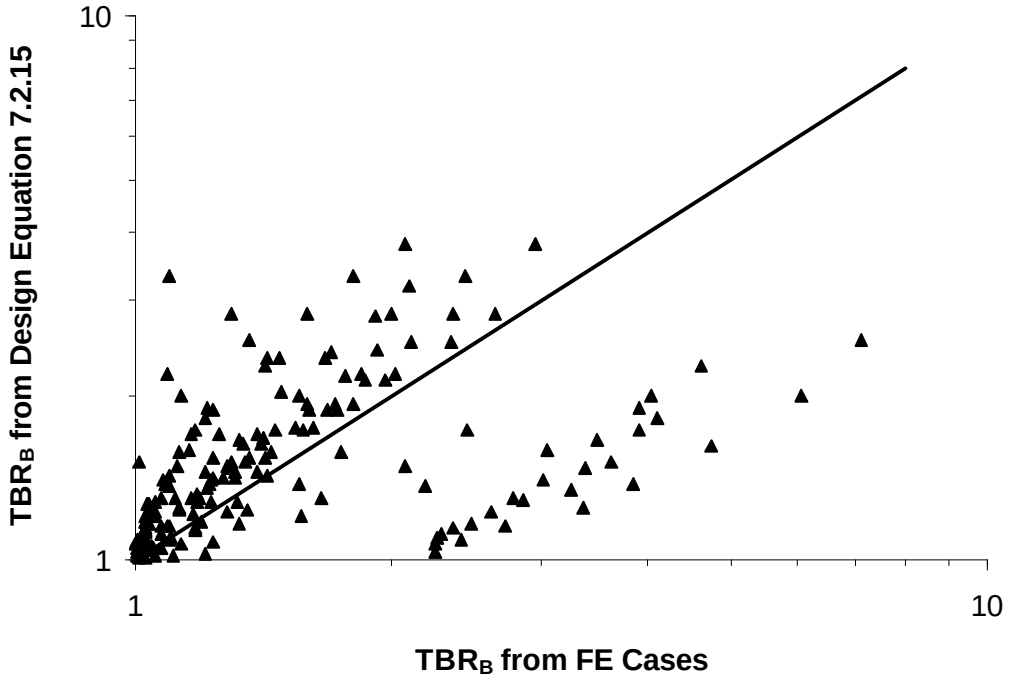


**Figure 7.2.5** $TBR_B$ comparison from FE model and Equation 7.2.15.

## 7.3 Influence of Geosynthetic Modulus Anisotropy on *TBR*

Effects of anisotropy of the elastic modulus of the geosynthetic between the machine and cross-machine directions were evaluated by comparison of values of *TBR* obtained from the model cases listed in Table 6.2.4 to corresponding cases with isotropic modulus values. Design equations for $TBR_{S\text{-}GM}$ and $TBR_{B\text{-}GM}$ were developed in Section 7.2 and were given by Equations 7.2.8-7.2.13 and 7.2.15, respectively. A reduction factor for geosynthetic modulus ratio was defined according to Equation 7.3.1 and evaluated for the finite element model cases listed in Table 6.2.4. Reduction factors were evaluated for corresponding *TBR* values for subgrade and base reinforcement effects.

$$RF_{GMR} = \frac{TBR_{GMR}}{TBR_{GM}} \quad (7.3.1)$$

For values of $TBR_S$, values of $RF_{GMR}$ were found to be approximated by straight line relationships given by Equation 7.3.2, where $m$ is the slope of the lines and was seen to be a function of $TBR_{S\text{-}GM}$, as given by Equation 7.3.3 and $G_{MR}$ is the ratio of moduli and is given by Equation 7.3.4.

$$RF_{GMR} = m\, G_{MR} + 1 - m \tag{7.3.2}$$

$$m = 0.62 \log(TBR_{S-GM}) \tag{7.3.3}$$

$$G_{MR} = \frac{E_{G-\min}}{E_{G-\max}} \tag{7.3.4}$$

Combination of Equations 7.3.1, 7.3.2 and 7.3.3 yields Equation 7.3.5.

$$TBR_{S-GMR} = TBR_{S-GM}\left[0.62 \log(TBR_{S-GM})\, G_{MR} + 1 - 0.62 \log(TBR_{S-GM})\right] \tag{7.3.5}$$

A similar analysis for values of $TBR_B$ showed that the reduction factor was dependent primarily on $G_{MR}$, which allowed Equation 7.3.6 to be developed.

$$TBR_{B-GMR} = TBR_{B-GM}\left(0.2\, G_{MR} + 0.8\right) \tag{7.3.6}$$

Evaluation of $TBR_{S\text{-}GM}$ and $TBR_{B\text{-}GM}$ from Equations 7.2.8-7.2.13 and 7.2.15, respectively, for the case of isotropic geosynthetic modulus values allows these values to be reduced by the use of Equations 7.3.5 and 7.3.6 when $G_{MR}$ from Equation 7.3.4 is evaluated.

## 7.4 Influence of Geosynthetic Poisson's Ratio and Shear Modulus on *TBR*

The finite element model cases presented in Tables 6.2.5 and 6.2.6 were used to examine the effect of reducing Poisson's ratio and shear modulus to zero from the values used for the case of isotropic material properties. A reduction factor was computed for the effect of reducing each variable according to Equations 7.4.1 and 7.4.2, where $TBR_n$ and $TBR_G$ were values of *TBR* obtained directly from the cases examined where either $n$ or $G$ was reduced to zero and $TBR_{GM}$

was the *TBR* for the corresponding model case where isotropic elastic values were used for the geosynthetic material. A reduction factor was also computed for the combined effect of reducing both *n* and *G* according to Equation 7.4.3. Geosynthetic property cases from Table 6.2.5 of G*nG*3 and G*nG*4 were used to evaluate $RF_{Gn}$. Cases G*nG*5 and G*nG*6 were used to evaluate $RF_{GG}$. Cases G*nG*7 and G*nG*8 were used to evaluate $RF_{GnG}$. Reduction factors for both values of $TBR_S$ and $TBR_B$ were evaluated.

$$RF_{Gn} = \frac{TBR_n}{TBR_{GM}} \tag{7.4.1}$$

$$RF_{GG} = \frac{TBR_G}{TBR_{GM}} \tag{7.4.2}$$

$$RF_{GnG} = \frac{TBR_{nG}}{TBR_{GM}} \tag{7.4.3}$$

Table 7.4.1 summarizes average values of reduction factors obtained for each reinforcement effect (i.e. base and subgrade). From these results, it appears that the combined effect of reducing both Poisson's ratio and shear modulus to zero corresponds to the product of the two reduction factors for each individual effect. Based on these results, reduction factors can be used either individually or in series and applied to $TBR_{S\text{-}GM}$ and $TBR_{B\text{-}GM}$ for reduction of these *TBR*'s according to Equations 7.4.1-7.4.3.

**Table 7.4.1** Reduction factors for reinforcement Poisson's ratio and shear modulus.

| | $RF_{Gn}$ | $RF_{GG}$ | $RF_{GnG}$ |
|---|---|---|---|
| $TBR_S$ | 0.83 | 0.92 | 0.75 |
| $TBR_B$ | 0.96 | 0.99 | 0.95 |

## 7.5 Influence of Interface Properties on *TBR*

Specific finite element model cases were not created to examine the effect of varying geosynthetic-base aggregate interface properties for the reasons described in Section 4.3, where it was argued that the influence of interface shear properties should be accounted for by comparison of predictions from the design model to test section results. The computation of *TBR* accounting for all the effects described above implicitly assumes optimal interface properties. A

reduction factor for interface properties is introduced to account for the influence of interface shear properties as given in Equation 7.5.1. Calibration of this reduction factor for the geosynthetics previously used in test sections reported in Perkins (1999a) is described in Section 7.6.

$$RF_{GI} = \frac{TBR_I}{TBR_{GM}} \tag{7.5.1}$$

## 7.6 Calibration of Design Model

The model described above was calibrated by comparison of the model to test section results described in Section 3. From Section 3, values of $TBR_B$, $TBR_S$ and $TBR_T$ are available for several reinforced test sections. The model is calibrated by comparison of these values to corresponding predictions from the design model. A match is sought for values of $TBR_S$ because of the generally conservative nature of values for $TBR_B$ predicted from the model. Values for 2 % secant tensile modulus for the geosynthetic products used in the test sections were given in Table 3.1.2 and are related to values of geosynthetic elastic modulus as described below.

Calibration began by the use of test sections CS5 and CS11, which used Geogrid B and A, respectively. These geosynthetics are rigid, extruded geogrids with different values of 2 % secant tensile modulus. As discussed previously in Section 2.1, existing but limited data shows high values of reinforcement benefit with this type of product. For this reason, reduction factors for Poisson's ratio, shear modulus and interface shear were all set to one. This presumes that this class of geosynthetic provides optimal properties described in terms of Poisson's ratio, shear modulus and interface shearing resistance. Values of 2 % secant tensile modulus given in Table 3.1.2 were used to determine values of geosynthetic modulus ratio ($G_{MR}$) of 0.595 for Geogrid A and a ratio of 0.614 for Geogrid B. Using these values, it was seen that the maximum values of 2 % secant modulus (i.e. values in the cross-machine directions) of 425 and 595 kN/m for Geogrid A and B, respectively, required multiplication by a factor of 4400 to produce values of $TBR_S$ that provided an average of the values reported in Table 3.2.1 for test sections CS11 and CS5. This factor was then taken as the factor necessary to relate the wide-width tensile modulus measured at 2 % axial strain ($G_{SM\text{-}2\%}$) to the value of elastic modulus used in the material model described in Section 4.3. This relationship is expressed in Equation 7.6.1. As described in Section 4.3, a one-to-one correspondence between these values was not expected. The majority of the factor of

4400 is due to the difference in units (i.e. kPa for $E_G$ and kN/m for $G_{SM\text{-}2\%}$) and the assumed thickness of the geosynthetic of 1 mm when defining $E_G$. This feature alone accounts for a factor of 1000. The remaining factor of 4.4 is most likely due to differences in loading rate between wide-width tension tests and pavement loading applications, and the use of a relatively high strain value for definition of the secant tensile modulus in comparison to the small dynamic strains induced in the geosynthetic in the roadway. A summary of the input values for these two test sections is provided in Table 7.6.1.

$$E_G = 4400 \times G_{SM-2\%} \tag{7.6.1}$$

Results from test section CS10 could be compared to the model predictions at this point. Test section CS10 also used Geogrid A and therefore the same values for this material were used as those used for test section CS11. The thickness of the base layer was increased to 375 mm. The model predicted a value of $TBR_S$ of 2.45 while a value from the test section of 2.23 was observed.

Results from test section CS6 were then used to calibrate a reduction factor for interface shear resistance. Test section CS6 used Geotextile A, which was a relatively lightweight woven material. The qualitative application guidelines given in Table 2.1.2, which are based on a review of the literature, suggest that reduction factors for Poisson's ratio and shear modulus, as given in Table 7.4.1, be used. Values of reduction factors given in Table 7.4.1 for Poisson's ratio and shear modulus corresponding to a Poisson's ratio of zero and a shear modulus of zero were used. Using a modulus ratio of 0.313 and a secant tensile modulus at 2 % strain of 680 kN/m, and keeping the reduction factor for interface shearing resistance to one for the time being, a $TBR_S$ of 2.17 was predicted from the model. A value of 1.66 was observed from test section CS6. The remainder of the reduction was assumed to be due to differences in interface shear conditions. To produce a $TBR_S$ of 1.66, a reduction factor for interface shearing resistance ($RF_{GI}$) of 0.765 was required. This reduction factor is taken as also being applicable to values of $TBR_B$. This value, along with the other reduction factors assumed, is taken as representative for this type of geosynthetic material.

Tables 7.6.1 and 7.6.2 provide a summary of all properties used in the design model for the test sections described above and values of $TBR_B$, $TBR_S$ and $TBR_T$ from the design model and

from the test sections. Due to the method used for calibration of the design model, the values of $TBR_S$ from the design model are seen to offer good predictions of values from the test sections. The predicted values of $TBR_B$ are considerably less and conservative in comparison to those seen from the test sections. The reasons for this are believed to be due to the inability of the material model for the base aggregate to properly show the effects of increases in bulk stress on base layer behavior. The comparatively low and conservative predictions of $TBR_T$ is due to the conservative values predicted for $TBR_B$ and the conservative procedure for multiplication of $TBR_B$ and $TBR_S$ to produce $TBR_T$.

**Table 7.6.1** Summary input parameters for design model and test section comparisons.

| Test Section | CS5 | CS6 | CS10 | CS11 |
|---|---|---|---|---|
| Geosynthetic | geogrid B | geotextile A | geogrid A | geogrid A |
| AC Thickness, $D_1$ (mm) | 75 | 75 | 75 | 75 |
| Base Thickness, $D_2$ (mm) | 300 | 300 | 375 | 300 |
| Subgrade *CBR* | 1.5 | 1.5 | 1.5 | 1.5 |
| 2 % Secant Modulus, $G_{SM\text{-}2\%}$ (kN/m) | 595 | 680 | 425 | 425 |
| Geosynthetic Modulus Ratio, $G_{MR}$ | 0.615 | 0.313 | 0.595 | 0.595 |
| Reduction factor for interface shear, $RF_I$ | 1 | 0.765 | 1 | 1 |
| RF for Poisson's ratio, $RF_{Gn}$, on $TBR_S$ | 1 | 0.83 | 1 | 1 |
| RF for Poisson's ratio, $RF_{Gn}$, on $TBR_B$ | 1 | 0.96 | 1 | 1 |
| RF for shear modulus, $RF_{GG}$, on $TBR_S$ | 1 | 0.92 | 1 | 1 |
| RF for shear modulus, $RF_{GG}$, on $TBR_B$ | 1 | 0.99 | 1 | 1 |

**Table 7.6.2** Summary output for design model and test section comparisons.

| Test Section | | | CS5 | CS6 | CS10 | CS11 |
|---|---|---|---|---|---|---|
| $TBR_{BCR=0}$ | Test section values | Subgrade | 2.95 | 1.66 | 2.23 | 2.61 |
| | | Base | 7.74 | 1.43 | 2.63 | 3.01 |
| | | Total | 29.7 | 2.90 | 9.82 | 13.5 |
| | Design model predictions | Subgrade | 3.02 | 1.66 | 2.45 | 2.54 |
| | | Base | 1.82 | 1.27 | 1.71 | 1.71 |
| | | Total | 5.51 | 2.10 | 4.19 | 4.34 |

## 7.7 Comparison of Model to Other Published Results

Berg et al. (2000) provided summary tables of pavement design parameters, geosynthetic type and reinforcement benefit for test sections published in the literature. Many sections used Geogrids A and B described in Table 3.1.2. The manufacturer provided values of tensile strength at 2 % axial strain for Geogrids H, K and L (Tenax, 2001) listed in Table 2-5 of Berg et al.

(2000). Values of other model parameters for this material are as assumed in Table 7.7.1. These conditions were input into the design model to provide a comparison of predicted reinforcement benefit. The studies described in Berg et al. (2000) listed either a total *TBR* or total *BCR* for reinforcement benefit. As such, these corresponding numbers from the model are used as comparison

In general, the predicted values of benefit from the model are seen to be conservative with respect to those observed from the test sections. The cases where the model over predicted results appear to be mostly from the studies of Barksdale et al. (1989) and Collin et al. (1996). The study of Barksdale et al. (1989) used a relatively light wheel load (6.6 kN) and may be partly responsible for the lack of benefit seen for this test section. The wheel load in the study of Collin et al. (1996) was 20 kN and is also relatively light in comparison to that assumed in the design model. The design model appears to be not as sensitive to base aggregate thickness as the results from Collin et al. (1996) and Kinney et al. (1998) suggest.

**Table 7.7.1** Summary output for design model and test section comparisons.

| Study | $D_1$ (mm) | $D_2$ (mm) | Subgrade *CBR* | $G_{SM\text{-}2\%}$ (kN/m) | $G_{MR}$ | $RF_{GI}$ | $RF_{Gn}$ $(TBR_B)$ | $RF_{Gn}$ $(TBR_S)$ | $RF_{GG}$ $(TBR_B)$ | $RF_{GG}$ $(TBR_S)$ |
|---|---|---|---|---|---|---|---|---|---|---|
| 1 | 38 | 200 | 2.5 | 425 | 0.595 | 1.0 | 1.0 | 1.0 | 1.0 | 1.0 |
| 2 (1) | 75 | 300 | 1.0 | 425 | 0.595 | 1.0 | 1.0 | 1.0 | 1.0 | 1.0 |
| 3 (1) | 75 | 300 | 8.0 | 425 | 0.595 | 1.0 | 1.0 | 1.0 | 1.0 | 1.0 |
| 3 (2) | 75 | 300 | 3.0 | 425 | 0.595 | 1.0 | 1.0 | 1.0 | 1.0 | 1.0 |
| 3 (3) | 75 | 400 | 3.0 | 425 | 0.595 | 1.0 | 1.0 | 1.0 | 1.0 | 1.0 |
| 3 (4) | 75 | 500 | 3.0 | 425 | 0.595 | 1.0 | 1.0 | 1.0 | 1.0 | 1.0 |
| 4 (1) | 50 | 175 | 1.9 | 425 | 0.595 | 1.0 | 1.0 | 1.0 | 1.0 | 1.0 |
| 4 (2) | 50 | 200 | 1.9 | 425 | 0.595 | 1.0 | 1.0 | 1.0 | 1.0 | 1.0 |
| 4 (3) | 50 | 225 | 1.9 | 425 | 0.595 | 1.0 | 1.0 | 1.0 | 1.0 | 1.0 |
| 4 (4) | 50 | 250 | 1.9 | 425 | 0.595 | 1.0 | 1.0 | 1.0 | 1.0 | 1.0 |
| 4 (5) | 50 | 275 | 1.9 | 425 | 0.595 | 1.0 | 1.0 | 1.0 | 1.0 | 1.0 |
| 5 (1) | 100 | 200 | 8.0 | 425 | 0.595 | 1.0 | 1.0 | 1.0 | 1.0 | 1.0 |
| 5 (2) | 75 | 200 | 3.5 | 425 | 0.595 | 1.0 | 1.0 | 1.0 | 1.0 | 1.0 |
| 5 (3) | 75 | 200 | 1.0 | 425 | 0.595 | 1.0 | 1.0 | 1.0 | 1.0 | 1.0 |
| 5 (4) | 75 | 300 | 0.5 | 425 | 0.595 | 1.0 | 1.0 | 1.0 | 1.0 | 1.0 |
| 5 (5) | 75 | 200 | 3.5 | 425 | 0.595 | 1.0 | 1.0 | 1.0 | 1.0 | 1.0 |
| 6 | 100 | 280 | 4 | 425 | 0.595 | 1.0 | 1.0 | 1.0 | 1.0 | 1.0 |
| 2 (2) | 75 | 300 | 1 | 325 | 0.677 | 1.0 | 1.0 | 1.0 | 1.0 | 1.0 |
| 2 (3) | 75 | 300 | 3 | 325 | 0.677 | 1.0 | 1.0 | 1.0 | 1.0 | 1.0 |
| 2 (4) | 75 | 300 | 8 | 325 | 0.677 | 1.0 | 1.0 | 1.0 | 1.0 | 1.0 |
| 2 (5) | 75 | 300 | 18 | 325 | 0.677 | 1.0 | 1.0 | 1.0 | 1.0 | 1.0 |
| 3 (5) | 75 | 300 | 3 | 325 | 0.677 | 1.0 | 1.0 | 1.0 | 1.0 | 1.0 |
| 3 (6) | 75 | 400 | 3 | 325 | 0.677 | 1.0 | 1.0 | 1.0 | 1.0 | 1.0 |
| 3 (7) | 75 | 500 | 3 | 325 | 0.677 | 1.0 | 1.0 | 1.0 | 1.0 | 1.0 |
| 3 (8) | 75 | 300 | 8 | 325 | 0.677 | 1.0 | 1.0 | 1.0 | 1.0 | 1.0 |
| 3 (9) | 75 | 400 | 3 | 595 | 0.615 | 1.0 | 1.0 | 1.0 | 1.0 | 1.0 |
| 3 (10) | 75 | 1000 | 1 | 595 | 0.615 | 1.0 | 1.0 | 1.0 | 1.0 | 1.0 |
| 4 (6) | 50 | 175 | 1.9 | 595 | 0.615 | 1.0 | 1.0 | 1.0 | 1.0 | 1.0 |
| 4 (7) | 50 | 200 | 1.9 | 595 | 0.615 | 1.0 | 1.0 | 1.0 | 1.0 | 1.0 |
| 4 (8) | 50 | 225 | 1.9 | 595 | 0.615 | 1.0 | 1.0 | 1.0 | 1.0 | 1.0 |
| 4 (9) | 50 | 250 | 1.9 | 595 | 0.615 | 1.0 | 1.0 | 1.0 | 1.0 | 1.0 |
| 4 (10) | 50 | 275 | 1.9 | 595 | 0.615 | 1.0 | 1.0 | 1.0 | 1.0 | 1.0 |
| 7 (1) | 61 | 250 | 2.5 | 595 | 0.615 | 1.0 | 1.0 | 1.0 | 1.0 | 1.0 |
| 7 (2) | 61 | 300 | 2.5 | 595 | 0.615 | 1.0 | 1.0 | 1.0 | 1.0 | 1.0 |
| 7 (3) | 61 | 350 | 2.5 | 595 | 0.615 | 1.0 | 1.0 | 1.0 | 1.0 | 1.0 |
| 3 (11) | 75 | 400 | 3 | 450 | 0.677 | 1.0 | 1.0 | 1.0 | 1.0 | 1.0 |
| 3 (12) | 75 | 1000 | 1 | 450 | 0.677 | 1.0 | 1.0 | 1.0 | 1.0 | 1.0 |
| 3 (13) | 75 | 300 | 3 | 500 | 0.600 | 1.0 | 1.0 | 1.0 | 1.0 | 1.0 |
| 3 (14) | 75 | 400 | 3 | 500 | 0.600 | 1.0 | 1.0 | 1.0 | 1.0 | 1.0 |
| 3 (15) | 75 | 500 | 3 | 500 | 0.600 | 1.0 | 1.0 | 1.0 | 1.0 | 1.0 |
| 3 (16) | 75 | 1000 | 1 | 500 | 0.600 | 1.0 | 1.0 | 1.0 | 1.0 | 1.0 |

Study References: Study 1: Barksdale et al. (1989); Study 2: Cancelli et al. (1996)
Study 3: Cancelli and Montanelli (1999); Study 4: Collin et al. (1996)
Study 5: Haas et al. (1988); Study 6: Huntington and Ksaibati (1999)
Study 7: Kinney et al. (1998)

**Table 7.7.2** Summary output for design model and test section comparisons.

| Study | $TBR_T$ Study | $TBR_T$ Model | $BCR_T$ Study | $BCR_T$ Model |
|---|---|---|---|---|
| 1 | 1.0 | 3.3 | NA | NA |
| 2 (1) | 17 | 6.8 | NA | NA |
| 3 (1) | 1.2 | 1.2 | NA | NA |
| 3 (2) | 220 | 2.2 | NA | NA |
| 3 (3) | 340 | 2.1 | NA | NA |
| 3 (4) | 8.4 | 1.9 | NA | NA |
| 4 (1) | 1.7 | 4.2 | NA | NA |
| 4 (2) | 1.8 | 4.1 | NA | NA |
| 4 (3) | 1.7 | 4.1 | NA | NA |
| 4 (4) | 3.3 | 4.0 | NA | NA |
| 4 (5) | 2.6 | 4.0 | NA | NA |
| 5 (1) | 3.3 | 1.1 | NA | NA |
| 5 (2) | 3.0 | 2.0 | NA | NA |
| 5 (3) | 1.8 | 7.2 | NA | NA |
| 5 (4) | 0.8 | 15.2 | NA | NA |
| 5 (5) | NA | NA | 50 | 20 |
| 6 | NA | NA | 35 | 14 |
| 2 (2) | 15 | 5.9 | NA | NA |
| 2 (3) | 5.2 | 2.0 | NA | NA |
| 2 (4) | 3.2 | 1.1 | NA | NA |
| 2 (5) | 4.5 | 1.0 | NA | NA |
| 3 (5) | 300 | 2.0 | NA | NA |
| 3 (6) | 330 | 1.9 | NA | NA |
| 3 (7) | 13 | 1.8 | NA | NA |
| 3 (8) | 1.6 | 1.1 | NA | NA |
| 3 (9) | 410 | 2.5 | NA | NA |
| 3 (10) | NA | NA | < 50 | 11 |
| 4 (6) | 2.1 | 4.9 | NA | NA |
| 4 (7) | 2.8 | 4.9 | NA | NA |
| 4 (8) | 6.1 | 4.8 | NA | NA |
| 4 (9) | 10.0 | 4.8 | NA | NA |
| 4 (10) | 3.2 | 4.8 | NA | NA |
| 7 (1) | 10 | 3.4 | NA | NA |
| 7 (2) | 4.8 | 3.4 | NA | NA |
| 7 (3) | 2.0 | 3.3 | NA | NA |
| 3 (11) | 410 | 2.2 | NA | NA |
| 3 (12) | NA | NA | > 50 | 10 |
| 3 (13) | 250 | 2.4 | NA | NA |
| 3 (14) | 670 | 2.3 | NA | NA |
| 3 (15) | 13 | 2.0 | NA | NA |
| 3 (16) | NA | NA | > 50 | 10 |

## 7.8 Discussion of Design Model

The design model developed and presented in Section 7 and summarized in Section 8 is capable of describing general trends relating reinforcement benefit to pavement design variables that have previously been identified as having a significant impact on reinforced pavement performance. In particular, the model is capable of showing that reinforcement benefit increases with decreasing subgrade strength/stiffness, increasing geosynthetic modulus and is related to the pavement structural thickness.

The model is expressed in terms of easily identifiable and well-recognized parameters related to the pavement structure and the subgrade condition. Geosynthetic tensile modulus and the ratio of modulus for the weak and strong directions of the material are determined from wide-width tension tests (ASTM 4595). Reduction factors for other geosynthetic properties used in the model, namely Poisson's ratio and shear modulus, and for interface shearing resistance have been developed for the geosynthetics used in test sections from which the model was calibrated. These values provide initial guidance for selection of these reduction factors for other geosynthetic types. Results from test sections using a wider range of geosynthetic products and results from additional laboratory interface and tension tests are needed to further define these reduction factors. In the absence of this information, the values provided in this report along with general application guidelines provided in Berg et al. (2000) should be used for selection of these factors.

The model presents a means of calculating reinforcement benefit for reinforcement effects on the subgrade, the base aggregate or the total system. Equations for calculating benefit due to each effect are provided and allow pavement designers to use their discretion in choosing which effect or effects to design for.

The model is believed to be conservative on several accounts. Use of only benefit accounting for effects in the subgrade layer results in a conservative design since effects in the base layer are ignored. Comparisons of the model to test section results indicate that partial benefits for reinforcement effects in the subgrade are considerably less than that for the entire system. The method used to calculate reinforcement benefit for the base aggregate layer was shown to yield values of benefit that are consistently less than those determined for test sections. The equation used to calculate total *TBR* from the partial values for the base and subgrade layers was shown to be conservative as compared to test section results. Given these observations, it is

recommended that total values of *TBR* be used for design purposes. Finally, the method used to calculate *BCR* and *TBR/BCR* combinations was shown to be conservative with respect to that predicted by the finite element model.

The design model is based on certain conditions to which the model should be limited. The response measures extracted from the finite element model are used to define pavement performance in terms of permanent surface deformation or rutting. Furthermore, the design model has been calibrated against test section results where pavement life was defined in terms of rutting due to the accumulation of permanent strain in the base and subgrade layers. As such, the model specifically addresses designs for which rutting is the controlling pavement distress feature. It should be noted, however, that test sections have shown that the dynamic deflection of the pavement surface is decreased by the use of reinforcement, which suggests that dynamic tensile strain in the bottom of the asphalt concrete layer is reduced and fatigue life is increased.

The distress feature of rutting generally controls for pavement cross sections containing relatively thin layers of asphalt concrete and base course aggregate and for pavement structural layers resting on weak subgrade. The design model predicts the greatest levels of benefit for those situations, meaning that the design model will tend to predict useful levels of benefit for pavement designs for which rutting controls. The AASHTO ’93 pavement design guide does not provide specific design checks for the individual pavement distress features of rutting and asphalt fatigue cracking. Rather, designs developed using the AASHTO ’93 guide assume that both pavement distress features are adequately addressed. For pavement designers who use methods for individually checking rutting and fatigue cracking criteria (namely mechanistic-empirical approaches), a method is presented in Section 8.7 to evaluate the effective increase in resilient modulus of the base aggregate layer with reinforcement. This increased modulus should be used to evaluate the fatigue cracking criteria for the asphalt concrete layer.

The design model was based on the results of finite element analyses calibrated against test section results. The parametric study using the finite element response model employed a range of input variables to which the design model should be limited. Furthermore, the regression equations developed from the results of the parametric study contain certain limitations on the range of values for input parameters. A summary of the permissible range of design model input parameters is as follows:

1. 50 mm = $D_1$ = 150 mm

2. 150 mm = $D_2$ = 600 mm
3. 0.5 = Subgrade *CBR* = 15 *or* 5.2 MPa = $M_S$ = 155 MPa
4. 33 kN/m = $G_{SM\text{-}2\%}$ = 2000 kN/m

As discussed in Section 7.1.2, it is recommended that values of *BCR* > 0 be used only for subgrades with a *CBR* = 1.0 (or $M_S$ = 10.3 MPa).

The finite element response model was used to evaluate cases only where the geosynthetic was placed at the bottom of the base aggregate layer. Guidance for evaluation of benefit when the geosynthetic is placed up within the base for thick base layer designs has not been provided. The finite element models developed did not contain a subbase aggregate layer. For designs using a subbase layer, recommendations are provided in Section 8.6 for accounting for this layer.

The model is based on results from a finite element model where pavement load has been simulated by the application of a 40 kN load applied over a circular plate. Experimental test section results from which the model has been validated used a similar load. The design model is therefore designed to describe reinforcement benefit for conventional roadway applications where the pavement load can be approximated in terms of a standard axle wheel load. The model may not be appropriate for either lightly loaded traffic or for excessively loaded traffic.

The model is calibrated largely from results based on a permanent pavement surface deformation of 12.5 mm. It is anticipated that roadways that can be designed for a rut depth greater than 12.5 mm will realize reinforcement benefits greater than those predicted from this model, meaning that this model should be conservative for roadways designed for a rut depth in excess of 12.5 mm.

The model is based on asphalt concrete and base aggregate properties that correspond to structural layer coefficients of approximately 0.4 and 0.14, respectively. To account for pavement designs with different materials yielding different layer coefficients, recommendations are provided in Section 8.5.

## 8.0 DESIGN MODEL SUMMARY

Section 7 described the methods used to interpret the data from the parametric study described in Section 6. Through this interpretation process, a design model emerged and was compared to results from test sections described in Section 3 and validated against others given in Berg et al.

(2000). The purpose of this section is to summarize the essential elements of the design model from that which was given in Section 7.

## 8.1 Design Inputs

The inputs to the design model are given in Table 8.1.1. The use of parameters $D_3$, $a_1$, $a_2$, $a_3$, $m_2$ and $m_3$ are introduced in Sections 8.5 and 8.6. Values of $D_1$ and $D_2$ should come from the design of the unreinforced pavement for the project. The subgrade *CBR* used should be the design value for the project. If some other subgrade property is given as the design value for the project (resilient modulus, R-value, subgrade support value, etc.) this value should be correlated to *CBR* through existing correlation equations such as Equation 4.2.9 relating *CBR* to resilient modulus. A value for $G_{SM\text{-}2\%}$ should be determined from test ASTM D 4595 (ASTM, 2001a). The secant tensile modulus should be computed from the tensile strength at 2 % axial strain ($T_{2\%}$) from Equation 8.1.1 and should represent the maximum value for either the machine or cross-machine direction of the material. Reduction factors for geosynthetic interface shearing resistance should be less than or equal to one. Reduction factors for geosynthetic Poisson's ratio and shear modulus should be either 1 or the values listed in Table 8.1.2.

$$G_{sm-2\%} = \frac{T_{2\%}}{0.02} \tag{8.1.1}$$

Values of $RF_{GI}$ were calibrated as 1.0 for Geogrid A and B and as 0.765 for the Geotextile listed in Table 3.1.2. Values of $RF_{Gn}$ and $RF_{GG}$ were calibrated as 1.0 for Geogrid A and B, while the values listed in Table 8.1.2 were used for the Geotextile. These values resulted from the design model calibration work described in Section 7.6. Selection of values for these factors for other geosynthetic products should be based on the values used here with assistance from the application guidelines given in Berg et al. (2000).

**Table 8.1.1** Design model input parameters.

| Design Parameter | Units | Description of Design Parameter |
|---|---|---|
| $D_1$ | mm | Design thickness of asphalt concrete layer |
| $a_1$ | none | Design asphalt concrete structural layer coefficient |
| $D_2$ | mm | Design thickness of unreinforced base aggregate layer |
| $a_2$ | none | Design base aggregate structural layer coefficient |
| $m_2$ | none | Design base aggregate drainage coefficient |
| $D_3$ | mm | Design thickness of unreinforced subbase aggregate layer |
| $a_3$ | none | Design subbase aggregate structural layer coefficient |
| $m_3$ | none | Design subbase aggregate drainage coefficient |
| $CBR$ | (%) | Subgrade CBR |
| $G_{SM\text{-}2\%}$ | kN/m | Geosynthetic secant tensile modulus at 2 % axial strain, maximum value of machine and cross-machine direction |
| $G_{MR}$ | none | Ratio minimum to maximum geosynthetic 2 % secant tensile modulus |
| $RF_{GI}$ | none | Reduction factor for geosynthetic interface shearing resistance |
| $RF_{Gn}$ for $TBR_B$ | none | Reduction factor for geosynthetic Poisson's ratio applied to $TBR_B$ |
| $RF_{Gn}$ for $TBR_S$ | none | Reduction factor for geosynthetic Poisson's ratio applied to $TBR_S$ |
| $RF_{GG}$ for $TBR_B$ | none | Reduction factor for geosynthetic Poisson's ratio applied to $TBR_B$ |
| $RF_{GG}$ for $TBR_S$ | none | Reduction factor for geosynthetic Poisson's ratio applied to $TBR_S$ |

**Table 8.1.2** Reduction factors for geosynthetic Poisson's ratio and shear modulus.

| | $RF_{Gn}$ | $RF_{GG}$ |
|---|---|---|
| $TBR_S$ | 0.83 | 0.92 |
| $TBR_B$ | 0.96 | 0.99 |

## 8.2 Designing for a *TBR* for *BCR* = 0

The structural number for the unreinforced pavement design is determined from Equation 8.2.1 where section thicknesses have been converted to units of inches in this equation. The geosynthetic material model elastic modulus ($E_G$) is calculated from the secant tensile modulus at 2 % axial strain ($G_{SM\text{-}2\%}$) from Equation 8.2.2.

$$SN = 0.4\,\frac{D_1}{25.4} + 0.14\,\frac{D_2}{25.4} \tag{8.2.1}$$

$$E_G = 4400 \times G_{SM-2\%} \tag{8.2.2}$$

Equations 8.2.3 – 8.2.11 are used to calculate the *TBR* for reinforcement effects in the subgrade. This value of *TBR* accounts for the influence of thickness of the structural section,

strength/stiffness of the subgrade and the value for the geosynthetic secant tensile modulus. Depending on the value of *SN* from Equation 8.2.1, either Equation 8.2.6 or 8.2.9 is used to calculate $TBR_{S\text{-}GM}$. The model has not been validated for values of SN ≤ 1.6 or ≥ 6.0. Computed values of $y_{1\text{-}GM}$ less than one should be assigned a value of one. Similarly, computed values of $TBR_{S\text{-}GM}$ less than one should be taken as one.

$$y_{1-GM} = \frac{49.8 \log(E_G)}{100}\left(10^{(\log 8 - \log CBR)} - 1\right) + 1 \tag{8.2.3}$$

$$y_{2-GM} = \frac{1.8\times10^{-6}\ \log(CBR) + 1.57\times10^{-6}}{100} E_G \left(10^{(\log 100 - 1.7 \log CBR)} - 1\right) + 1 \tag{8.2.4}$$

$$SN_{TBR_{S-GM}=1} = 2.54\ (CBR - 0.28)^{0.028}\ E_G^{\ 0.0504} \tag{8.2.5}$$

$1.6 \le SN \le 3.3$

$$TBR_{S-GM} = 10^{(m_1 SN + \log y_{o1})} \tag{8.2.6}$$

$$m_1 = \frac{\log \dfrac{y_{2-GM}}{y_{1-GM}}}{1.7} \tag{8.2.7}$$

$$y_{o1} = \frac{y_{1-GM}}{10^{(1.6 m_1)}} \tag{8.2.8}$$

$3.3 \le SN \le 6.0$

$$TBR_{S-GM} = 10^{(m_2 SN + \log y_{o2})} \tag{8.2.9}$$

$$m_2 = \frac{-\log y_{2-GM}}{SN_{(TBR_{S-GM}=1)} - 3.3} \tag{8.2.10}$$

$$y_{o2} = \frac{y_{2-GM}}{10^{(3.3 m_2)}} \tag{8.2.11}$$

Equation 8.2.12 is used to calculate the *TBR* for reinforcement effects in the base. This value of *TBR* accounts for the influence of thickness of the structural section, strength/stiffness

of the subgrade and the value for the geosynthetic secant modulus. Computed values of $TBR_{B\text{-}GM}$ less than one should be taken as one.

$$TBR_{B-GM} = \frac{55.8 \log(E_G) - 288}{100}\left[\left(1 - 4.45\, CBR^{-0.522}\right)\frac{D_1}{160} + 4.45\, CBR^{-0.522} - 1\right] + 1 \qquad (8.2.12)$$

The effects of geosynthetic secant modulus ratio on *TBR* are accounted for by the use of $TBR_{S\text{-}GM}$ and $TBR_{B\text{-}GM}$ in Equations 8.2.13 and 8.2.14.

$$TBR_{S-GMR} = TBR_{S-GM}\left[0.62 \log(TBR_{S-GM})\, G_{MR} + 1 - 0.62 \log(TBR_{S-GM})\right] \qquad (8.2.13)$$

$$TBR_{B-GMR} = TBR_{B-GM}\left(0.2\, G_{MR} + 0.8\right) \qquad (8.2.14)$$

The effects of geosynthetic interface shearing resistance, Poisson's ratio and shear modulus are accounted for by the use of $TBR_{S\text{-}GMR}$ and $TBR_{B\text{-}GMR}$ in Equations 8.2.15 and 8.2.16. A total *TBR* for the pavement system is then computed from Equation 8.2.17. Values of $TBR_S$, $TBR_B$ and $TBR_T$ from Equations 8.2.15 - 8.2.17 represent final values of *TBR* for accounting for all design variables and for the condition that no base course reduction is used (i.e. *BCR*=0). Designs may be based on the use of any of the three *TBR* values. Given the conservative aspects of the design approach, as discussed in Section 7.8, it is recommended that $TBR_T$ be used.

$$TBR_S = TBR_{S-GMR} \times RF_{GI} \times RF_{Gn\ TBR_S} \times RF_{GG\ TBR_S} \qquad (8.2.15)$$

$$TBR_B = TBR_{B-GMR} \times RF_{GI} \times RF_{Gn\ TBR_B} \times RF_{GG\ TBR_B} \qquad (8.2.16)$$

$$TBR_T = TBR_S \times TBR_B \qquad (8.2.17)$$

## 8.3 Designing for a *BCR* for *TBR* = 1

To compute values of *BCR* for a life equivalent to the unreinforced pavement design, the steps described in Section 8.2 are first followed to obtain a *TBR* accounting for all pavement variable

effects. A $TBR_S$, $TBR_B$ or $TBR_T$ may be used for design and as input to the remaining design steps described below.

Equations 8.3.1 - 8.3.3 are used to calculate the number of ESAL's for the unreinforced pavement design. In this equation, certain values have been assumed for parameters in the AASHTO 1993 pavement design equation. Since the design model has been calibrated against these assumed values, the equation should be used as given.

$$W_{18-U} = 10\wedge\left[9.36\log(SN+1) - \frac{0.15261}{0.4+\frac{1094}{(SN+1)^{5.19}}} + 2.32\log(M_S) - 8.84575\right] \quad (8.3.1)$$

$$SN = 0.4\frac{D_1}{25.4} + 0.14\frac{D_2}{25.4} \quad (8.3.2)$$

$$M_S = 1500 \times CBR \quad (8.3.3)$$

With the design value of $TBR_S$, $TBR_B$ or $TBR_T$ selected from the computations performed in Section 8.2, a value for $W_{18\text{-}R}$ is computed from Equation 8.3.4.

$$W_{18-R} = W_{18-U}\ TBR \quad (8.3.4)$$

The value of $W_{18\text{-}R}$ from Equation 8.3.4 is then used in Equation 8.3.1 to calculate a value of $SN$ for the reinforced pavement, with this value used in Equation 8.3.2 to determine a new value of $a_2$ for the reinforced pavement, with all other parameters in Equations 8.3.1 and 8.3.2 being equal to those used for the unreinforced pavement. This calculation requires an iterative solution for $SN$ in Equation 8.3.1. Once a value of $a_2$ for the reinforced pavement is obtained ($a_{2\text{-}R}$), this value is used in Equation 8.3.2 along with a reduced base thickness for the reinforced pavement ($D_{2\text{-}R}$) such that a $SN$ identical to the unreinforced pavement is obtained. The reduced base thickness is calculated from

$$D_{2-R} = \frac{SN_U - a_1 D_1}{a_{2-R}\, m_2} \quad (8.3.5)$$

This allows for the determination of a value of *BCR* when *TBR* = 1 from Equation 8.3.6. Depending on the value of *TBR* used in Equation 8.3.4 ($TBR_B$, $TBR_S$ or $TBR_T$), the computed *BCR* then pertains to reinforcement effects on the base, subgrade or total system.

$$BCR = 100\,\frac{D_{2-U} - D_{2-R}}{D_{2-U}} \tag{8.3.6}$$

This method described in Section 8.3 is recommend only for values of subgrade $CBR \geq 1$

## 8.4 Designing for a *TBR/BCR* Combination

From Sections 8.2 and 8.3, corresponding values of *TBR* when *BCR* = 0 and *BCR* when *TBR* = 1 are known. If a value of *TBR* less than $TBR_{BCR=0}$ is used, it should be expected that the remaining benefit can be expressed in terms of a *BCR*. Conversely, if a value of *BCR* less than $BCR_{TBR=1}$ is used, remaining benefit can be expressed in terms of a *TBR*. The same general approach described in Section 8.3 is used to determine combinations of *BCR* and *TBR*. Each approach uses the predetermined value of $TBR_{BCR=0}$ selected for design. For the case where a desired *BCR* is specified, the reinforced base layer thickness is determined from Equation 8.4.1.

$$D_{2-R} = \left(1 - \frac{BCR}{100}\right) D_{2-U} \tag{8.4.1}$$

The structural number of the reinforced pavement is then determined from Equation 8.4.2.

$$SN_R = 0.4\,\frac{D_1}{25.4} + a_{2-R}\,\frac{D_{2-R}}{25.4} \tag{8.4.2}$$

where $a_{2\text{-}R}$ is determined from the method described in Section 8.3 and by knowing the design value of $TBR_{BCR=0}$ from Section 8.2. A value of $W_{18\text{-}R}$ is then determined using Equation 8.3.1 using the value of *SN* from Equation 8.4.2. A value of remaining *TBR* is then computed by Equation 8.4.3, where this value should lie between 1 and $TBR_{BCR=0}$ provided the desired value of *BCR* used was less than or equal to $BCR_{TBR=1}$.

$$TBR = \frac{W_{18-R}}{W_{18-U}} \tag{8.4.3}$$

For the case where a desired *TBR* is specified, Equation 8.3.4 is used to calculate the number of ESAL's required of the reinforced section. Equation 8.3.1 is then solved iteratively to give the required *SN* for the reinforced section ($SN_R$). Equation 8.4.5 is then used to determine the base layer thickness necessary to produce this *SN*, where the reinforced structural base layer coefficient is used in this equation.

$$D_{2-R} = \frac{SN_R - a_1 D_1}{a_{2-R}\, m_2} \tag{8.4.5}$$

The remaining *BCR* is then determined from Equation 8.3.6, where the value obtained should lie between 0 and $BCR_{TBR=1}$ provided the desired value of *TBR* was less than $TBR_{BCR=0}$.

This method described in Section 8.4 is recommend only for values of subgrade $CBR \geq 1$.

## 8.5 Adjustment of Structural Layer Coefficients

The material models used for the asphalt concrete and base aggregate layers were calibrated to match the properties of these layers from test sections reported in Section 3 and were shown to approximate layer coefficients of 0.4 and 0.14, respectively. Furthermore, a base aggregate drainage layer coefficient ($m_2$) of 1.0 was used for calibration of the model. To use the design model developed in this project for designs involving material layers having other layer and drainage coefficients, it is suggested that the design AC thickness ($D_{1\text{-}d}$), design base aggregate thickness ($D_{2\text{-}d}$) be adjusted to equivalent values ($D_{1\text{-}e}$, $D_{2\text{-}e}$) using Equations 8.5.1 and 8.5.2, where $a_{1\text{-}d}$ and $a_{2\text{-}d}$ are the design values for the layer coefficients and $m_{2\text{-}d}$ is the design value for the drainage coefficient.

$$D_{1-e} = D_{1-d}\left(\frac{a_{1-d}}{0.4}\right) \tag{8.5.1}$$

$$D_{2-e} = D_{2-d}\left(\frac{a_{2-d}}{0.14}\right)\left(\frac{m_{2-d}}{1.0}\right) \tag{8.5.2}$$

Equivalent values of layer thickness ($D_{1\text{-}e}$, $D_{2\text{-}e}$) are then used directly for $D_1$ and $D_2$ in all equations given in Sections 8.1-8.4.

## 8.6 Accounting for Subbase Aggregate Layers

The finite element response models did not contain a subbase layer. For designs using a subbase layer, and where the reinforcement will be placed at the bottom of the subbase, it is suggested that the design layer thickness of the subbase ($D_{3\text{-}d}$) be converted to an equivalent base aggregate thickness ($D_{3\text{-}e}$) having a structural layer coefficient of 0.14 and a drainage coefficient of 1.0 and added to the base aggregate thickness ($D_2$). The equivalent thickness can be calculated from Equation 8.6.1, where $a_{3\text{-}d}$ is the design value of the structural coefficient for the subbase aggregate layer and $m_{3\text{-}d}$ is the design value of the drainage coefficient for the subbase layer.

$$D_{3-e} = D_{3-d}\left(\frac{a_{3-d}}{0.14}\right)\left(\frac{m_{3-d}}{1.0}\right) \tag{8.6.1}$$

Designs using a subbase according to Equation 8.6.1 are valid only when the geosynthetic is placed at the bottom of the subbase layer. Special attention should be given to the selection of the reduction factor for geosynthetic interface shearing resistance ($R_{GI}$) because of the typically large particle sizes and lack of angularity associated with common subbase aggregate materials.

## 8.7 Evaluating Asphalt Fatigue Cracking Criteria

As discussed in Section 7.8, the design model is based on response measures extracted from the finite element model used to define pavement performance in terms of permanent surface deformation or rutting. The design model has been calibrated against test section results where pavement life was defined in terms of rutting due to the accumulation of permanent strain in the base and subgrade layers. As such, the model specifically addresses designs for which rutting is the controlling pavement distress feature. It should be noted, however, that test sections have shown that the dynamic deflection of the pavement surface is decreased by the use of reinforcement, which suggests that dynamic tensile strain in the bottom of the asphalt concrete layer is reduced and fatigue life is increased.

The distress feature of rutting generally controls for pavement cross sections containing relatively thin layers of asphalt concrete and base course aggregate and for pavement structural

layers resting on weak subgrade. The design model predicts the greatest levels of benefit for those situations, meaning that the design model will tend to predict useful levels of benefit for pavement designs for which rutting controls. The AASHTO ’93 pavement design guide does not provide specific design checks for the individual pavement distress features of rutting and asphalt fatigue cracking. Rather, designs developed using the AASHTO ’93 guide assume that both pavement distress features are adequately addressed. For pavement designers who use methods for individually checking rutting and fatigue cracking criteria (namely mechanistic-empirical approaches), a method is needed to evaluate the effective increase in resilient modulus of the base aggregate layer with reinforcement such that fatigue cracking criteria for the asphalt concrete layer may be checked.

Such a method is possible from the equations presented in Section 8.3 where a *BCR* value is determined from a known *TBR* value. Equation 8.3.2 presumes the use of a base layer coefficient for the unreinforced base of 0.14. Equation 8.7.1 (AASHTO, 1993) is used to relate the unreinforced base layer coefficient ($a_{2\text{-}U}$) to an unreinforced base aggregate layer resilient modulus ($M_{R\text{-}U}$).

$$M_R = 10\wedge\left(\frac{a_2 + 0.977}{0.249}\right) \tag{8.7.1}$$

The method described in Section 8.3, through the use of Equations 8.3.1-8.3.4, is then used to evaluate the base layer coefficient of the reinforced pavement ($a_{2\text{-}R}$), which is then used in Equation 8.7.1 to evaluate the effective resilient modulus of the reinforced base aggregate layer ($M_{R\text{-}R}$). A ratio of the reinforced to unreinforced resilient moduli can then be determined from Equation 8.7.2.

$$M_{R-R/U} = \frac{M_{R-R}}{M_{R-U}} \tag{8.7.2}$$

Since any of the three values of *TBR* ($TBR_S$, $TBR_B$ or $TBR_T$) can be used in Equation 8.3.4, a ratio of resilient moduli can be computed for each reinforcement effect. Since this method has not been experimentally validated, it is recommended that $TBR_B$ be used in Equation 8.3.4 and the remaining equations described in this section to evaluate the ratio of resilient moduli. $TBR_B$ is

based on results from finite element analyses showing increases in bulk stress in the base aggregate layer. Since this effect is directly tied to an increase in resilient modulus of the aggregate layer, it is believed to be most representative for an effect on dynamic tensile strain in the bottom of the asphalt concrete layer.

It is recommended that the ratio of resilient moduli defined from Equation 8.7.2 be used to modify the unreinforced base aggregate layer resilient modulus used in the design being evaluated. The modified value for the reinforced section can then be used for designs where *TBR*, *BCR* or a combination of the two are used to check asphalt fatigue cracking criteria. It is recommended that the effective resilient modulus of the reinforced aggregate layer be used only for this purpose.

## 8.8 Design Model Software Program

A spreadsheet program was written to perform the design calculations described in Sections 8.1 – 8.7. The program was written in Microsoft Excel Office 2000 and can be downloaded from the following URL: http://www.mdt.state.mt.us/departments/researchmgmt/grfp/grfp.html; or made available by contacting the Montana Department of Transportation Research, Development and Technology Transfer Program. The program consists of a single visible sheet where input and output parameters are displayed. The input parameters described in Table 8.1.1, with the exception of the four parameters for $RF_{G?}$ and $RF_{GG}$ for $TBR_S$ and $TBR_B$, are specified with the units listed in Table 8.1.1. Since values for $RF_{G?}$ and $RF_{GG}$ are either 1.0 or the values listed in Table 8.1.2, check boxes have been provided in the spreadsheet program to toggle between the two sets of values. Two check boxes have been given. The check box labeled “Reduction for Poisson’s Ratio” selects values for $RF_{G?}$ listed in Table 8.1.2 when checked. Similarly, the check box labeled “Reduction for Shear Modulus” selects values for $RF_{GG}$ listed in Table 8.1.2 when checked. When unchecked, values of 1.0 are used for each parameter.

The program incorporates the material contained in Sections 8.5 and 8.6. Changes made to the effective pavement layer thicknesses due to the use of pavement layers with structural layer coefficients differing from those assumed in the design model and/or the use of a subbase layer are not displayed on the MASTER sheet but are accounted for in the program’s computations.

As input, the MASTER sheet also contains six cells where desired *TBR* or *BCR* for reinforcement effects for the subgrade, base or total system can be specified. These values are

specified when combinations of *TBR/BCR* are desired. Changing any of the input values or options automatically causes the program to run and compute values listed in the output table.

Output consists of values for $TBR_{BCR=0}$ and $BCR_{TBR=1}$ for reinforcement effects in the subgrade, base and total system. The designer may choose to use any of the three sets of values. For the desired values of *TBR* and *BCR* listed as input, values of remaining *TBR* and *BCR* are computed and listed as output. The output also contains computed values of effective base aggregate resilient modulus ratio for evaluation of asphalt concrete fatigue cracking criteria as described in Section 8.7. Limitations associated with the use of the model were discussed in Section 7.8 and are presented again in Appendix B.

## 9.0 INCORPORATION OF DESIGN MODEL INTO A STANDARD OF PRACTICE

This report presents a design model for computing reinforcement benefit of geosynthetics used in the base course of flexible pavements. Computed benefit is in terms of a *TBR*, *BCR* or combination of the two. These values can be used directly in the recommended standard of practice given by Berg et al. (2000). These values can be used to directly modify an unreinforced pavement according to step 4 of the recommended standard of practice (see Section 2.3 of this report). Further guidance is provided in Appendix B of this report. The example specification provided in Berg et al. (2000) will require revisions to account for the design model proposed herein. Lastly, the AASHTO Subcommittee on Materials Technical Section 4E, Task Force on Geogrids/Geotextiles is encouraged to consider adoption of this design method into the existing AASHTO Designation PP 46-01.

## 10.0 CONCLUSIONS

The work described in this report has resulted in the development of a generic design model for geosynthetic reinforced flexible pavements. The model is expressed solely in terms of equations relating reinforcement benefit to pavement and geosynthetic input design parameters. These equations are based on the results of predictions of reinforcement benefit from a finite element based mechanistic-empirical model from over 465 analyzed cases. The mechanistic-empirical model and the design model were calibrated from test section results for reinforced pavements presented in Perkins (1999a). The design model was further validated by comparison of

predictions to values of benefit from other studies reported in the literature and summarized in Berg et al. (2000).

The design model presents a means of calculating reinforcement benefit for reinforcement effects on the subgrade, the base aggregate or both. Equations for calculating benefit due to each effect are provided and allow pavement designers to use their discretion in choosing for which effect to design.

The design model has been shown to be sensitive to pavement design variables that have previously been identified as having a significant impact on reinforced pavement performance. In particular, the model is capable of showing that reinforcement benefit increases with decreasing subgrade strength/stiffness, increasing geosynthetic tensile modulus and is sensitive to the pavement structural thickness. Furthermore, the model is shown to be sensitive to the ratio of geosynthetic tensile modulus in the weak to strong directions of the material. The model is calibrated from the use of geosynthetic secant tensile modulus values determined at 2 % axial strain according to ASTM 4595 (ASTM, 2001a).

The design model attempts to account for geosynthetic properties pertinent to the type and structure of the material through the assignment of reduction factors for geosynthetic material Poisson's ratio, shear modulus and geosynthetic/aggregate shear interaction. Geosynthetic material Poisson's ratio and shear modulus are parameters existing in the anisotropic elastic material model used for the geosynthetic and were shown to have a moderate influence on reinforcement benefit. Reduction factors for Poisson's ratio and shear modulus correspond to one of two values for either good or poor material property conditions and were calibrated for the two types of geosynthetics used in test sections reported in Perkins (1999a). Similarly, the reduction factor for interface shearing resistance was calibrated from these test section results. These values serve as a starting point for selection of values for other geosynthetic types. In the absence of additional results from test sections using a broader range of geosynthetic products, judgment and experience are required for selection of final values for design.

The design model appears to yield mostly conservative predictions of reinforcement benefit when compared to results available in the literature. Conservatism in the model results from several sources. Use of only benefit accounting for effects in the subgrade layer would result in a conservative design since effects in the base layer would be ignored. Comparisons of the model to test section results indicate that partial benefits for reinforcement effects in the subgrade are

considerably less than that for the entire system. The method used to calculate reinforcement benefit for the base aggregate layer was shown to yield values of benefit that are consistently less than those determined for test sections. The equation used to calculate total *TBR* from the partial values for the base and subgrade layers was shown to be conservative as compared to test section results. Finally the method used to calculate *BCR* and *TBR/BCR* combinations was shown to be conservative with respect to that predicted by the finite element model. In spite of this inherent conservatism, use of the model is shown to offer significant life-cycle cost benefits for several pavement design examples illustrated in Appendix B.

The design model is based on certain conditions to which the model should be limited. The model is based on results from a finite element model where pavement load has been simulated by the application of a 40 kN load applied over a circular plate. Experimental test section results from which the model has been validated used a similar load. The design model is therefore designed to describe reinforcement benefit for conventional roadway applications where the pavement load can be approximated in terms of a standard axle wheel load. The model may not be appropriate for either lightly loaded traffic or for excessively loaded traffic.

The design model is calibrated largely from results based on a permanent pavement surface deformation of 12.5 mm. It is anticipated that roadways that can be designed for a rut depth greater than 12.5 mm will realize reinforcement benefits greater than those predicted from this model, meaning that this model should be conservative for roadways designed for a rut depth in excess of 12.5 mm.

The model is based on asphalt concrete and base aggregate properties that correspond to structural layer coefficients of approximately 0.4 and 0.14, respectively. Recommendations were provided to account for pavement designs with different materials yielding different layer coefficients.

All cases of reinforcement were modeled by placement of the geosynthetic at the bottom of the base aggregate layer. As such, the design model cannot account for situations where it might be desirable to place the geosynthetic further up in the base aggregate layer. Work involving the assessment of benefit for situations where the geosynthetic was elevated up into the base layer was not performed because of the relatively low values of benefit that were derived for the base aggregate layer. Reliable values of benefit for cases where the geosynthetic is elevated up into

the base aggregate layer requires a material model for the base aggregate that is more suited for demonstrating benefits observed in experimental test sections.

Values of reinforcement benefit from the design model can be used directly in a recommended standard of practice for reinforced pavement design presented in Berg et al. (2000) and AASHTO (2001). Appendix B of this report describes the steps necessary to carry out a pavement design using geosynthetic reinforcement, where the material presented in this report can be used in place of step 4 of the previously recommended standard of practice. The AASHTO Subcommittee on Materials Technical Section 4E, Task Force on Geogrids/Geotextiles is encouraged to consider adoption of this design method into the existing AASHTO Designation PP 46-01.

Further work for improvement of the design model should focus on a better description of reinforcement benefit for reinforcement effects in the base aggregate layer. The design model as presented in this report yields conservative predictions of this reinforcement component. Improvements in the material model used for the base aggregate layer would be required to improve upon predictions of this component of benefit. These improvements would then also warrant examining the model for predictions of benefit for cases where the geosynthetic is moved up into the base aggregate layer. Further work should also be performed to allow assignment of reduction factors for geosynthetic Poisson's ratio, shear modulus and geosynthetic/aggregate shear interaction to different geosynthetics types. Finally, future results from new test sections should be used to further refine and update the model.

## 11.0 REFERENCES

AASHTO (2001), *Recommended Practice for Geosynthetic Reinforcement of the Aggregate Base Course of Flexible Pavement Structures*, AASHTO Designation PP 46-01.

AASHTO (1997a), *Standard Specification for Geotextiles – M288*, Standard Specifications for Transportation Materials and Methods of Sampling and Testing, 18th Edition, American Association of State Highway and Transportation Officials, Washington, D.C., USA.

AASHTO (1997b), *AASHTOWare DARWin 3.1, Pavement Design and Analysis System*, American Association of State Highway and Transportation Officials, Washington, D.C., USA.

AASHTO (1993), *AASHTO Guide for Design of Pavement Structures*, American Association of State Highway and Transportation Officials, Washington, D.C., USA.

AASHTO (1991), "Standard Method of Test for Resilient Modulus of Subgrade Soils and Untreated Base/Subbase Materials", AASHTO Designation T 292-91, *Standard*

*Specifications for Transportation Materials and Methods of Sampling and Testing, Part II, Methods of Sampling and Testing*, American Association of State Highway and Transportation Officials, Washington, D.C., USA.

Allied Engineering (2000), *Final Geotechnical Report, Rosebud County Line East Roadway Reconstruction, Montana Department of Transportation, Project Number STPP 14-6(8)207, Control Number 4060, Rosebud Country, Montana*, Allied Engineering Services, Incorporated Project 99-048, Bozeman, MT, USA.

AMOCO (1996). Personal Fax Communication, 6-12-1996.

AMOCO (2001). Personal Email Communication, 4-23-2001.

Asphalt Institute (1991), *Computer Program DAMA, Pavement Structural Analysis Using Multi-Layered Elastic Theory*, Asphalt Institute, Lexington, KY, USA.

ASTM (2001a), *Annual Book of ASTM Standards, Soil and Rock (II): D4943-Latest; Geosynthetics*, Vol. 04.09, Section 4, American Society of Testing and Materials, West Conshohocen, PA, USA.

ASTM (2001b), *Annual Book of ASTM Standards, Road and Paving Materials; Vehicle Pavement Systems*, Vol. 04.03, Section 4, American Society of Testing and Materials, West Conshohocen, PA, USA.

Barksdale, R.D., Brown, S.F. and Chan, F. (1989), "*Potential Benefits of Geosynthetics in Flexible Pavement Systems*", National Cooperative Highway Research Program Report No. 315, Transportation Research Board, National Research Council, Washington DC.

Berg R.R., Christopher, B.R. and Perkins, S.W. (2000), *Geosynthetic Reinforcement of the Aggregate Base Course of Flexible Pavement Structures, GMA White Paper II*, Geosynthetic Materials Association, Roseville, MN, USA, 130p.

Burd, H.J. and Brocklehurst, C.J. (1992), "Parametric Studies of a Soil Reinforcement Problem Using Finite Element Analysis", *Proceedings of the Conference on Computer Methods and Advances in Geomechanics*, Balkema, pp. 1783-1788.

Burd, H.J. and Brocklehurst, C.J. (1990), "Finite Element Studies of the Mechanics of Reinforced Unpaved Roads", *Proceedings of the 4th International Conference on Geotextiles, Geomembranes and Related Products*, The Hauge, Netherlands, pp. 217-221.

Burd, H.J. and Houlsby, G.T. (1986), "A Large Strain Finite Element Formulation for One Dimensional Membrane Elements", *Computers and Geotechnics*, Vol. 2, pp. 3-22.

Cancelli, A. and Montanelli, F. (1999), "In-Ground Test for Geosynthetic Reinforced Flexible Paved Roads", *Proceedings of the Conference Geosynthetics '99*, Boston, MA, USA, Vol. 2, pp. 863-878.

Cancelli, A., Montanelli, F., Rimoldi, P. and Zhao, A. (1996), "Full Scale Laboratory Testing on Geosynthetic Reinforced Paved Roads", *Proceedings of the International Symposium on Earth Reinforcement*, Fukuoka/Kyushu, Japan, November, Balkema, pp. 573-578.

Chen, D.-H., Zaman, M., Laguros, J. and Soltani, A. (1995), "Assessment of Computer Programs for Analysis of Flexible Pavement Structure", In *Transportation Research Record 1482*, TRB, National Research Council, Washington, DC, USA, pp. 123-133.

Christopher, B.R., Berg, R.R. and Perkins, S.W. (2001), *Geosynthetic Reinforcements in Roadway Sections*, NCHRP Synthesis for NCHRP Project 20-7, Task 112, Transportation Research Board, Washington, D.C., In-Print.

Colbond (1998), *TRC-Grid, Design and Installation Guide*, Akzo Nobel Geosynthetics, Arnhem, the Netherlands, 24p.

Collin, J. G., Kinney, T. C. and Fu, X. (1996), "Full Scale Highway Load Test of Flexible Pavement Systems With Geogrid Reinforced Base Courses" *Geosynthetics Intentional*, Vol. 3, No. 4, pp. 537-549.

Dafalias, Y.F. and Hermann, L.R. (1986), "Bounding Surface Plasticity. II: Application to Isotropic Cohesive Soils", *Journal of Engineering Mechanics*, ASCE, Vol. 112, No. 12, pp. 1263-1291.

Dafalias, Y.F. and Hermann, L.R. (1982), "Bounding Surface Formulation of Soil Plasticity", *Soil Mechanics-Transient and Cyclic Loads*, Chapter 10, John Wiley and Sons, Ltd., pp. 253-282.

Dafalias, Y.F. (1975), *On Cyclic and Anisotropic Plasticity*, Ph.D. Thesis, University of California at Berkeley.

Davies, M.C.R. and Bridle, R.J. (1990), "Predicting the Permanent Deformation of Reinforced Flexible Pavement Subject to Repeated Loading," *Proceedings of the International Reinforced Soil Conference, Performance of Reinforced Soil Structures*, Glasgow, UK, A. McGown, K.C. Yeo and K.Z. Andrawes, eds., British Geotechnical Society, Thomas Telford, London, pp. 421 - 425, UK.

Desai, C.S., Somasundaram, S. and Frantziskonis, G.N. (1986), "A Hierarchical Approach for Constitutive Modeling of Geologic Materials", *International Journal of Numerical Methods in Geomechanics*, Vol. 10, pp.25-257.

Dondi, G. (1994), "Three-Dimensional Finite Element Analysis of a Reinforced Paved Road", *Proceedings of the Fifth International Conference on Geotextiles, Geomembranes and Related Products*, Singapore, pp. 95-100.

Dorman, G.M. and Metcalf, C.T. (1965), "Design Curves for Flexible Pavements Based on Layered System Theory", *Highway Research Record 71*, Highway Research Board, Washington, D.C. USA, pp. 69-84.

GRI (2001), *GRI Test Methods and Standards*, Geosynthetic Research Institute, Drexel University, Philadelphia, PA, USA.

Haas R., Wall, J. and Carroll, R.G. (1988), "Geogrid Reinforcement of Granular Bases in Flexible Pavements," In *Transportation Research Record 1188*, TRB, National Research Council, Washington DC, USA, pp. 19 - 27.

Harichandran, R.S., Yeh, M.S. and Baladi, G.Y. (1989), *MICH-PAVE User's Manual*, Final Report, FHWA-MI-RD-89-032, Department of Civil and Environmental Engineering, Michigan State University, East Lansing, MI, USA.

Heukelom, W. and Klomp, A.J.G. (1962), "Dynamic Testing as a Means of Controlling Pavements During and After Construction", *Proceedings of the First International Conference on the Structural Design of Asphalt Pavements*, pp. 667-685.

Hibbitt, Karlson and Sorensen (1998), *ABAQUS Standard User's Manuals*, Version 5.8, Pawtucket, RI, USA.

Holtz, R.D. and Kovacs, W.D. (1981), *An Introduction to Geotechnical Engineering*, Prentice Hall, Englewood Cliffs, NJ, USA., 733p.

Huang, Y.H. (1993), *Pavement Analysis and Design*, Prentice Hall, Englewood Cliffs, NJ, USA, 805p.

Huntington, G. and Ksaibati, K. (1999), "Evaluation of Geogrid-Reinforced Granular Base", *Geotechnical Special Publication No. 89, Recent Advances in the Characterization of Transportation Geo-Materials*, ASCE, pp. 13-24.

IFAI (1994), *1995 Specifier's Guide*, Geotechnical Fabrics Report, Vol. 12, No. 9, pg. 169.

ILLI-PAVE (1990), *ILLI-PAVE PC Version User's Manual*, NCHRP 1-26, Transportation Faculties Group, University of Illinois at Urbana-Champaign.

Kaliakin, V.N., Dafalias, Y.F. and Hermann, L.R. (1987), *Time Dependent Bounding Surface Model for Isotropic Cohesive Soils*, notes for a short course held in conjunction with the Second International Conference on Constitutive Laws for Engineering Materials, Tucson, AZ, January.

Kinney, T.C., Abbott, J. and Schuler, J. (1998), "Benefits of Using Geogrids for Base Reinforcement with Regard to Rutting", *Transportation Research Record 1611*, Transportation Research Board, National Research Council, Washington, DC, USA, pp. 86-96.

Kopperman, S.G., Tiller, and Tseng, M. (1986), *ELSYM5, Interactive Microcomputer Version, User's Manual*, Report No. FHWA-TS-87-206, Federal Highway Administration, Washington, D.C., USA.

Liu, X., Scarpas, A., Blaauwendraad, J. and Genske, D.D. (1998), "Geogrid Reinforcing of Recycled Aggregate Materials for Road Construction", *77th Annual Meeting of the Transportation Research Board*, Preprint 981343, Washington, D. C.

Meyer, N. and Elias, J.M. (1999), "Design Methods for Roads Reinforced with Multifunctional Geogrids for Subbase Stabilization", Translation of a paper in German presented at the *German Conference on Geosynthetics, Kunststoffe in der Geotechnik*, Technical University of Munich, March.

Mirafi (1982), *Guidelines for Design of Flexible Pavements Using Mirafi Woven Geotextiles*, TC Mirafi, Pendergrass, GA, USA, 23 p.

Miura, N., Sakai, A., Taesiri, Y., Yamanouchi, T. and Yasuhara, K. (1990), "Polymer Grid Reinforced Pavement on Soft Clay Grounds", *Geotextiles and Geomembranes*, Vol. 9, pp. 99-123.

MDT (2001), Montana Department of Transportation Internet Resource, "MDT Contractor's System": *http://www.mdt.state.mt.us/cntrct/contract.htm*.

Penner, R., Haas, R., Walls, J. and Kennepohl, G. (1985), "Geogrid Reinforcement of Granular Bases", Paper Presented at the *Roads and Transportation Association of Canada Annual Conference*, Vancouver, Canada, September.

Perkins, S.W. (2001a), *Numerical Modeling of Geosynthetic Reinforced Flexible Pavements*, Montana Department of Transportation, Helena, Montana, Report No. FHWA/MT-01/003/99160-2, 97p.

Perkins, S.W. (2001b), *Mechanistic-Empirical Modeling and Design Model Development of Geosynthetic Reinforced Flexible Pavements: Appendix C - DARWin Output*, Montana Department of Transportation, Helena, Montana, Report No. FHWA/MT-01/002/99160-1B, 89p.

Perkins, S.W. (1999a), *Geosynthetic Reinforcement of Flexible Pavements: Laboratory Based Pavement Test Sections*, Montana Department of Transportation, Helena, Montana, Report No. FHWA/MT-99/8106-1, 140 p.

Perkins, S.W. (1999b), "Mechanical Response of Geosynthetic-Reinforced Flexible Pavements", *Geosynthetics International*, Vol. 6, No. 5, pp. 347-382.

Perkins, S.W., Ismeik M. and Fogelsong, M.L (1999), "Influence of Geosynthetic Placement Position on the Performance of Reinforced Flexible Pavement Systems", *Proceedings of the Conference Geosynthetics'99*, Boston, MA, USA, V. 1, pp. 253-264.

Perkins, S.W., Ismeik, M., Fogelsong, M.L., Wang, Y. and Cuelho, E.V. (1998a), "Geosynthetic-

Reinforced Pavements: Overview and Preliminary Results", *Proceedings of the Sixth International Conference on Geosynthetics*, Atlanta, GA, USA, Vol. 2, pp. 951-958.

Perkins, S.W., Ismeik, M. and Fogelsong, M.L. (1998b), "Mechanical Response of a Geosynthetic-Reinforced Pavement System to Cyclic Loading", *Fifth International Conference on the Bearing Capacity of Roads and Airfields*, Trondheim, Norway, Vol. 3, pp. 1503-1512.

Perkins, S.W. and Ismeik, M. (1997a), "A Synthesis and Evaluation of Geosynthetic Reinforced Base Course Layers in Flexible Pavements: Part I", *Geosynthetics International*, Vol. 4, No. 6, pp. 549-604, 1997.

Perkins, S.W. and Ismeik, M. (1997b), "A Synthesis and Evaluation of Geosynthetic Reinforced Base Course Layers in Flexible Pavements: Part II", *Geosynthetics International*, Vol. 4, No. 6, pp. 605-621, 1997.

Schofield, A.N. and Wroth, C.P. (1968), *Critical State Soil Mechanics*, McGraw-Hill, Inc., London.

Seed, H.B., Mitry, F.G., Monismith, C.L. and Chan, C.K. (1967), *Prediction of Flexible Pavement Deflections From Laboratory Repeated Load Tests*, NCHRP Report No. 35, Transportation Research Board, National Research Council, Washington, DC, USA.

Sellmeijer, J.B. (1990), "Design of Geotextile Reinforced Paved Roads and Parking Areas", *Proceedings of the Conference Geotextiles, Geomembranes and Related Products*, Balkema, Rotterdam, pp.177-182.

Tenax (2001), Personal email communication, 5-7-2001.

Tensar (2001), Personal fax communication, 4-23-2001, 37 p.

Tensar (1996), *Design Guidelines for Flexible Pavements with Tensar Geogrid Reinforced Base Layers*, Technical Note BR96, The Tensar Corporation, Atlanta, GA, 77p.

Wathugala, G.W., Huang, B. and Pal, S. (1996), "Numerical Simulation of Geosynthetic Reinforced Flexible Pavement", In *Transportation Research Record 1534*, Transportation Research Board, National Research Council, Washington, DC, USA, pp. 58-65.

Wathugala, G.W. and Desai, C.S. (1993), "Constitutive Model for Cyclic Behavior of Clay I: Theory", *Journal of Geotechnical Engineering*, ASCE, Vol. 119, No. 4, pp.714-729.

Webster, S. L. (1993), *Geogrid Reinforced Base Courses For Flexible Pavements For Light Aircraft, Test Section Construction, Behavior Under Traffic, Laboratory Tests, and Design Criteria*, Technical Report GL-93-6, USAE Waterways Experiment Station, Vicksburg, Mississippi, USA, 86 p.

Zhao and Foxworthy (1999), "Geogrid Reinforcement of Flexible Pavements: A Practical Perspective", *Geotechnical Fabrics Report*, Vol. 17, No. 4, IFAI, Roseville, MN, pp. 28-34.

## APPENDIX A: NOTATION

Provided below is a list of symbols and their definitions. Given the fact that certain symbols have been used more than once for different material definitions, the notation list below is broken down by various categories. Duplicate definitions for the same symbol was necessary to avoid confusion with symbols used in original references.

### General

| | |
|---|---|
| $A$ | Material constant for subgrade rutting model (unitless) |
| $a_1$ | Asphalt concrete structural layer coefficient (unitless) |
| $a_{1\text{-}d}$ | Design value for asphalt concrete structural layer coefficient (unitless) |
| $a_2$ | Base aggregate structural layer coefficient (unitless) |
| $a_{2\text{-}d}$ | Design value for base aggregate structural layer coefficient (unitless) |
| $a_{2\text{-}R}$ | Base aggregate structural layer coefficient for a reinforced pavement (unitless) |
| $a_3$ | Subbase aggregate structural layer coefficient (unitless) |
| $a_{3\text{-}d}$ | Design value for subbase aggregate structural layer coefficient (unitless) |
| $B$ | Material constant for subgrade rutting model (unitless) |
| $BCR$ | Base course reduction ratio (%) |
| $BCR_{TBR=1}$ | Base course reduction ratio (%) when $TBR$ is 1 |
| $CBR$ | California Bearing Ratio (%) |
| $D_1$ | Asphalt concrete thickness (in or mm) |
| $D_{1\text{-}d}$ | Design value for asphalt concrete thickness (in or mm) |
| $D_{1\text{-}e}$ | Equivalent value for asphalt concrete thickness (in or mm) |
| $D_2$ | Base aggregate thickness (in or mm) |
| $D_{2\text{-}d}$ | Design value for base aggregate thickness (in or mm) |
| $D_{2\text{-}e}$ | Equivalent value for base aggregate thickness (in or mm) |
| $D_{2\text{-}R}$ | Base aggregate thickness of a reinforced pavement (in or mm) |
| $D_{2\text{-}U}$ | Base aggregate thickness of an unreinforced pavement (in or mm) |
| $D_3$ | Subbase aggregate thickness (in or mm) |
| $D_{3\text{-}d}$ | Design value for subbase aggregate thickness (in or mm) |
| $D_{3\text{-}e}$ | Equivalent value for subbase aggregate thickness (in or mm) |

| | |
|---|---|
| $E_G$ | Isotropic value of elastic modulus for the geosynthetic material model (kPa) |
| $E_{G\text{-}max}$ | Maximum value of elastic modulus for the geosynthetic material model (kPa) |
| $E_{G\text{-}min}$ | Minimum value of elastic modulus for the geosynthetic material model (kPa) |
| $G_{MR}$ | Ratio of minimum to maximum 2 % secant modulus of the geosynthetic (unitless) |
| $G_{SM\text{-}2\%}$ | Secant tensile modulus from ASTM 4595 measured at 2 % axial strain (kN/m) |
| $k_1$ | Material constant in $k_1$-$q$-$k_2$ non-linear model for resilient modulus (unitless) |
| $k_2$ | Material constant in $k_1$-$q$-$k_2$ non-linear model for resilient modulus (unitless) |
| $m_2$ | Base layer drainage coefficient (unitless) |
| $m_{2\text{-}d}$ | Design value for base layer drainage coefficient (unitless) |
| $m_3$ | Subbase layer drainage coefficient (unitless) |
| $m_{3\text{-}d}$ | Design value for subbase layer drainage coefficient (unitless) |
| $M_R$ | Base aggregate resilient modulus (psi) |
| $M_{R\text{-}R}$ | Effective base aggregate resilient modulus of a reinforced base (psi) |
| $M_{R\text{-}U}$ | Effective base aggregate resilient modulus of an unreinforced base (psi) |
| $M_{R\text{-}R/U}$ | Ratio of base aggregate resilient moduli for a reinforced and unreinforced base |
| $M_S$ | Subgrade resilient modulus (psi) |
| $N$ | Traffic load cycles necessary to for a given level of permanent surface deformation |
| $N_{12.5\ mm}$ | Traffic load cycles necessary to reach 12.5 mm of permanent surface deformation |
| $N_{12.5\ mm\text{-}R}$ | $N_{12.5\ mm}$ for a reinforced pavement |
| $N_{12.5\ mm\text{-}U}$ | $N_{12.5\ mm}$ for an unreinforced pavement |
| $n$ | Number of integration points within base volume examined |
| $r_i$ | Radius to an integration point (m) |
| $R_{GI}$ | Reduction factor for geosynthetic interface shearing resistance (unitless) |
| $R_{GM}$ | Reduction factor for geosynthetic isotropic secant modulus at 2 % strain (unitless) |
| $R_{GMR}$ | Reduction factor for geosynthetic modulus ratio (unitless) |
| $R_{Gn}$ | Reduction factor for geosynthetic Poisson's ratio (unitless) |
| $R_{GG}$ | Reduction factor for geosynthetic shear modulus (unitless) |
| $R_{GnG}$ | Reduction factor for geosynthetic Poisson's ratio and shear modulus (unitless) |
| $S$ | Subgrade support value (unitless) |
| $SN$ | Structural number (unitless) |

| | |
|---|---|
| $SN_R$ | Structural number of a reinforced section (unitless) |
| $S_o$ | Combined standard error (unitless) |
| $TBR$ | Traffic benefit ratio (unitless) |
| $TBR_B$ | Traffic benefit ratio for reinforcement effects in the base aggregate layer (unitless) |
| $TBR_{B\text{-}GM}$ | $TBR_B$ accounting for geosynthetic isotropic secant modulus (unitless) |
| $TBR_{B\text{-}GMR}$ | $TBR_B$ accounting for geosynthetic modulus and modulus ratio (unitless) |
| $TBR_{B\text{-}PR}$ | $TBR_B$ for case of perfect reinforcement (unitless) |
| $TBR_{BCR=0}$ | Traffic benefit ratio (unitless) when $BCR$ is 0 |
| $TBR_S$ | Traffic benefit ratio for reinforcement effects in the subgrade layer (unitless) |
| $TBR_{S\text{-}GM}$ | $TBR_S$ accounting for geosynthetic isotropic secant modulus (unitless) |
| $TBR_{S\text{-}GMR}$ | $TBR_S$ accounting for geosynthetic modulus and modulus ratio (unitless) |
| $TBR_{S\text{-}PR}$ | $TBR_S$ for case of perfect reinforcement (unitless) |
| $TBR_T$ | Traffic benefit ratio for reinforcement effects on the total system (unitless) |
| $T$ | Tensile strength of the geosynthetic (kN/m) |
| $T_{2\%}$ | Tensile strength of the geosynthetic at 2 % axial strain (kN/m) |
| $V_i$ | Volume associated with an integration point ($m^3$) |
| $W_{18}$ | ESAL's |
| $W_{18\text{-}R}$ | ESAL's for a reinforced pavement |
| $W_{18\text{-}U}$ | ESAL's for an unreinforced pavement |
| $z_i$ | Vertical distance above bottom of base for an integration point (m) |
| $Z_R$ | Standard normal deviate (unitless) |
| $e_a$ | Axial strain of geosynthetic in a wide-width tension test (m/m) |
| $e_v$ | Vertical strain in the top of the subgrade for subgrade rutting model (m/m) |
| $e_{v\text{-}R}$ | Vertical strain in the top of the subgrade for a reinforced pavement (m/m) |
| $e_{v\text{-}U}$ | Vertical strain in the top of the subgrade for an unreinforced pavement (m/m) |
| $DPSI$ | Loss of design serviceability (unitless) |
| $q$ | Bulk stress (psi) |
| $q_{avg}$ | Average bulk stress for base aggregate layer (psi) |
| $q_i$ | Bulk stress for an integration point (psi) |

## Asphalt Concrete Material Model

| | |
|---|---|
| $E_x$ | Elastic modulus in the x direction (MPa) |
| $E_y$ | Elastic modulus in the y direction (MPa) |
| $E_z$ | Elastic modulus in the z direction (MPa) |
| $G_{xy}$ | Shear modulus in the x – y plane (MPa) |
| $G_{xz}$ | Shear modulus in the x – z plane (MPa) |
| $G_{yz}$ | Shear modulus in the y – z plane (MPa) |
| $R_x$ | Yield stress ratio for the x direction (unit less) |
| $R_y$ | Yield stress ratio for the y direction (unit less) |
| $R_z$ | Yield stress ratio for the z direction (unit less) |
| $R_{xy}$ | Yield stress ratio for the x – y plane (unit less) |
| $R_{xz}$ | Yield stress ratio for the x – z plane (unit less) |
| $R_{yz}$ | Yield stress ratio for the y – z plane (unit less) |
| $n_{xy}$, $n_{yx}$ | Poisson's ratio in the x – y plane (unitless) |
| $n_{xz}$, $n_{zx}$ | Poisson's ratio in the x – z plane (unitless) |
| $n_{yz}$, $n_{zy}$ | Poisson's ratio in the y – z plane (unitless) |
| $s^0_{AC}$ | Ultimate yield stress (kPa) |

## Base Aggregate and Subgrade Bounding Surface Material Model

| | |
|---|---|
| $A$ | Shape parameter (unitless) |
| $C$ | Projection center parameter (unitless) |
| $C_c$ | Compression index (unitless) |
| $C_s$ | Swelling/recompression index (unitless) |
| $C_1$ | Coefficient 1 for modification of equation for bulk modulus (unitless) |
| $C_2$ | Coefficient 2 for modification of equation for bulk modulus (unitless) |
| $E$ | Elastic modulus (kPa) |
| $e_{in}$ | Initial void ratio (unitless) |
| $G$ | Shear modulus (kPa) |
| $h$ | Hardening parameter (unitless) |
| $I$ | First stress invariant (kPa) |

| | |
|---|---|
| $I_L$ | Atmospheric pressure (kPa) |
| $I_o$ | Size of ellipse 1 of the bounding surface (kPa) and preconsolidation pressure |
| $J$ | Square root of the second deviatoric stress invariant (kPa) |
| $K$ | Bulk modulus (kPa) |
| $m$ | Hardening parameter (unitless) |
| $M$ | Slope of critical state line in *p-q* stress space (unitless) |
| $M_E/M_C$ | Ratio of $M$ in extension to compression (unitless) |
| $N(a)$ | Slope of critical state line in *I-J* stress space (unitless) |
| $R$ | Shape parameter (unitless) |
| $s_p$ | Elastic zone parameter (unitless) |
| $T$ | Shape parameter (unitless) |
| $a$ | Lode angle (degrees) |
| $f$ | Drained soil friction angle in triaxial compression (degrees) |
| $k$ | Swell/recompression slope (unitless) |
| $l$ | Virgin compression slope (unitless) |
| $\nu$ | Poisson's ratio (unitless) |
| $q$ | First invariant of stress or bulk stress (kPa) |

## Geosynthetic Material Model

| | |
|---|---|
| $E_m$ | Elastic modulus in the machine direction (kPa) |
| $E_n$ | Elastic modulus in the direction through the thickness of the material (kPa) |
| $E_{xm}$ | Elastic modulus in the cross-machine direction (kPa) |
| $G_{m\text{-}n}$ | Shear modulus in the machine – normal to the geosynthetic plane (kPa) |
| $G_{xm\text{-}m}$ | Shear modulus in the cross-machine - machine plane (kPa) |
| $G_{xm\text{-}n}$ | Shear modulus in the cross-machine – normal to the plane direction (kPa) |
| $n_{m\text{-}n}$, $n_{n\text{-}m}$ | Poisson's ratio in the machine – normal to the geosynthetic plane (unitless) |
| $n_{m\text{-}xm}$, $n_{xm\text{-}m}$ | Poisson's ratio in the machine – cross-machine plane (unitless) |
| $n_{n\text{-}xm}$, $n_{xm\text{-}n}$ | Poisson's ratio in the cross-machine – normal to the geosynthetic plane (unitless) |

# APPENDIX B: DESIGN GUIDE

## B.1.0 INTRODUCTION

This appendix has been prepared for the final report of a research project titled "Mechanistic-Empirical Modeling and Design Model Development of Geosynthetic Reinforced Flexible Pavements" and is intended to serve as a stand-alone document summarizing the design model described in the main body of the report and how this model should be used within the context of pavement design practice. The intended audience for this appendix is the interested user of the design model who is concerned principally with use of the model in practice. As such, information concerning the development of the design model is excluded. Given the relatively large number of equations associated with the design model and the availability of a spreadsheet program through this project that performs these computations, non-essential design equations are not contained in this guide but can be found in the body of the main report. It is assumed that the spreadsheet program will be used and hence the design model is described within the context of the program. The spreadsheet program may be downloaded from the following URL: http://www.mdt.state.mt.us/departments/researchmgmt/grfp/grfp.html; or obtained by contacting the Montana Department of Transportation, Development and Technology Transfer Program at the address listed in the Technical Report Standard Page of this report.

## B.2.0 APPLICATION BACKGROUND

The design guide presented in this appendix addresses the use of geosynthetics for reinforcement in flexible pavement systems when placed at the bottom of the base or subbase aggregate layer. Geosynthetic reinforcement within this context is intended to provide structural support of traffic loads over the life of the pavement and principally addresses the pavement distress feature of rutting due to the accumulation of permanent strain in the unbound aggregate and subgrade layers. The geosynthetic is expected to provide one or a combination of the following two primary benefits: 1) improved or extended service life of the pavement; 2) a reduction in base or subbase aggregate thickness for equal service life. The types of geosynthetics that may be used for this application include geotextiles, geogrids or geogrid/geotextile composites. The use of geotextiles for separation and stabilization applications is addressed in AASHTO Specification M-288 (AASHTO, 1997a).

## B.3.0 DESIGN MODEL BACKGROUND

The research project from which this appendix was developed provides a design model for the application described in Section B.2.0. The design model was developed to describe reinforcement benefit in terms of generic material and pavement layer parameters, thereby allowing for the consideration of geosynthetic reinforcement for a range of pavement design conditions and geosynthetic products.

The design model was developed within the context of a mechanistic-empirical analysis framework. A finite element response model, including specific elements and material properties for the geosynthetic reinforcement, was developed to provide key stress and strain response measures that relate to the pavement distress feature of permanent surface deformation due to the development of permanent strain in the unbound aggregate and subgrade layers. Empirical distress models were either adopted and modified, or developed to relate the response measures from the mechanistic finite element model to pavement performance defined in terms of permanent surface deformation.

The finite element response model was used within the context of a parametric study to analyze and provide response measures for over 465 pavement design configurations. The empirical distress models used in the study were calibrated by the comparison of response measures from certain finite element model cases to stress and strain measures from large-scale tests sections reported by Perkins (1999a). The design model itself was further calibrated by comparison of reinforcement benefit predicted from the model to that observed in these same pavement test sections.

Regression equations were developed from the results of the parametric study to relate reinforcement benefit to the range of input parameters used. These parameters included thickness of the asphalt concrete and base course aggregate layers, strength/stiffness of the subgrade layer, secant tensile modulus of the geosynthetic measured at 2 % axial strain in the strong direction of the material, the ratio of secant tensile modulus between the weak and strong directions of the material and two other elastic properties (Poisson's ratio and shear modulus) that may be related to geosynthetic type and structure. These regression equations form the basis of the design model. The relatively large number of regression equations developed and the need for iterations of several equations prompted the need to program them into a relatively simple spreadsheet program available through this project.

The design model, expressed in the form of the spreadsheet program, provides quantitative descriptions of reinforcement benefit for the input parameters contained in the model. The purpose of this design guide is to describe the operation of the design model including the input required and the use of the benefit values for pavement design.

## B.4.0 REINFORCEMENT BENEFIT DEFINITIONS

The design model predicts reinforcement benefit in terms of two basic parameters, namely Traffic Benefit Ratio (*TBR*) and Base Course reduction Ratio (*BCR*). *TBR* describes the increase in service life of an unreinforced pavement design when a particular geosynthetic reinforcement is added. *TBR* is formally defined as the ratio of the number of traffic loads between an otherwise identical reinforced and unreinforced pavement that are applied to reach a particular pavement permanent surface deformation. *BCR* describes the reduction of base course aggregate allowed for equivalent service life. *BCR* is formally defined as the percentage reduction of the base course thickness of an unreinforced pavement such that equivalent life, defined in terms of traffic loads, is obtained between the thinner reinforced pavement and the thicker unreinforced pavement. As defined above, *TBR* corresponds to no reduction in base course aggregate thickness and is more formally denoted as $TBR_{BCR=0}$. *BCR* as defined above corresponds to no increase in service life and is more formally denoted as $BCR_{TBR=1}$. The design model allows for the combined use of the two benefits described above by the determination of combined values of *TBR* and *BCR*. When combined values are used, values will fall within the following ranges: $1 = TBR = TBR_{BCR=0}$; $0 = BCR = BCR_{TBR=1}$.

The use of a $BCR_{TBR=1}$ will be most familiar conceptually because of its similarity to methods employed for comparison of bound aggregate (i.e. cement treated base) to unbound crushed base options. The use of bound aggregate requires that a more expensive material be used with savings being realized by a reduction in the thickness of the layer for an equivalent service life. This option will also require the least amount of effort in terms of a cost savings analysis. It should be recognized, however, that the use of a *TBR* value, either as $TBR_{BCR=0}$ or combined with a *BCR*, will most likely yield the greatest economic benefits when life-cycle costs are considered over the increased service life of the reinforced pavement. Transportation agencies are encouraged to consider options involving the use of *TBR* to examine cost savings

for typical projects. Examples are provided at the end of this guide that illustrate these considerations.

The design model has been formulated to determine separate values of *TBR* and *BCR* for reinforcement effects in the subgrade, base aggregate layer and for the total system. The report for this project describes the conservatism and apparent safety associated with the steps taken to develop the design model and concludes that reinforcement effects for the total system be used. It is recommended, therefore, that the *Total* values column for *TBR* and/or *BCR* values in the design spreadsheet program be used. Values for each reinforcement effect are provided, however, such that designers may choose values at their discretion. All examples contained in this guide use benefit values for the total system.

## B.5.0 DESIGN MODEL

### B.5.1 Design Model Input

The design model spreadsheet program requires specification of 20 input parameters. Figure B.5.1 provides a diagram of the selection boxes for the input parameters with typical values provided for one of the cases examined in the project. Comment boxes in the active program provide information on each input item.

Table B.5.1 provides a listing of the 14 input parameters contained in the input selection boxes for the *Pavement Section Parameters* and *Geosynthetic Properties* boxes shown in Figure B.5.1. The parameters $a_1$, $a_2$ and $a_3$ are dimensionless structural layer coefficients for the asphalt concrete, base aggregate and subbase layers, respectively as defined for use in the AASHTO 1993 pavement design guide. While this design guide is general in the sense that the unreinforced pavement can be designed according to any technique, as described later in this appendix, input parameters for layer coefficients must be specified within the context of the AASHTO 1993 guide. The 1993 guide contains equations and charts for relating dimensionless layer coefficients to other commonly used parameters describing the mechanical properties of these pavement layers and should be used to determine appropriate values of layer coefficients for the design in question. A recently completed survey of US State transportation agencies indicated that 70 % of the 34 responding agencies used the AASHTO 1993 method for pavement design (Christopher et al., 2001).

| INPUT | | | |
|---|---|---|---|
| **PAVEMENT SECTION PARAMETERS** | | | |
| AC Thickness, $D_1$ (mm) | 75 | | |
| AC Structural Layer Coefficient, $a_1$ | 0.40 | | |
| Base Thickness, $D_2$ (mm) | 300 | | |
| Base Strucural Layer Coefficient, $a_2$ | 0.14 | | |
| Base Layer Drainage Coefficient, $m_2$ | 1.0 | | |
| Subbase Thickness, $D_3$ (mm) | 0 | | |
| Subbase Structural Layer Coefficient, $a_3$ | 0.10 | | |
| Subbase Layer Drainage Coefficient, $m_3$ | 1.0 | | |
| Subgrade CBR | 1.5 | | |
| | | | |
| **GEOSYNTHETIC PROPERTIES** | | | |
| Geosynthetic Modulus, $G_{SM\text{-}2\%}$ (kN/m) | 425 | | |
| Geosynthetic Modulus Ratio, $G_{MR}$ | 0.595 | | |
| Reduction Factor for Interface Shear | 1.00 | | |
| ☐ Reduction for Poisson's Ratio | | | |
| ☐ Reduction for Shear Modulus | | | |
| **DESIRED REINFORCEMENT BENEFIT** | | | |
| | Subgrade | Base | Total |
| Desired TBR | 1.00 | 1.00 | 2.00 |
| Desired BCR | 0.0 | 0.0 | 25.0 |

**Figure B.5.1** Design model software program input selection boxes.

**Table B.5.1** Design model input parameters.

| | |
|---|---|
| $a_1$ | Asphalt concrete structural layer coefficient (unitless) |
| $a_2$ | Base aggregate structural layer coefficient (unitless) |
| $a_3$ | Subbase aggregate structural layer coefficient (unitless) |
| $CBR$ | Subgrade California Bearing Ratio (%) |
| $D_1$ | Asphalt concrete thickness (mm) |
| $D_2$ | Base aggregate thickness (mm) |
| $D_3$ | Subbase aggregate thickness (mm) |
| $G_{MR}$ | Ratio of minimum to maximum 2 % secant modulus of the geosynthetic (unitless) |
| $G_{SM\text{-}2\%}$ | Secant tensile modulus from ASTM 4595 measured at 2 % axial strain (kN/m) |
| $m_2$ | Base layer drainage coefficient (unitless) |
| $m_3$ | Subbase layer drainage coefficient (unitless) |
| $R_{GI}$ | Reduction factor for interface shear (unitless) |
| $R_{Gn}$ | Reduction for geosynthetic Poisson's ratio (unitless) |
| $R_{GG}$ | Reduction for geosynthetic shear modulus (unitless) |

The strength or stiffness of the subgrade material is specified by the design value for its California Bearing Ratio (*CBR*). If the subgrade has been characterized in terms of a design value for resilient modulus ($M_S$), then subgrade *CBR* should be estimated from Equation B.5.1, where resilient modulus in this equation should have units of *psi*. The survey contained in Christopher et al. (2001) indicated that 41 % of responding agencies use *CBR* to characterize the subgrade while 47 % use resilient modulus. Values of either *CBR* or $M_S$ should be the values used for development of the unreinforced pavement design.

$$CBR = \frac{M_S}{1500} \tag{B.5.1}$$

The parameters $D_1$, $D_2$ and $D_3$ describe the layer thickness of the asphalt concrete, base aggregate and subbase layers, respectively, for the unreinforced pavement design, where these parameters should be specified in units of millimeters. The program internally converts the calculated structural number in units of millimeters to units of inches for use in the AASHTO design equation. The parameters $m_2$ and $m_3$ are the drainage coefficients for the base and subbase layers, where these values must also be determined within the guidelines of the AASHTO 1993 method.

The parameters introduced above correspond to conventional pavement design parameters used within the context of the AASHTO 1993 method. The remainder of this section describes parameters pertinent to the geosynthetic reinforcement. As an aid for understanding these

parameters, Table B.5.2 provides a listing of the geosynthetic products used in the study that served as the basis for this design model. Table B.5.2 lists material characteristics for these products as provided by the manufacturer. Table B.5.3 provides a summary of the geosynthetic input parameters for the design model as they were used in the study for these materials. It should be noted that only the "wide-width tensile strength at 2 % axial strain" data in Table B.5.2 is used for the determination of design model input parameters.

**Table B.5.2** Material properties of geosynthetics used for design model development.

| | Geogrid A: | Geogrid B: | Geotextile: |
|---|---|---|---|
| Material | Polypropylene | Polypropylene | Polypropylene |
| Structure | Punched Drawn, Biaxial | Punched Drawn, Biaxial | Woven |
| Mass/Unit Area ($g/m^2$) | 215 | 309 | 250 |
| Aperature Size (mm) | | | |
| Machine Direction | 25 | 25 | None |
| Cross-Machine Direction | 33 | 33 | |
| Wide-Width Tensile Strength at 2 % Strain (kN/m) | | | |
| Machine Direction | 5.06 | 7.32 | 4.25 |
| Cross-Machine Direction | 8.5 | 11.9 | 13.6 |
| Wide-Width Tensile Strength at 5 % Strain (kN/m) | | | |
| Machine Direction | 9.71 | 13.4 | 11.9 |
| Cross-Machine Direction | 16.5 | 22.9 | 26.4 |
| Ultimate Wide-Width Tensile Strength (kN/m) | | | |
| Machine Direction | 13.8 | 21.1 | 40.2 |
| Cross-Machine Direction | 21.2 | 31.3 | 42.9 |

**Table B.5.3** Design model parameters for geosynthetics.

| | Geogrid A: | Geogrid B: | Geotextile: |
|---|---|---|---|
| $G_{SM\text{-}2\%}$ (kN/m) | 425 | 595 | 680 |
| $G_{MR}$ (unitless) | 0.595 | 0.615 | 0.313 |
| $R_{Gn}$ (unitless) | unchecked | unchecked | checked |
| $R_{GG}$ (unitless) | unchecked | unchecked | checked |
| $R_{GI}$ (unitless) | 1.0 | 1.0 | 0.765 |

The parameters $G_{SM\text{-}2\%}$ and $G_{MR}$ describe secant tensile modulus data for the two principal directions of the geosynthetic. The parameter $G_{SM\text{-}2\%}$ is the greatest value of secant tensile

modulus for the two principal directions of the geosynthetic, where all modulus values have been measured at an axial strain of 2 %. For example, $G_{SM\text{-}2\%}$ for Geogrid A equals 8.5/0.02 = 425. ASTM 4595 (ASTM, 2001a) should be followed to determine these values in each principal direction of the geosynthetic. Values of modulus in units of kN/m should be used. The parameter $G_{MR}$ is the ratio of the minimum to maximum 2 % secant tensile modulus for the two principal directions of the geosynthetic. This parameter should be expressed in decimal form and should be = 1. For Geogrid A, $G_{MR}$ = 5.06/8.5 = 0.595.

The parameters $R_{Gn}$ and $R_{GG}$ are reduction factors for two other geosynthetic material properties (in-plane Poisson's ratio and shear modulus), which relate to the type and structure of the geosynthetic. Each reduction factor corresponds to a check box in the spreadsheet program. When unchecked, each factor has a value of 1.00 and corresponds to a good geosynthetic type and structure for this application. When checked, reduction factors, as summarized in Table 7.6.1 of the main report, are applied to base, subgrade and total system reinforcement effects and correspond to a less favorable geosynthetic type and structure for this application. Calibration of the design model from large-scale test sections resulted in reduction factors of 1.00 (i.e. unchecked boxes) for two rigid, extruded geogrid products and checked boxes for a woven, slit-film geotextile. Suitable tests for the definition of these parameters have not been developed. In the absence of a suitable test method and additional results from test sections using a broader range of geosynthetic products, the values used above along with general geosynthetic application guidelines provided in Berg et al. (2000) and summarized in Table 2.1.2 should serve as the basis for selection of these parameters.

The parameter $R_{GI}$ defines a reduction factor for shear interaction characteristics between the unbound aggregate and the geosynthetic layers and should have a value = 1. Calibration of the design model from large-scale test sections resulted in a reduction factor of 1.00 for Geogrids A and B and 0.765 for the Geotextile. Like the situation for definition of parameters $R_{Gn}$ and $R_{GG}$, suitable tests for the definition of $R_{GI}$ have not been developed. The values provided above should serve as a guide until additional information becomes available.

Figure B.5.1 contains six other input parameters contained in the *Desired Reinforcement Benefit* selection boxes. Values of *Desired TBR* or *BCR* can be listed for reinforcement effects on the subgrade, base or total system. These input boxes are provided for computing combined values of *TBR* and *BCR*. When desired values are specified within the ranges 1 = *Desired TBR* =

$TBR_{BCR=0}$ and 0 = *Desired BCR* = $BCR_{TBR=1}$, for any of the three categories of reinforcement effect, remaining values of *TBR* or *BCR* are computed and listed in the output section. Values in the *Total* column are recommended for use.

### B.5.2 Design Model Output

Figure B.5.2 shows the output boxes for the spreadsheet program for the input parameters contained in Figure B.5.1. Table B.5.4 provides a list of the parameters contained in the output boxes.

| OUTPUT | | | |
|---|---|---|---|
| | Subgrade | Base | Total |
| $TBR_{BCR=0}$ | 2.54 | 1.71 | 4.34 |
| $BCR_{TBR=1}$ | 21.5 | 13.3 | 31.0 |
| Desired TBR | 1.00 | 1.00 | 2.00 |
| Remaining BCR | 21.5 | 13.3 | 17.1 |
| Desired BCR | 0.0 | 0.0 | 25.0 |
| Remaining TBR | 2.54 | 1.71 | 1.36 |
| $M_{R\text{-}R/U}$ | 1.43 | 1.22 | 1.79 |

**Figure B.5.2** Design model software program output boxes.

**Table B.5.4** Design model output parameters.

| | |
|---|---|
| $BCR_{TBR=1}$ | Base course reduction ratio (%) when *TBR* is 1 |
| *Desired BCR* | Input value for desired *BCR (%)* |
| *Remaining BCR* | Computed value of remaining *BCR* (%) for desired *TBR* specified as input |
| $M_{R\text{-}R/U}$ | Ratio of reinforced to unreinforced base aggregate resilient moduli |
| $TBR_{BCR=0}$ | Traffic benefit ratio (unitless) when *BCR* is 0 |
| *Desired TBR* | Input value for desired *TBR* (unitless) |
| *Remaining TBR* | Computed value of remaining *TBR* for desired *BCR* specified as input |

Values of $TBR_{BCR=0}$ and $BCR_{TBR=1}$ are provided for each of the three reinforcement effects of base, subgrade and total system, and where recommended values for the total system have been highlighted in yellow in the active spreadsheet. For the input parameters listed in Figure B.5.1, values of $TBR_{BCR=0}$ and $BCR_{TBR=1}$ of 4.34 and 31.0 % are obtained. Values of *Desired TBR* and *Desired BCR* in the output boxes are repeated from the input values provided. Values of

*Remaining TBR* and *Remaining BCR* are computed based on the desired values specified and the computed values for $TBR_{BCR=0}$ and $BCR_{TBR=1.}$ As seen from the example provided, when values of *Desired TBR* and *Desired BCR* of 1 and 0, respectively, are specified, then values of *Remaining TBR* = $TBR_{BCR=0}$ and *Remaining BCR* = $BCR_{TBR=1.}$ For the case of reinforcement benefits for the total system, a *Desired TBR* = 2.0 results in a *Remaining BCR* = 17.1 %. A *Desired BCR* = 25.0 % results in a *Remaining TBR* = 1.36.

Use of $BCR_{TBR=1}$ typically requires only a consideration of construction costs when performing a cost analysis of various pavement design options. Use of this parameter is conceptually similar to consideration of stabilized base options, such as cement-treated base, where a more expensive material with a reduced thickness is considered for construction. Since an extension of service life is not involved in the use of $BCR_{TBR=1}$, a life-cycle cost analysis is generally not required. Use of $TBR_{BCR=0}$ or combined values of *TBR* and *BCR* require that a life-cycle cost analysis be performed to assess economic benefits. In general, it is anticipated that options involving the use of *TBR* will yield the greatest economic benefits when life-cycle costs are considered over the increased service life of the reinforced pavement. Transportation agencies are encouraged to consider options involving the use of *TBR* to examine cost savings for typical projects. Examples are provided at the end of this guide that illustrate these considerations.

The last output parameter listed is the computed ratio of effective resilient modulus of the reinforced and unreinforced base for reinforcement effects in the subgrade, base and total system. These ratios are provided to allow a check on asphalt concrete fatigue cracking criteria and should be used only for this purpose. It is recommended that the value listed for reinforcement effects in the base layer be used, where this box has been highlighted in yellow in the active spreadsheet. The design value for resilient modulus of the unreinforced base aggregate layer should be multiplied by this ratio to obtain a design value for resilient modulus of the base layer for the reinforced pavement. This value can then be used in a mechanistic analysis (layered elastic or finite element) when checking the design for asphalt fatigue cracking. The user of this factor should be reminded that the only pavement distress feature observed in the support testing for this model was permanent surface deformation, meaning that this value is derived indirectly from test results reflecting permanent deformation in the base aggregate and subgrade layers. Consequently, this factor should be used with discretion and judgment.

### B.5.3 Design Model Input Limitations

The design model has been developed for a certain range of input parameters. Recommended limits on critical parameters are given below:

1. 50 mm = $D_1$ = 150 mm
2. 150 mm = $D_2$ = 600 mm
3. 0.5 = Subgrade *CBR* = 15 *or* 5.2 MPa = $M_S$ = 155 MPa
4. 33 kN/m = $G_{SM\text{-}2\%}$ = 2000 kN/m
5. *BCR* > 0 be used only for subgrades with a *CBR* = 1.0 (or $M_S$ = 10.3 MPa).

## B.6.0 DESIGN STEPS

The design steps described below are an extension of those provided as the recommended standard of practice in Berg et al. (2000) and AASHTO (2001). Additional details may be obtained by referring to Berg et al. (2000).

Step 1. Initial assessment of applicability of the technology.
Step 2. Design of the unreinforced pavement.
Step 3. Definition of the qualitative benefits of reinforcement for the project.
Step 4. Definition of the quantitative benefits of reinforcement (*TBR* and/or *BCR*).
Step 5. Design of the reinforced pavement using the benefits defined in Step 4.
Step 6. Analysis of life-cycle costs.
Step 7. Development of a project specification.
Step 8. Development of construction drawings and bid documents.
Step 9. Construction of the roadway.

Step 1 involves consideration of project conditions for the design to determine whether geosynthetic reinforcement is applicable and remains unchanged from that contained in Berg et al. (2000). Step 2 involves designing the thickness of an unreinforced pavement section based on representative material parameters. Step 2 may be accomplished by any recognized pavement design procedure, provided that the pavement layer material properties can be related to the layer coefficients and drainage coefficients required in the design model. Step 3 should emphasize the

definition of benefits for use of reinforcement other than the main benefits defined in terms of a *TBR* and /or *BCR*, where these benefits have been summarized in Berg et al. (2000).

Step 4 should be accomplished by the use of the design model described in Section B.5.0. The values of *TBR* and/or *BCR* calculated from the design model are then used in Step 5 to alter the unreinforced pavement design. Equation B.6.1 results from the definition of *TBR* and states that the number of ESAL's that can be applied to the reinforced pavement is equal to the design ESAL's for the unreinforced pavement multiplied by *TBR*. Recognizing that the service life, or performance period, of the pavement is related to the number of ESAL's that the pavement can carry, it follows that the service life of the reinforced pavement can be determined from Equation B.6.2. Equation B.6.3 allows *BCR* to be used to adjust the design thickness of the base course aggregate layer for the reinforced pavement. The design should also consider separation, filtration and drainage requirements.

$$W_{18-R} = W_{18-U}\ TBR \tag{B.6.1}$$

$$Service\ Life_{(Reinforced\ Pavement)} = Service\ Life_{(Unreinforced\ Pavement)} * TBR \tag{B.6.2}$$

$$D_{2-R} = D_{2-U}\left(1 - \frac{BCR}{100}\right) \tag{B.6.3}$$

Use of values of *BCR* through Equation B.6.3 results in potential economic savings during the initial construction phase of the pavement. Use of a *TBR* through Equation B.6.2 results in potential economic savings seen over the life-cycle of the pavement. Step 6 is used to define life-cycle costs for the various pavement design alternatives such that design decisions can be based on economic benefits. Examples are provided in Section B.7.0 to illustrate this step. Sample specifications for Step 7 have been provided in Berg et al. (2000) and will require revisions according to the new methods proposed for Steps 4 and 5. Steps 8 and 9 should consider geosynthetic survivability criteria.

## B.7.0 DESIGN EXAMPLES

Two basic examples are provided to illustrate use of the design model for pavement design. The first example uses life-cycle cost information contained in Chapter 6 of Berg et al. (2000). The rehabilitation steps contained in this example are kept relatively simple to avoid confusion. The second example uses information from a project design recently prepared for the Montana Department of Transportation. All examples were analyzed using the computer program DARWin (AASHTO, 1997b), which is based on the AASHTO 1993 pavement design guide (AASHTO, 1993). Copies of DARWin output are provided for each example in Appendix C as a separate volume to this report (Perkins 2001b). Each example incorporates assumptions for rehabilitation and maintenance steps and costs. These design assumptions will differ between agencies, geographic locations, projects, designers and clients. The purpose of these examples is to illustrate how reinforcement concepts and results from the design model can be incorporated into life-cycle cost analyses. The focus should not be on the validity of the design assumptions made for a particular agency or project, as these may vary as described above.

### B.7.1 Illustrative Example

The first example is designed primarily to illustrate the operation of the design model and the incorporation of the results into a life-cycle cost analysis. Table B.7.1 provides the input used for the DARWin Flexible Structural Design module. These input design parameters result in a structural number of 80 mm (3.1 in).

**Table B.7.1** Flexible structural design module input for example 1.

| | |
|---|---|
| ESAL's ($W_{18}$) | 35,000 |
| Initial Serviceability | 4.2 |
| Terminal Serviceability | 2.5 |
| Reliability Level (%) | 90 |
| Overall Standard Deviation | 0.44 |
| Roadbed Soil Resilient Modulus (kPa) | 15,500 |
| Design Structural Number (mm) | 80 |
| Asphalt Concrete Layer One-Directional Lane Width (m) | 4 |
| Base Course Aggregate Layer One-Directional Lane Width (m) | 5 |

Table B.7.2 lists the thickness design for the unreinforced pavement (Option 1) satisfying the design structural number of 80 mm. Several design options with three different geosynthetics

were considered. Geogrid A and B, and the Geotextile listed previously in Table B.5.2 were used. Figures B.7.1 – B.7.3 provide a copy of the input and output from the design model for each of the three geosynthetics. Each of the geosynthetic input parameter sets corresponds to those values used for calibration of the model and are representative of these material types. For cases where a $TBR_{BCR=0}$ greater than 2 was obtained, options involving the combined use of *BCR* and *TBR* were examined. Tables B.7.2 and B.7.3 provide a listing of the thickness design and benefit values used for the design options examined. It should be noted that for the Geotextile, a value of $TBR_{BCR=0} = 2$ was rounded up from the value of 1.97 computed from the design model. The reduced base course aggregate thickness listed in Table B.7.2 for options using a *BCR* is computed using Equation B.6.3.

**Table B.7.2** Thickness designs for design options for example 1.

| Design Option | Structural Section Type | Asphalt Concrete | | Base Course Aggregate | |
|---|---|---|---|---|---|
| | | Thickness (mm) | Structural Coefficient | Thickness (mm) | Structural Coefficient |
| Option 1 | Unreinforced | 85 | 0.4 | 325 | 0.14 |
| Option 2 | Geogrid A | 85 | 0.4 | 325 | 0.14 |
| Option 3 | Geogrid A | 85 | 0.4 | 275 | 0.14 |
| Option 4 | Geogrid A | 85 | 0.4 | 228 | 0.14 |
| Option 5 | Geogrid B | 85 | 0.4 | 306 | 0.14 |
| Option 6 | Geogrid B | 85 | 0.4 | 259 | 0.14 |
| Option 7 | Geogrid B | 85 | 0.4 | 215 | 0.14 |
| Option 8 | Geotextile | 85 | 0.4 | 325 | 0.14 |
| Option 9 | Geotextile | 85 | 0.4 | 271 | 0.14 |

**Table B.7.3** *TBR* and *BCR* values for design options for example 1.

| Design Option | Structural Section Type | $TBR_T$ | $BCR_T$ |
|---|---|---|---|
| Option 1 | Unreinforced | NA | NA |
| Option 2 | Geogrid A | 4 | 0 |
| Option 3 | Geogrid A | 2 | 15.5 |
| Option 4 | Geogrid A | 1 | 29.7 |
| Option 5 | Geogrid B | 4 | 5.7 |
| Option 6 | Geogrid B | 2 | 20.3 |
| Option 7 | Geogrid B | 1 | 33.7 |
| Option 8 | Geotextile | 2 | 0 |
| Option 9 | Geotextile | 1 | 16.6 |

| INPUT | |
|---|---|
| **PAVEMENT SECTION PARAMETERS** | |
| AC Thickness, $D_1$ (mm) | 85 |
| AC Structural Layer Coefficient, $a_1$ | 0.40 |
| Base Thickness, $D_2$ (mm) | 325 |
| Base Strucural Layer Coefficient, $a_2$ | 0.14 |
| Base Layer Drainage Coefficient, $m_2$ | 1.0 |
| Subbase Thickness, $D_3$ (mm) | 0 |
| Subbase Structural Layer Coefficient, $a_3$ | 0.10 |
| Subbase Layer Drainage Coefficient, $m_3$ | 1.0 |
| Subgrade CBR | 1.5 |
| | |
| **GEOSYNTHETIC PROPERTIES** | |
| Geosynthetic Modulus, $G_{SM\text{-}2\%}$ (kN/m) | 425 |
| Geosynthetic Modulus Ratio, $G_{MR}$ | 0.595 |
| Reduction Factor for Interface Shear | 1.00 |
| ☐ Reduction for Poisson's Ratio | |
| ☐ Reduction for Shear Modulus | |

| DESIRED REINFORCEMENT BENEFIT | | | |
|---|---|---|---|
| | Subgrade | Base | Total |
| Desired TBR | 1.00 | 1.00 | 2.00 |
| Desired BCR | 0.0 | 0.0 | 0.0 |

| OUTPUT | | | |
|---|---|---|---|
| | Subgrade | Base | Total |
| $TBR_{BCR=0}$ | 2.47 | 1.62 | 4.00 |
| $BCR_{TBR=1}$ | 21.1 | 12.1 | 29.7 |
| Desired TBR | 1.00 | 1.00 | 2.00 |
| Remaining BCR | 21.1 | 12.1 | 15.5 |
| Desired BCR | 0.0 | 0.0 | 0.0 |
| Remaining TBR | 2.48 | 1.62 | 4.00 |
| $M_{R\text{-}R/U}$ | 1.41 | 1.20 | 1.73 |

**Figure B.7.1** Design model input/output for Geogrid A for example 1.

| INPUT | |
|---|---|
| **PAVEMENT SECTION PARAMETERS** | |
| AC Thickness, $D_1$ (mm) | 85 |
| AC Structural Layer Coefficient, $a_1$ | 0.40 |
| Base Thickness, $D_2$ (mm) | 325 |
| Base Strucural Layer Coefficient, $a_2$ | 0.14 |
| Base Layer Drainage Coefficient, $m_2$ | 1.0 |
| Subbase Thickness, $D_3$ (mm) | 0 |
| Subbase Structural Layer Coefficient, $a_3$ | 0.10 |
| Subbase Layer Drainage Coefficient, $m_3$ | 1.0 |
| Subgrade CBR | 1.5 |
| | |
| **GEOSYNTHETIC PROPERTIES** | |
| Geosynthetic Modulus, $G_{SM\text{-}2\%}$ (kN/m) | 595 |
| Geosynthetic Modulus Ratio, $G_{MR}$ | 0.615 |
| Reduction Factor for Interface Shear | 1.00 |
| ☐ Reduction for Poisson's Ratio | |
| ☐ Reduction for Shear Modulus | |

| DESIRED REINFORCEMENT BENEFIT | | | |
|---|---|---|---|
| | Subgrade | Base | Total |
| Desired TBR | 1.00 | 1.00 | 2.00 |
| Desired BCR | 0.0 | 0.0 | 0.0 |

| OUTPUT | | | |
|---|---|---|---|
| | Subgrade | Base | Total |
| $TBR_{BCR=0}$ | 3.01 | 1.72 | 5.16 |
| $BCR_{TBR=1}$ | 24.8 | 13.5 | 33.7 |
| Desired TBR | 1.00 | 1.00 | 2.00 |
| Remaining BCR | 24.8 | 13.5 | 20.3 |
| Desired BCR | 0.0 | 0.0 | 0.0 |
| Remaining TBR | 3.01 | 1.72 | 5.16 |
| $M_{R\text{-}R/U}$ | 1.53 | 1.22 | 1.93 |

**Figure B.7.2** Design model input/output for Geogrid B for example 1.

| INPUT | |
|---|---|
| **PAVEMENT SECTION PARAMETERS** | |
| AC Thickness, $D_1$ (mm) | 85 |
| AC Structural Layer Coefficient, $a_1$ | 0.40 |
| Base Thickness, $D_2$ (mm) | 325 |
| Base Strucural Layer Coefficient, $a_2$ | 0.14 |
| Base Layer Drainage Coefficient, $m_2$ | 1.0 |
| Subbase Thickness, $D_3$ (mm) | 0 |
| Subbase Structural Layer Coefficient, $a_3$ | 0.10 |
| Subbase Layer Drainage Coefficient, $m_3$ | 1.0 |
| Subgrade CBR | 1.5 |
| | |
| **GEOSYNTHETIC PROPERTIES** | |
| Geosynthetic Modulus, $G_{SM\text{-}2\%}$ (kN/m) | 680 |
| Geosynthetic Modulus Ratio, $G_{MR}$ | 0.313 |
| Reduction Factor for Interface Shear | 0.77 |
| ☑ Reduction for Poisson's Ratio | |
| ☑ Reduction for Shear Modulus | |

| DESIRED REINFORCEMENT BENEFIT | | | |
|---|---|---|---|
| | Subgrade | Base | Total |
| Desired TBR | 1.00 | 1.00 | 2.00 |
| Desired BCR | 0.0 | 0.0 | 0.0 |

| OUTPUT | | | |
|---|---|---|---|
| | Subgrade | Base | Total |
| $TBR_{BCR=0}$ | 1.66 | 1.19 | 1.98 |
| $BCR_{TBR=1}$ | 12.8 | 4.7 | 16.6 |
| Desired TBR | 1.00 | 1.00 | 2.00 |
| Remaining BCR | 12.8 | 4.7 | -0.2 |
| Desired BCR | 0.0 | 0.0 | 0.0 |
| Remaining TBR | 1.66 | 1.19 | 1.98 |
| $M_{R\text{-}R/U}$ | 1.21 | 1.07 | 1.29 |

**Figure B.7.3** Design model input/output for Geotexile for example 1.

A life-cycle cost analysis was performed for each design option. Table B.7.4 lists the assumed construction and rehabilitation dates and performance periods for each design option. This relatively simple example assumes that the performance period of the new pavement for the unreinforced option is 10 years. The example assumes that the pavement will be milled and overlaid every 10 years. An overlay thickness of 50 mm is assumed. These assumptions are purposefully simplistic in order to illustrate the incorporation of reinforcement concepts and results from the design model into a life-cycle cost analysis.

**Table B.7.4** Construction and rehabilitation dates and performance periods for example 1.

| Step | Date of Step Taken and Performance Period (years) | | |
|---|---|---|---|
| | Options 1, 4 & 7 | Options 3, 6 & 8 | Options 2 & 5 |
| New Construction | 2000 / 10 | 2000 / 20 | 2000 / 40 |
| Asphalt Concrete Milling and Overlay | 2010 / 10 | 2020 / 20 | |
| Asphalt Concrete Milling and Overlay | 2020 / 10 | | |
| Asphalt Concrete Milling and Overlay | 2030 / 10 | | |

Use of a *TBR* of 2 for options 3, 6 and 8 allows the performance period for the new construction to be extended from 10 years to 20 years. In addition, it is assumed that the milling and overlay rehabilitation at year 2020 has a performance period of 20 rather than 10 years. Use of a *TBR* of 4 for options 2 and 5 allows the performance period for the new construction of 10 years to be extended to 40 years such that no rehabilitations are required within the analysis period of 40 years. This approach assumes that rutting in the pavement is due primarily to permanent deformation in the base and subgrade layers, which is influenced by reinforcement. This is generally believed to be true of relatively thin pavement sections. For thick pavement layers, rutting and subsequent milling and overlays will most likely be controlled more by flow within the AC layer, which is not effected by reinforcement. The example given in Section B.7.2 assumes that milling and overlays are required equally for all options, but that reconstruction costs are impacted by the extension of service life.

Other design inputs and pay item costs for the analysis are listed in Tables B.7.5 and B.7.6. The maintenance cost listed in Table B.7.6 is assumed to begin 5 years after each performance period, meaning that 20 years of maintenance is included for options 1, 4 and 7, 30 years is included for options 3, 6 and 8 and 35 years is included for options 2 and 5. The costs used for the three geosynthetics are based on the author's experience and best judgment. These costs, and

the relative cost between products, should not be considered as representative of any particular geographic region. Actual geosynthetic material costs will be dependent on project location, project size, experience of the contractor and other factors.

**Table B.7.5** Life-cycle cost analysis input parameters for example 1.

| | |
|---|---|
| Analysis Period (years) | 40 |
| Project Length (km) | 10 |
| Number of Lanes in One Direction | 1 |
| Discount Rate (%) | 3.5 |
| Type of Roadway | Undivided |
| Evaluation Method | NPV |
| Cost Method | Cost per km for Both Directions |

**Table B.7.6** Pay items for example 1.

| Item | Cost |
|---|---|
| Asphalt Concrete – New and Overlay ($/metric ton) | 38.00 |
| Asphalt Concrete Milling ($/m$^2$) | 0.80 |
| Base Course Aggregate ($/metric ton) | 22.00 |
| Geogrid A ($/m$^2$) | 1.50 |
| Geogrid B ($/m$^2$) | 3.00 |
| Geotextile ($/m$^2$) | 0.75 |
| Maintenance Costs ($/lane km) | 62.50 |
| Annual Percent Increase in Maintenance Costs | 0 |
| Year Maintenance Costs Begin | 5 years after beginning of performance period |
| Salvage Values | None for initial construction and rehabilitations |

Total life-cycle costs for each design option are listed in Table B.7.7, where costs are listed per km of the entire road (i.e. both traffic lanes). The costs listed in Table B.7.7 include the reduced construction cost for options using a *BCR*. For this design example, the optimal cost benefit is seen by the use of a combination of *TBR* and *BCR* (option 3). This example was presented only to illustrate the use of the design model and its results in a relatively simple life-cycle cost analysis. Optimal cost benefit for the options presented will depend upon specific project conditions and pay item costs.

**Table B.7.7** Total life-cycle costs for design options for example 1.

| Design Option | Structural Section Type | Total Life Cycle Cost per km ($) | Percent Savings |
|---|---|---|---|
| Option 1 | Unreinforced | 269,210 | NA |
| Option 2 | Geogrid A | 221,641 | 17.7 |
| Option 3 | Geogrid A | 219,159 | 18.6 |
| Option 4 | Geogrid A | 240,484 | 10.7 |
| Option 5 | Geogrid B | 228,076 | 15.3 |
| Option 6 | Geogrid B | 226,947 | 15.7 |
| Option 7 | Geogrid B | 249,624 | 7.3 |
| Option 8 | Geotextile | 234,198 | 13.0 |
| Option 9 | Geotextile | 252,368 | 6.3 |

## B.7.2 Project Example

The second example uses design and analysis information from a project recently developed for the Montana Department of Transportation (Allied Engineering, 2000). The example attempts to use more comprehensive construction and life-cycle cost rehabilitation information. Assumptions were necessary for rehabilitation and maintenance steps and costs. These assumptions will differ from user to user. The purpose of this example is to illustrate the use of reinforcement benefit within the context of a more complex project example. Agencies are encouraged to examine life-cycle cost scenarios pertinent to conditions within their jurisdictions.

The project consists of the reconstruction of 17.5 km of US Highway 12 between the towns of Melstone and Sumatra located approximately 130 km northeast of Billings, Montana. The age of the roadway required complete removal and replacement of the existing pavement structure and partial realignment. Input for the flexible structural design module is listed in Table B.7.8, which assumes a 20-year design life. Four design options are considered. Option 1 uses an unbound, unreinforced crushed base aggregate. Option 2 uses a cement treated base for the base aggregate layer. Options 3 and 4 use Geogrid A for base reinforcement. Input to the spreadsheet design model is shown in Figure B.7.4, where a $TBR_{BCR=0}$ = 2.21 was obtained. Option 3 is developed by specifying a desired *TBR* of 2, which provides a remaining *BCR* of 2.3 %. Option 4 uses a *BCR* of 18.5 % for a *TBR* = 1. Thickness designs and *TBR/BCR* values used for options 3 and 4 are listed in Tables B.7.9 and B.7.10.

| INPUT | |
|---|---|
| **PAVEMENT SECTION PARAMETERS** | |
| AC Thickness, $D_1$ (mm) | 90 |
| AC Structural Layer Coefficient, $a_1$ | 0.33 |
| Base Thickness, $D_2$ (mm) | 486 |
| Base Strucural Layer Coefficient, $a_2$ | 0.10 |
| Base Layer Drainage Coefficient, $m_2$ | 1.0 |
| Subbase Thickness, $D_3$ (mm) | 0 |
| Subbase Structural Layer Coefficient, $a_3$ | 0.10 |
| Subbase Layer Drainage Coefficient, $m_3$ | 1.0 |
| Subgrade CBR | 3.0 |
| | |
| **GEOSYNTHETIC PROPERTIES** | |
| Geosynthetic Modulus, $G_{SM\text{-}2\%}$ (kN/m) | 425 |
| Geosynthetic Modulus Ratio, $G_{MR}$ | 0.595 |
| Reduction Factor for Interface Shear | 1.00 |
| ☐ Reduction for Poisson's Ratio | |
| ☐ Reduction for Shear Modulus | |

| DESIRED REINFORCEMENT BENEFIT | | | |
|---|---|---|---|
| | Subgrade | Base | Total |
| Desired TBR | 1.00 | 1.00 | 2.00 |
| Desired BCR | 0.0 | 0.0 | 0.0 |

| OUTPUT | | | |
|---|---|---|---|
| | Subgrade | Base | Total |
| $TBR_{BCR=0}$ | 1.60 | 1.38 | 2.21 |
| $BCR_{TBR=1}$ | 11.3 | 8.0 | 18.0 |
| Desired TBR | 1.00 | 1.00 | 2.00 |
| Remaining BCR | 11.3 | 8.0 | 2.3 |
| Desired BCR | 0.0 | 0.0 | 0.0 |
| Remaining TBR | 1.60 | 1.38 | 2.21 |
| $M_{R\text{-}R/U}$ | 1.18 | 1.12 | 1.33 |

**Figure B.7.4** Design model input/output for example 2.

**Table B.7.8** Flexible structural design module input for example 2.

| | |
|---|---|
| ESAL's ($W_{18}$) | 165,549 |
| Initial Serviceability | 4.2 |
| Terminal Serviceability | 2.5 |
| Reliability Level (%) | 90 |
| Overall Standard Deviation | 0.35 |
| Roadbed Soil Resilient Modulus (kPa) | 31,000 |
| Design Structural Number (mm) | 76 |

**Table B.7.9** Thickness designs for design options for example 2.

| Design Option | Structural Section Type | Asphalt Concrete | | Base Course Aggregate | | |
|---|---|---|---|---|---|---|
| | | Thickness (mm) | Structural Coefficient | Thickness (mm) | Structural Coefficient | Drainage Coefficient |
| Option 1 | Unreinforced | 90 | 0.33 | 486 | 0.095 | 1.0 |
| Option 2 | CTB | 90 | 0.33 | 257 | 0.18 | 1.0 |
| Option 3 | Geogrid A | 90 | 0.33 | 475 | 0.095 | 1.0 |
| Option 4 | Geogrid A | 90 | 0.33 | 398 | 0.095 | 1.0 |

**Table B.7.10** *TBR* and *BCR* values for design options for example 2.

| Design Option | Structural Section Type | $TBR_T$ | $BCR_T$ |
|---|---|---|---|
| Option 1 | Unreinforced | NA | NA |
| Option 2 | Cement Treated Base | NA | NA |
| Option 3 | Geogrid A | 2 | 1.5 |
| Option 4 | Geogrid A | 0 | 18.5 |

The life-cycle cost analysis used the construction and rehabilitation steps, dates and performance periods listed in Table B.7.11. In this example, the newly constructed road was chip sealed immediately after construction. Crack sealing and chip sealing is a rehabilitation step required every 5 years and is assumed not to be effected by *TBR*. A milling thickness of 75 mm was used for determining the overlay thickness. An overlay design within DARWin using the remaining life method resulted in a total overlay thickness of 79 mm. Milling and overlays were required every 10 years for all options and were assumed to be necessary because of asphalt concrete rutting due to flow within the AC layer, which is not effected by reinforcement. Some of this rutting may in fact be due to permanent deformation in the base and subgrade layers, in which case reinforcement would limit this for option 3.

A design life of 20 years required that the asphalt concrete layer be removed and reconstructed at year 2020 for options 1, 2 and 4. A *TBR* of 2 eliminated the need for this rehabilitation step for option 3. This constitutes the major difference between option 3 and the

others. The asphalt concrete was removed by complete milling of the layer and incorporation of the material back into the base aggregate layer. Traffic control was assumed to be required for this rehabilitation step.

**Table B.7.11** Construction and rehabilitation dates and performance periods for example 2.

| Date of Step & Performance Period (years) | Step Taken | |
|---|---|---|
| | Options 1, 2 & 4 | Option 3 |
| 2000 / 5 | New Construction and Chip Seal | New Construction and Chip Seal |
| 2005 / 5 | Crack Sealing and Chip Seal | Crack Sealing and Chip Seal |
| 2010 / 5 | Asphalt Concrete Milling, Overlay and Chip Seal | Asphalt Concrete Milling, Overlay and Chip Seal |
| 2015 / 5 | Crack Sealing and Chip Seal | Crack Sealing and Chip Seal |
| 2020 /5 | Remove/Reconstruct Asphalt Concrete and Chip Seal | Asphalt Concrete Milling, Overlay and Chip Seal |
| 2025 / 5 | Crack Sealing and Chip Seal | Crack Sealing and Chip Seal |
| 2030 / 5 | Asphalt Concrete Milling, Overlay and Chip Seal | Asphalt Concrete Milling, Overlay and Chip Seal |
| 2035 / 5 | Crack Sealing and Chip Seal | Crack Sealing and Chip Seal |

Reconstruction of the pavement section for options 1, 2 and 4 at year 20 was different between the options. Since option 1 did not contain any type of geosynthetic, a certain amount of base course contamination was assumed to occur over the first 20-year design life. At year 20, it was assumed that the base aggregate had gone from a material in a damp to dry state having a resilient modulus of 139 MPa and a layer coefficient of 0.095 to a material in a moist to damp state having a resilient modulus of 100 MPa and a layer coefficient of 0.06. In addition, assumed contamination of the base required that the drainage coefficient be reduced from 1.0 for the original construction to 0.6 for the reconstruction. Based on these values, a new AC thickness was computed to carry the 20-year design ESAL's for the second 20-year period. Table B.7.12 provides a summary of these details for each option.

**Table B.7.12** Thickness designs for options 1, 2 and 4 for reconstruction at year 20.

| Design Option | Asphalt Concrete | | Base Course Aggregate | | |
|---|---|---|---|---|---|
| | Thickness (mm) | Structural Coefficient | Thickness (mm) | Structural Coefficient | Drainage Coefficient |
| Option 1 | 177 | 0.33 | 486 | 0.06 | 0.6 |
| Option 2 | 145 | 0.33 | 257 | 0.11 | 1.0 |
| Option 4 | 137 | 0.33 | 398 | 0.079 | 0.8 |

Cement treated bases are known to deteriorate and lose strength in the presence of moisture. For option 2, it was assumed that the cement treated base lost approximately 50 % of its assumed modulus when it was originally constructed. This results in the use of a layer coefficient of 0.11 for the cement treated base for the reconstruction design. The drainage coefficient was maintained at a value of 1.0.

Some level of contamination of the base aggregate layer was assumed for option 4 using a geogrid reinforcement. The reduction in layer properties was assumed to be approximately half of that used for option 1. The resilient modulus of the base aggregate was assumed to reduce from the initial value of 139 MPa to 120 MPa, yielding a layer coefficient of 0.079. The drainage coefficient was assumed to reduce from 1.0 to 0.8.

The lane and layer widths were established such that the minimum one-lane AC surface deck width of 4.6 m was maintained throughout the 40-year analysis period. In addition, the design side slope of 1V:11H was maintained for all layers.

Tables B.7.13 and B.7.14 give life-cycle cost analysis input parameters and pay item information. The pay item information was derived from the project report (Allied Engineering, 2000) and average contractor bid summaries for the year 2000, as available from the Montana DOT (MDT, 2001). Maintenance costs were not included as the pay items of crack and chip sealing required every 5 years were considered as maintenance.

Total life-cycle cost figures for each design option are listed in Table B.7.15. For this particular example, it is seen that option 3 is the least expensive, followed by options 2 and 4.

This example disregards several considerations that may be examined for other cases. Any differences in subexcavation costs between the different options were ignored. Options 2, 3 and 4 all involve a total pavement layer thickness at year-40 which is less than that of option 1, with option 2 yielding the smallest total thickness. Reduced subexcavation costs would be anticipated for options 2, 3 and 4. General assumptions were made regarding the level of deterioration of

unbound and cement treated base layers. Additional work should be performed to refine these figures for specific projects. Finally, no consideration was given to issues concerning conservation of aggregate resources in areas where resources are in danger of becoming depleted.

**Table B.7.13** Life-Cycle Cost analysis input parameters for example 2.

| | |
|---|---|
| Analysis Period (years) | 40 |
| Project Length (km) | 17.5 |
| Number of Lanes in One Direction | 1 |
| Discount Rate (%) | 3.5 |
| Type of Roadway | Undivided |
| Evaluation Method | NPV |
| Cost Method | Cost per km for Both Directions |

**Table B.7.14** Pay items for example 2.

| Item | Cost |
|---|---|
| Asphalt Concrete – New and Overlay ($/metric ton) | 28.00 |
| Asphalt Concrete Milling ($/$m^2$) | 0.80 |
| Chip Seal ($/$m^2$) | 1.10 |
| Crack Sealing ($/m) | 2.00 |
| Asphalt Concrete Removal ($/$m^2$) | 2.50 |
| Base Course Aggregate ($/metric ton) | 9.20 |
| Cement Treated Base ($/metric ton) | 16.20 |
| Geogrid A ($/$m^2$) | 2.50 |
| Traffic Control ($, lump sum) | 70,000 |
| Maintenance Costs ($/lane km) | 0.00 |
| Salvage Values | None for initial construction and all rehabilitations |

**Table B.7.15** Total life-cycle costs for design options for example 2.

| Design Option | Total Life Cycle Cost per km ($) | Percent Savings |
|---|---|---|
| Option 1 | 446,151 | NA |
| Option 2 | 384,133 | 13.9 |
| Option 3 | 369,524 | 17.2 |
| Option 4 | 401,531 | 10.0 |